strip globally. However, such a path can rarely be found in practice due to the complexity of the resulting vector field. An algorithm to find a suboptimal solution of this problem is presented in [20]. The authors introduce an "initial" tool path which has the largest average machining strip. Next, the entire tool path is constructed by propagating the initial path inside the region until it substantially deviates from the streamlines.

A few papers explore other "iso" methods such as the iso-distance and the iso-curvature methods (see, for instance, [47]). In [63] an additional tool path segments are appended to the basic tool path in order to achieve constant cutting forces and to avoid chatter vibrations in the entire machining area. Furthermore, the necessity to create geometric patterns suitable for the so-called pocket milling leaded to a series of methods designed for parts with one or more complex shaped "islands" inside. The methods are also needed to machined the so-called trimmed surfaces when the boundaries of the surface are defined by intersections with other surfaces.

In 1998, Choi and Jerard [21] introduced a term regional milling referring to situations when the machining operation, occurs in a region specified by boundary curves. According to [96] the regional milling can be performed using the same types of tool path topologies, namely, the contour-based offset type and the direction-parallel type. The direction-parallel type has been analyzed in [45, 46, 49], whereas the direction-parallel type in [21, 48, 51, 94].

One of the most important problems in the contour-based machining is linking the contours in such a way that the number of tool retractions is minimized. Held et al. [51] presents an algorithm designed for this type of machining based on the proximity maps and the Voronoi diagrams. The author suggests a linking procedure requiring a spanning tree of the planar graph of the monotonic pouches. Park and Chung [95] propose a contour linking algorithm accommodating minimization of slotting, tool-retractions and drilling holes.

Park et al. [96] presented a tool path linking algorithm, which guarantees a "zero" number of tool-retractions. The algorithm employs the concept of tool path element net providing information on the parent/child relationships. Jeong and Kim [57] present an algorithm designed to offset the boundary curves in the complex shaped region using the Voronoi diagram. Each curve segment is offset within the corresponding Voronoi polygon to avoid the degeneracy problem. Jeong and Kim [58] introduce a distance map algorithm which effectively finds the characteristic points and self intersection points of the offset curve segments and as the result eliminates such topological problems as loops, ridges and cusps. A forward locus tracing method is introduced in [68]. The algorithm searches for all intervals split by intersections of the planar curves and maps the 2D transversal intersections onto a 1D interval.

Suppose that the part is partitioned into a grid of cells each of them being a curvilinear triangle or a curvilinear rectangle. The optimization can then be considered as constructing a path which visits each cell, does not have intersections, requires minimal number of tool retractions and satisfies some error related criteria. Pocket machining using staircase or window frame patterns were proposed in [97]. Hansen and Arbab [46] developed a scan line algorithm for generating NC tool paths for arbitrarily shaped flat bottom pockets with islands. Flat pocket machining based on grids was suggested by Bao and Yim [11].

Treating the tool path generation as a navigation problem on grids leaded to approaches exploiting the shortest path optimization and related techniques. Suh and Shin [110] developed a neural network model to obtain the tool path in rough pocket machining as a solution to the traveling salesman problem. A good mathematical analysis of such strategies is given in [9]. The problem is formulated as follows: given a region in the parametric plane and the shape of a cutter find a shortest tour/path for the cutter such that every point within the region is covered by the cutter at some position along the tour (tool path). Additionally the cutter could be constrained to stay within a certain region. Narayanaswami and Choi [91] present a grid-based 3D navigation approach for generating NC tool path data for both linear interpolation and a combination of linear and circular interpolation for three-axis milling. The approach can be extended to the five-axis case.

The space-filling curves (SFC), having been applied in computer graphics, image processing, information systems, can be also seen as a suitable navigation pattern for generation of five-axis paths. The first application of the SFC to NC tool path generation was reported in [23, 44]. Griffiths [44] proposed the use of the Hilbert's curve as a tool path, while Cox et al. [23] used various forms of space-filling curves such as Moore's curve. Fractal based techniques were suggested by Chen et al. [18].

However, neither SFCs nor fractals have never been very popular in the five-axis machining community due to a large number of sharp turns produced by the conventional SFCs. A concept of an adaptive space-filling curve for tool path planning for five-axis NC machining was proposed in [8]. The space-filling curves, adapted to the local optimal cutting direction, produce shorter tool paths. Besides, the tool path correction stage suggested in [8] makes it possible to eliminate the effect of sharp angular turns which characterize the standard SFC patterns. These techniques will be presented in Chap. 4 of this book.

Finally, the entire tool path can be considered in the framework of the grid generation technologies. The concept was first introduced by Makhanov [82] and developed in [15, 83]. The grid generation techniques are surprisingly well-adapted to tool path optimizations. As a matter of fact, the concept of a grid refinement contains almost all the main ingredients for tool path planning, such as grid adaptation to the regions of large milling errors, possibility to easily construct curvilinear versions of the conventional zigzag and spiral patterns and adaptation to constraints related to the tool diameter and the scallop height. Moreover, in contrast to the standard techniques characterized by a local error estimate, grid generation deals with a global spatial error and consequently adapts all the CL points simultaneously. These ideas were developed further in [84], specifically for five-axis machining whereas Bieterman

and Sandstrom [12] suggested a similar approach, independently. Finally, Sun et al. [111] presented a spiral version of the grid generation algorithm applied to tool path generation. The advanced grid generation techniques for five-axis machining will be considered in Chap. 5 of this book.

## Tool posture and gouging avoidance

This section deals with techniques providing an optimal position and orientation of the tool in a particular neighborhood of the machined surface. The emphasis is on the orientations prescribed independently with regard to a certain criteria such as the local gouging avoidance, machining strip, scallop height, avoiding global gouging constraints, etc. The most important application of these techniques is cutting the part surface by the flat-end or fillet mill

In 1987, Marciniak [86] showed that in five-axis machining the maximum width of machined strip on the surface could be obtained if the tool moved on the surface approximately along the minimum curvature line. The maximum width of the strip depends on the difference of the surface main curvatures at the contact point. Some of the early research papers exploiting this idea are [37, 67, 74]. Furthermore, Kruth and Klewais [67] introduced an optimal milling direction parallel to the principal direction of the surface with the minimum curvature.

Gani et al. [37] notice that "One of the critical problems in five-axis milling is the positioning of the cutter in relation to the surfaces in order to machine without having overcut (gouging) or undercut. Because of this problem, ballend cutters are preferred. Undercutting does not cause a big problem when using ball-end cutters. The calculation of the NC tool path for ball-end cutters is mainly a problem of surface offset. An important drawback of ball-end cutters is the varying cutting speed along the tool radius. The maximal cutting speed is reached on the tool diameter, and at the tool tip it is zero. This leads to cutting edge chipping as well as poor surface roughness".

Recall that as long as the five-axis machines are considered, the tool has five degrees of freedom relative to the surface. The three spatial degrees are used to locate the tool at the cutter location points point. The extra two rotational degrees are used to establish the orientation of the tool represented by the *inclination angle* and the *tilt angle* (see, for instance, [103]) or the *tilt angle* and the *yaw angle* [60]. The angles are evaluated in a local coordinate system usually defined by the feed direction, the surface normal and the corresponding cross product vector. In the case of the flat-end mill the boundary of the base of the tool, which is the part of the tool cylinder is called the *cutting circle* of the tool. The *effective cutting shape* (also referred to as the tool swept section) is defined as a projection of the base of the tool onto the plane normal to the feed direction. Actually, in the case of flat-end mill the projected bottom edge becomes an ellipse called the *effective cutting ellipse*.

The parameters of the ellipse depend on the tool orientation. The local gouging (or the curvature interference) is usually defined as the excess material removal in the vicinity of the cutter contact point due to the mismatch in curvatures between the tool cutting edge and the desired surface. Detecting and avoidance of the local gouging includes comparing the curvature of the effective cutting shape (also referred to as effective cutting curvature) and the normal curvature of the surface evaluated in the same plane where the effective cutting shape is defined.

If the effective cutting curvature is greater than the normal curvature of the surface then the local gouging will not occur. The mathematical description of the effective cutting shape for a flat-end cutter is given in [129] and for a fillet end mill in [71]. The gouging is then avoided by determining the smallest inclination angle that ensures the largest material removal, that is, the largest machining strip. Of course, gouging is still possible because the curvatures are compared only in one section. In order to eliminate this source of errors, Lee and Ji [72] suggested to compare the curvature of the effective cutting shape evaluated in two planes: along the tool path and normal to the tool path. These effective cutting curvatures are compared to the normal curvatures of the surface in the respective planes and the inclination angle is computed as the maximum from the two minimal inclinations. Unfortunately, the method is not applicable to the non-convex surfaces when the radius of the curvature of the part surface is negative in the both directions but the maximum principle curvature is positive. In these cases, the method produces a zero inclination. This "bug" often leads to local gouging. Lo [78] solves this problem by continuously checking for gouging in all directions. Some improvements and modifications of these techniques are given in [8].

Li and Chen [75] write "Not only the parameters of the part of cutter body that pierces into the stock, but also the parameters of the area on the designed surface that may have relations to the cutter is yet to be studied. But the cutter location point, just as its name, is only the common point both on the cutter and the designed surface, any methods only based on the geometric properties of it will not obtain the best cutter positions." In other words, the accuracy of the above single point gouging model may be insufficient. In this case multipoint strategies [123, 124, 130] could be applied to further enhance the accuracy of the tool positioning. Furthermore, Rao and Sarma [103] present a closed form, coordinate free method for the detection and elimination of local gouging, at a CC point, in five-axis machining of sculptured surfaces using flat-end tools. The method is based on finding the curvatures of the tool swept surface at CC points along the tool path. Local gouging can then be detected and eliminated by sampling a finite set of points on the tool path, while comparing curvatures of the tool swept surface and the designed surface. Pottmann et al. [100] proposed a local millability criterion that guarantees global millability (i.e., rear-gouge and collision free milling) for three-axis machining using ball-end tools. The local millability criterion is based on curvature matching, using Dupin indicatrices in the tangent plane at the CC point, between the designed surface and the tool swept surface. A five-axis version of these method is presented in [131].

The above curvature matching methods require iterative gouge checking and correction strategies. To eliminate the need for iterative gouge checking and correction algorithms, some five-axis tool positioning strategies attempt to match the tool's cutting geometry to the surface geometry such as the principal axis method [104] developed for three-axis ball nose cutter and the five-axis arc intersection methods [42] based on the fact that the widest machined strip width is cut when the tool is tilted along the feed direction. Then for a given feed direction, a tool position is computed for each CC point along the tool path. The tool vector is restricted to lie in the tilting plane. The tilt angles are measured around the cross vector. The idea is to find the minimum tilt angle of the tool axis about the cross vector at which the tool contacts another point on the surface and maintain its contact with the CC point without gouging the surface.

Gray et al. [43] propose a modification of the five-axis arc intersection method for the so-called  $3^{1}/2^{1}/2$ -axis machining. This type of machining is characterized by three linear axes and two temporary locked rotary axes. The rotary axis are locked during the entire cut (resulting in a fixed tool orientation) or during a certain fraction of the cut. The rotary axis, represented by a high precision indexing device, constitute an interesting inexpensive alternative to the five-axis machining.

It should be noted that the above methods are based on the properties of a single or several contact points and therefore the errors still are unavoidable during, for instance, the wide strip precision machining. Besides, there is always a possibility of the so-called rear gouging when the back side of the tool gouges the surface with an attempt to obtain a wider machining strip. When the gouge is detected the tool must be inclined further and checked for gouging again until it clears the part. This secondary check and gouge elimination can be performed using the rolling ball method suggested in [41]. The basic idea is to roll a varying radius ball along the tool path and position the tool inside the ball.

An interesting approach has been developed by Li and Chen [75]. An envelop surface created by the cutter movement is discretized into infinite characteristic curves. Each of these curves will exactly copy themselves on to the stock. Then an analysis of the characteristic curves is performed to solve the problem of cutter positioning. The authors use the concept of the instantaneous cutter position error employing the virtual cutting edge of the tool. The effective bandwidth of cutting strip is calculated and used in the optimization algorithm.

Finally, regardless of the tool orientation there always exists the possibility of a global interference of the workpiece with the tool holder, fixture or other parts of the machine. There also exists a possibility that given any orientation, the tool still flank-mills an unwanted part of the surface. It means that this portion of the surface is not accessible. Elber and Cohen [28] write "The

problem of accessibly, or the ability to verify and possibly correct gouging into the machined surface or even into other surfaces, is apparently the most fundamental hindering factor in the broad use of five-axis machining".

Solid modeling systems offer the possibility of doing both simulation and verification of tool paths off-line. However, the solid modeling approach is computationally expensive. The cost of simulation using the so-called constructive solid geometry is proportional to the fourth power of the number of the tool movements  $O(N^4)$  [16]. On the other hand, the solid model can detect both the local and the global interference, including collisions with the clamping device and the machine parts. A typical program for surface machining could contain more than 10,000 tool movements, therefore, current solid modeling research focuses on efficient and fast algorithms to compute the swept volume of the tool and perform Boolean operations to subtract the intersection from the stock. Bohez et al. [16] presents a short introduction to solid modeling schemes such as the extended Z-buffer algorithm [52], line graphic simulation approaches [59] and others.

The partition into elements and the corresponding data structures are the most important components of these procedures. The Z-buffer structure [7, 113], ray representation [56], Octree method [93, 106], K-D trees [50], BSP-trees [92], Brep-indices [65, 117], tetrahedral meshes [93] and regular grids [38] are examples of such spatial decomposition techniques. Each solid modeling algorithm has advantages and disadvantages in terms of accuracy, robustness, data structure and computation time. However, it seems that the simplicity of the data structure required for the Z-buffer scheme and the possibility to generate and update the part model very fast made many commercial CAM program to use the Z-buffer algorithm or its ramifications for the NC code verification and optimization [107].

The recent research papers include many improvements of the Z-buffer techniques such as the enhanced Z-buffer model [107], the stencil buffer [16], the adaptive depth buffer [105], the undo facilities for the Z-buffer scheme [13], etc. However, the above methods are not designed specifically for global interference detection. As a matter of fact, the solid model visualizes a general cut which may or may not include the global interferences. It may take hours of simulation and possibly an operator to visually detect possible collisions.

Therefore, methods based on the closed form mathematical solutions or their approximation are still valuable. The problem of the global gouging is treated mathematically using the concept of accessibility. The accessibility of a point in a given direction is defined as follows: a point belonging to a geometric entity is accessible in a given direction if a ray can be drawn from it in the given direction without intersecting with interior of the geometric entity.

The problem of accessibility in three-axis machining can be solved by a method of hidden surface removal of the same scene from a direction collinear with the tool axis [26, 53]. The fact that the tool has a finite thickness can be compensated for, by offsetting all the check surfaces by the radius of the tool.

The use of Z-buffer based hidden surface removal techniques to verify and correct the three-axis tool path, is a common practice in many contemporary computer-aided manufacturing schemes. For three-axis machining under certain conditions the absence of the local gouging implies the complete absence of collisions [99].

For five-axis machining it has been also shown that if all axis positions pass through a fixed point and if all points of the workpiece surface can be seen from this point then the local millability implies global millability [99]. Wallner and Pottmann [120] presented a global millability theorem for general workpieces. They analyzed several possible configuration manifolds of tool positions relative to a workpiece under different aspects; the degree of freedom of the motion of the tool, the correspondence between the contact point and the tool position, and the presence or absence of unwanted collisions between tool and workpiece.

Takeuchi et al. [114] proposed a method for computing the collision-free CL data using a trial and error approach. Morishige et al. [89] used the so-called C-space techniques to generate a smooth, continuously varying tool path. The C-space is a general concept of robotics where the configuration of a mechanism is specified by a sequence of values. A rigid body, for example, can be located in space by specifying six parameters related to all six of its degrees of freedom. The configuration space (C-space) of a mechanism is the space of these parameters, and a point in the C-space specifies a particular configuration. Obstacles can be mapped to the C-space as well, and the required collision-free access can theoretically be inferred by navigating the point in the C-space around the obstacles. Unfortunately, though intuitive and intellectually appealing, the C-space approach could lead to computationally intractable tasks.

The problem of accessibility can be approximated by a simpler requirement called visibility. A point on an object is visible from a point at infinity if there exists a straight line segment connecting the two points which does not intersect with the object. Visibility is a useful precursor for the accessibility computation because, for a certain class of tools and probes, visibility is a necessary condition for accessibility. Seminal theoretical results in the area were obtained by Elber and Cohen [27], Elber and Zussman [29], Woo [127]. Later research was focused on generating the so-called product visibility cones (see [62, 116]).

Lauwers et al. [70] describe a multi-axis tool path generation software where the tool orientation is optimized to avoid machine collisions and at the same time to maximize the material removal rate along the tool track. To perform efficient collision avoidance, the tool path generation module, the post processing and machine simulation has been integrated into one system. Xu et al. [128] combine the machine limits, collisions, and gouging to generate feasible gouge free tool orientations. Gian et al. [39] developed open regions and vector fields techniques to find rapidly the cutter paths and tool orientations for parts with cavity areas. In 2003, Balasubramaniam et al. [10] developed

methods for five-axis tool positioning that account for accessibility of the tool using visibility maps of the triangulated data. Using this visibility data for finish machining the authors show how it can be used to generate globally collision-free five-axis finishing tool paths while considering machine limits, tool tilt, cusp height limits and the tool pitch limits.

Young et al. [132] presented a new parametric method with an approximate constant cutting depth for the rough machining of an impeller. The initial tool spindle axis is considered as the initial orientation to determine the cutting tool posture for which the variation of rotational axes of the five-axis machine tool will be reduced. Hsuch et al. [54] propose to prevent the collisions using the two stages: the first stage is to obtain the tilting and collision-free angle range in the plane that is normal to the tool path obtained. Next, a checking cone generated from this collision-free tool axis range is used for the second collision check. The collision region is formed by the intersection of the neighboring surfaces.

Analyzing a proper sculptured surface orientation on the worktable of multi-axis CNC machine, Radzevich and Goodman [102] proposed the so-called spherical indicatrix of the sculptured surface machinability. This characteristic curve indicates whether the sculptured surface is machinable under a known scenario. The theory is developed in connection with a sculptured surface orientation on the worktable of a multi-axis CNC machine.

Radzevich [101] presents an approach that enables us to detect regions of a sculptured surface which are not accessible for a cutting tool of a given design, Furthermore, if any not-machinable regions exist, the developed approach enables us to subdivide the sculptured surface into the cutter-accessible and the cutter-not-accessible regions.

We have presented a survey on three selected topics in five-axis machining, namely, tool path interpolators, adaptable geometric patterns and methods for tool posture and gouging avoidance. We believe that the above procedures are the most important for constructing efficient numerical methods for five-axis machining

It should be noted that complete software systems designed for tool path generation and verification are now very important. The commercial CAD/CAM systems such as Unigraphics, PowerMill, Catia, MasterCam, each of them to a certain degree, include five-axis capabilities. In Chap. 2 we will demonstrate how the solid modeling features of Unigraphics can be used for the tool path simulation and verification.

Finally, we apologize to those authors whose works have not been cited. The exclusion of any such papers is due to our not being aware of their work.

# References

[1] The NURBS++ package, http://libnurbs.sourceforge.net/index.shtml.

- [2] NURBS Toolbox, http://www.aria.uklinux.net/nurbs.php3.
- [3] NIST/IGES, http://www.nist.gov/iges/.
- [4] .SLC file format, http://www-rp.me.vt.edu/bohn/rp/SLC.html.
- [5] CAD/CAM Software and File Format Compatibility Matrix, http://www.cs.cmu.edu/People/unsal/research/rapid/cadcam.html.
- [6] CAD File Formats, http://www.actify.com/v2/products/Importers/ formats.htm.
- [7] Anderson, R. O. 1978. Detecting and eliminating collisions in NC machining. *Computer-Aided Design*, 10(4):231–237.
- [8] Anotaipaiboon, W. and Makhanov, S. S. 2005. Tool path generation for five-axis NC machining using adaptive space-filling curves. *International Journal of Production Research*, 43(8):1643–1665.
- [9] Arkin, E. M., Fekete, S. P., and Mitchell, J. S. B. 2000. Approximation algorithms for lawn mowing and milling. *Computational Geometry: Theory* and Applications, 17(1-2):25-50.
- [10] Balasubramaniam, M., Sarma, S. E., and Marciniak, K. 2003. Collision-free finishing toolpaths from visibility data. Computer-Aided Design, 35(4):359–374.
- [11] Bao, H. P. and Yim, H. 1992. Tool path determination for end milling of non-convex shaped polygons. *NAMRI Transactions*, pages 151–158.
- [12] Bieterman, M. B. and Sandstrom, D. R. 2003. A curvilinear tool-path method for pocket machining. *Journal of Materials Processing Technology*, 125(4):709–715.
- [13] Blasquez, I. and Poiraudeau, J.-F. 2004. Undo facilities for the extended z-buffer in NC machining simulation. *Computers in Industry*, 53(2):193–204.
- [14] Bohez, E. L. J., Makhanov, S. S., and Sonthipermpoon, K. 2000a. Adaptive non-linear grid tool path optimization for 5-axis machining. *International Journal of Production Research*, 38(17):4329–4343.
- [15] Bohez, E. L. J., Makhanov, S. S., and Sonthipermpoon, K. 2000b. Adaptive nonlinear tool path optimization for 5-axis machining. *International Journal of Production Research*, 38(17):4329–4343.
- [16] Bohez, E. L. J., Minh, N. T. H., Kiatsrithanakorn, B., Natasukon, P., Ruei-Yun, H., and Son, L. T. 2003. The stencil buffer sweep plane algorithm for 5-axis CNC tool path verification. *Computer-Aided Design*, 35(12):1129– 1142.
- [17] Butler, J., Haack, B., and Tomizuka, M. 1988. Reference input generation for high speed coordinated motion of a two axis system. In Symposium on Robotics, Winter Annual Meeting of the American Society of Mechanical Engineers, pages 457–470.
- [18] Chen, C.-C. A., Juang, Y.-S., and Lin, W.-Z. 2002. Generation of fractal toolpaths for irregular shapes of surface finishing areas. *Journal of Materials Processing Technology*, 127(2):146–150.

- [19] Chen, Y. D., Ni, J., and Wu, S. M. 1993. Real-time CNC tool path generation for machining IGES surfaces. ASME Journal of Engineering for Industry, 115(4):480–486.
- [20] Chiou, C.-J. and Lee, Y.-S. 2002. A machining potential field approach to tool path generation for multi-axis sculptured surface machining. Computer-Aided Design, 34(5):357–371.
- [21] Choi, B. K. and Jerard, R. B. 1998. Computer Aided Machining the z-Map Way: Sculptured Surface Machining Theory and Applications. Kluwer Academic Publishers, Dordrecht, The Netherlands.
- [22] Choi, Y.-K. and Banerjee, A. Tool path generation and tolerance analysis for free-form surfaces. *International Journal of Machine Tools and Manu*facture. in press.
- [23] Cox, J. J., Takezaki, Y., Ferguson, H. R. P., Kohkonen, K. E., and Mulkay, E. L. 1994. Space-filling curves in tool-path applications. *Computer-Aided Design*, 26(3):215–224.
- [24] De Boor, C. 2001. A practical guide to splines. Springer, New York, USA.
- [25] Dragomatz, D. and Mann, S. 1997. A classified bibliography of literature on NC milling path generation. *Computer-Aided Design*, 29(3):239–247.
- [26] Elber, G. and Cohen, E. 1990. Hidden curve removal for free form surfaces. In SIGGRAPH '90: Proceedings of the 17th annual conference on Computer graphics and interactive techniques, pages 95–104.
- [27] Elber, G. and Cohen, E. 1995. Arbitrarily precise computation of gauss maps and visibility sets for freeform surfaces. In SMA '95: Proceedings of the third ACM symposium on Solid modeling and applications, pages 271–279.
- [28] Elber, G. and Cohen, E. 1999. A unified approach to verification in 5-axis freeform milling environments. *Computer-Aided Design*, 31(13):795–804.
- [29] Elber, G. and Zussman, E. 1998. Cone visibility decomposition of freeform surface. *Computer-Aided Design*, 30(4):315–320.
- [30] Erkorkmaz, K. and Altintas, Y. 2001. High speed CNC system design. Part I: jerk limited trajectory generation and quintic spline interpolation. International Journal of Machine Tools and Manufacture, 41(9):1323–1345.
- [31] Farin, G. E. 1999. NURBS: From Projective Geometry to Practical Use. A. K. Peters, Ltd., Natick, MA, USA.
- [32] Farouki, R. T. and Neff, C. A. 1995. Hermite interpolation by Pythagorean hodograph quintics. *Mathematics of Computation*, 64(212):1589–1609.
- [33] Farouki, R. T. and Sakkalis, T. 1994. Pythagorean-hodograph space curves. *Advances in Computational Mathematics*, 2(1):41–66.
- [34] Farouki, R. T., Tsai, Y.-F., and Wilson, C. S. 2000. Physical constraints on feedrates and feed accelerations along curved tool paths. *Computer Aided Geometric Design*, 17(4):337–359.
- [35] Farouki, R. T., Tsai, Y.-F., and Yuan, G.-F. 1999. Contour machining of free-form surfaces with real-time PH curve CNC interpolators. Computer Aided Geometric Design, 16(1):61-76.

- [36] Flutter, A. and Todd, J. 2001. A machining strategy for toolmaking. Computer-Aided Design, 33(13):1009–1022.
- [37] Gani, E. A., Kruth, J. P., Vanherck, P., and Lauwers, B. 1997. A geometrical model of the cut in five-axis milling accounting for the influence of tool orientation. *International Journal of Advanced Manufacturing Technology*, 13(10):677–684.
- [38] Garcia-Alonso, A., Serrano, N., and Flaquer, J. 1994. Solving the collision detection problem. *IEEE Computer Graphics and Applications*, 14(3):36–43.
- [39] Gian, R., Lin, T., and Lin, A. C. 2003. Planning of tool orientation for five-axis cavity machining. *International Journal of Advanced Manufacturing Technology*, 22(1-2):150–160.
- [40] Goldstein, B. L., Kemmerer, S. J., and Parks, C. H. 1998. A brief history of early product data exchange standards - NISTIR 6221. Technical report, National Institute of Standards and Technology.
- [41] Gray, P. J., Bedi, S., and Ismail, F. 2003. Rolling ball method for 5-axis surface machining. *Computer-Aided Design*, 35(4):347–357.
- [42] Gray, P. J., Bedi, S., and Ismail, F. 2005. Arc-intersect method for 5-axis tool positioning. *Computer-Aided Design*, 37(7):663–674.
- [43] Gray, P. J., Ismail, F., and Bedi, S. 2007. Arc-intersect method for 3<sup>11</sup>/<sub>22</sub>-axis tool paths on a 5-axis machine. *International Journal of Machine Tools and Manufacture*, 47(1):182–190.
- [44] Griffiths, J. G. 1994. Toolpath based on Hilbert's curve. Computer-Aided Design, 26(11):839–844.
- [45] Guyder, M. K. 1990. Automating the optimization of 2 1/2 axis milling. Computers in Industry, 15(3):163–168.
- [46] Hansen, A. and Arbab, F. 1992. An algorithm for generating NC tool paths for arbitrarily shaped pockets with islands. *ACM Trans. Graph.*, 11(2):152–182.
- [47] Hatna, A. and Grieve, B. 2000. Cartesian machining versus parametric machining: a comparative study. *International Journal of Production Research*, 38(13):3043–3065.
- [48] Held, M. 1991a. A geometry-based investigation of the tool path generation for zigzag pocket machining. *The Visual Computer*, 7(5-6):296–308.
- [49] Held, M. 1991b. On the computational geometry of pocket machining. Springer-Verlag New York, Inc., New York, NY, USA.
- [50] Held, M., Klosowski, J., and Mitchell, J. S. B. 1995. Evaluation of collision detection methods for virtual reality fly-throughs. In proceedings Seventh Canadian Conference on Computational Geometry, pages 205–210.
- [51] Held, M., Lukács, G., and Andor, L. 1994. Pocket machining based on contour-parallel tool paths generated by means of proximity maps. *Computer-Aided Design*, 26(3):189–203.
- [52] Hook, T. V. 1986. Real-time shaded NC milling display. In SIGGRAPH '86: Proceedings of the 13th annual conference on Computer graphics and interactive techniques, pages 15–20.

- [53] Hornung, C., Lellek, W., Rehwald, P., and Straßer, W. 1985. An areaoriented analytical visibility method for displaying parametrically defined tensor-product surfaces. *Computer Aided Geometric Design*, 2(1-3):197– 205.
- [54] Hsueh, Y.-W., Hsueh, M.-H., and Lien, H.-C. Automatic selection of cutter orientation for preventing the collision problem on a five-axis machining. *International Journal of Advanced Manufacturing Technology*. in press.
- [55] Hu, J., Xiao, L., Wang, Y., and Wu, Z. 2006. An optimal feedrate model and solution algorithm for a high-speed machine of small line blocks with look-ahead. *International Journal Advanced Manufacturing Technology*, 28(9):930–935.
- [56] Huang, Y. and Oliver, J. H. 1995. Integrated simulation, error assessment, and tool path correction for five-axis NC machining. *Journal of Manufacturing Systems*, 14(5):331334.
- [57] Jeong, J. and Kim, K. 1999a. Generating tool paths for free-form pocket machining using z-buffer-based Voronoi diagrams. *International Journal of Advanced Manufacturing Technology*, 15(3):182–187.
- [58] Jeong, J. and Kim, K. 1999b. Generation of tool paths for machining free-form pockets with islands using distance maps. *International Journal* of Advanced Manufacturing Technology, 15(5):311–316.
- [59] Jerard, R. B. and Drysdale, R. L. 1989. Methods for geometric modeling, simulation and spacial verification of NC machining programs. In Wozny, M. J., Turner, J. U., and Pegna, J., editors, *Product modeling for computer*aided design and manufacturing. Elsevier/North-Holland, New York, USA.
- [60] Jun, C.-S., Cha, K., and Lee, Y.-S. 2003. Optimizing tool orientations for 5-axis machining by configuration-space search method. *Computer-Aided Design*, 35(6):549–566.
- [61] Jüttler, B. 2001. Hermite interpolation by Pythagorean hodograph curves of degree seven. *Mathematics of Computation*, 70(235):1089–1111.
- [62] Kang, J.-K. and Suh, S.-H. 1997. Machinability and set-up orientation for five-axis numerically controlled machining of free surfaces. *International Journal of Advanced Manufacturing Technology*, 13(5):311–325.
- [63] Kim, H.-C., Lee, S.-G., and Yang, M.-Y. An optimized contour parallel tool path for 2D milling with flat endmill. *International Journal of Advanced Manufacturing Technology*. in press.
- [64] Ko, T. J., Kim, H. S., and Park, S. H. 2005. Machineability in NURBS interpolator considering constant material removal rate. *International Journal of Machine Tools and Manufacture*, 45(6):665–671.
- [65] Kondo, M. 1994. Decomposition of complex geometry for a manufacturing application. Computer-Aided Design, 26(3):244–252.
- [66] Koren, Y. 1976. Interpolator for a computer numerical control system. *IEEE Transactions on Computers*, 25(1):32–37.

- [67] Kruth, J.-P. and Klewais, P. 1994. Optimization and dynamic adaptation of the cutter inclination during five-axis milling of sculptured surfaces. *Anals CIRP*, 43(1):443–448.
- [68] Lai, Y.-L., Wu, J. S.-S., Hung, J.-P., and Chen, J.-H. 2006. A simple method for invalid loops removal of planar offset curves. *International Journal of Advanced Manufacturing Technology*, 27(11-12):1153–1162.
- [69] Langeron, J. M., Duc, E., Lartigue, C., and Bourdet, P. 2004. A new format for 5-axis tool path computation, using Bspline curves. Computer-Aided Design, 36(12):1219–1229.
- [70] Lauwers, B., Dejonghe, P., and Kruth, J. P. 2003. Optimal and collision free tool posture in five-axis machining through the tight integration of tool path generation and machine simulation. *Computer-Aided Design*, 35(5):421–432.
- [71] Lee, Y.-S. 1997. Admissible tool orientation control of gouging avoidance for 5-axis complex surface machining. Computer-Aided Design, 29(7):507– 521
- [72] Lee, Y.-S. and Ji, H. 1997. Surface interrogation and machining strip evaluation for 5-axis CNC die and mold machining. *International Journal of Production Research*, 35(1):225–252.
- [73] Li, F., Wang, X. C., Ghosh, S. K., Kong, D. Z., Lai, T. Q., and Wu, X. T. 1995. Tool-path generation for machining sculptured surface. *Journal of Materials Processing Technology*, 48(1):811–816.
- [74] Li, S. X. and Jerard, R. B. 1994. 5-axis machining of sculptured surfaces with a flat-end cutter. *Computer-Aided Design*, 26(3):165–178.
- [75] Li, Z. and Chen, W. 2006. A global cutter positioning method for multiaxis machining of sculptured surfaces. *International Journal of Machine Tools and Manufacture*, 46(12-13):1428–1434.
- [76] Lin, R.-S. and Koren, Y. 1996. Efficient tool-path planning for machining free-form surfaces. ASME Journal of Engineering for Industry, 118(1):20– 28.
- [77] Lo, C. C. 1997. Feedback interpolator for CNC machine tool. ASME. Journal of Manufacturing Science and Engineering, 119(4):587592.
- [78] Lo, C. C. 1999a. Efficient cutter-path planning for five-axis surface machining with a flat-end cutter. *Computer-Aided Design*, 31(9):557–566.
- [79] Lo, C. C. 1999b. Real-time generation and control of cutter path for 5-axis CNC machining. *International Journal of Machine Tools and Manufacture*, 39(3):471–488.
- [80] Lo, C. C. 2000. CNC machine tool surface interpolator for ball-end milling of free-form surfaces. *International journal of machine tools and manufacture*, 40(3):307–326.
- [81] Ma, W., But, W.-C., and He, P. 2004. NURBS-based adaptive slicing for efficient rapid prototyping. Computer-Aided Design, 36(13):1309–1325.
- [82] Makhanov, S. S. 1999. An application of variational grid generation techniques to the tool-path optimization of industrial milling robots. *Journal of Materials Processing Technology*, 39(9):1524–1535.

- [83] Makhanov, S. S., Batanov, D., Bohez, E., Sonthipaumpoon, K., Anotaipaiboon, W., and Tabucanon, M. 2002. On the tool-path optimization of a milling robot. *Computers & Industrial Engineering*, 43(3):455–472.
- [84] Makhanov, S. S. and Ivanenko, S. A. 2003. Grid generation as applied to optimize cutting operations of the five-axis milling machine. *Applied Numerical Mathematics*, 46(3-4):331–351.
- [85] Mani, K., Kulkarni, P., and Dutta, D. 1999. Region-based adaptive slicing. Computer-Aided Design, 31(5):317–333.
- [86] Marciniak, K. 1987. Influence of surface shape in admissible tool positions in 5-axis face milling. *Computer-Aided Design*, 19(5):233–236.
- [87] Monreal, M. and Rodríguez, C. A. 2003. Influence of tool path strategy on the cycle time of high-speed milling. Computer-Aided Design, 35(4):395– 401.
- [88] Moon, H. P., Farouki, R. T., and Choi, H. I. 2001. Construction and shape analysis of PH quintic hermite interpolants. Computer Aided Geometric Design, 18(2):93–115.
- [89] Morishige, K., Takeuchi, Y., and Kase, K. 1999. Tool path generation using C-space for 5-axis control machining. *Journal of Manufacturing Science and Engineering*, 121(1):144–149.
- [90] Müller, M., Erds, G., and Xirouchakis, P. C. 2004. High accuracy spline interpolation for 5-axis machining. Computer-Aided Design, 36(13):1379– 1393
- [91] Narayanaswami, R. and Choi, Y. 2001. NC machining of freeform pockets with arbitrary wall geometry using a grid-based navigation approach. International Journal of Advanced Manufacturing Technology, 18(10):708–716
- [92] Naylor, B., Amanatides, J., and Thibault, W. 1990. Merging BSP trees yields polyhedral set operations. In SIGGRAPH '90: Proceedings of the 17th annual conference on Computer graphics and interactive techniques, pages 115–124.
- [93] Noborio, H., Fukuda, S., and Arimoto, S. 1989. Fast interference check method using octree representation. *Advanced robotics*, 3(3):193–212.
- [94] Park, S. C. and Choi, B. K. 2000. Tool-path planning for direction-parallel area milling. *Computer-Aided Design*, 32(1):17–25.
- [95] Park, S. C. and Chung, Y. C. 2002. Offset tool-path linking for pocket machining. *Computer-Aided Design*, 34(4):299–308.
- [96] Park, S. C., Chung, Y. C., and Choi, B. K. 2003. Contour-parallel offset machining without tool-retractions. Computer-Aided Design, 35(9):841– 849
- [97] Persson, H. 1978. NC machining of arbitrarily shaped pockets. Computer-Aided Design, 10(3):169–174.
- [98] Piegl, L. and Tiller, W. 1995. The NURBS book. Springer-Verlag, London, UK.
- [99] Pottmann, H. and Ravani, B. 2000. Singularities of motions constrained by contacting surfaces. *Mechanism and Machine Theory*, 35(7):963–984.

- [100] Pottmann, H., Wallner, J., Glaeser, G., and Ravani, B. 1999. Geometric criteria for gouge-free three-axis milling of sculptured surfaces. ASME Journal of Mechanical Design, 121(2):241–248.
- [101] Radzevich, S. P. 2005. A cutting-tool-dependent approach for partitioning of sculptured surface. *Computer-Aided Design*, 37(7):767–778.
- [102] Radzevich, S. P. and Goodman, E. D. 2002. Computation of optimal workpiece orientation for multi-axis NC machining of sculptured part surfaces. ASME Journal of Mechanical Design, 124(2):201–212.
- [103] Rao, A. and Sarma, R. 2000. On local gouging in five-axis sculptured surface machining using flat-end tools. *Computer-Aided Design*, 32(7):409–420.
- [104] Rao, N., Ismail, F., and Bedi, S. 1997. Tool path planning for five-axis machining using the principal axis method. *International Journal of Machine Tools and Manufacture*, 37(7):1025–1040.
- [105] Roth, D., Ismail, F., and Bedi, S. 2003. Mechanistic modelling of the milling process using an adaptive depth buffer. *Computer-Aided Design*, 35(14):1287–1303.
- [106] Roy, U. and Xu, Y. 1999. Computation of a geometric model of a machined part from its NC machining programs. *Computer-Aided Design*, 31(6):401–411.
- [107] Sang-Kyu Lee, S.-L. K. 2002. Development of simulation system for machining process using enhanced Z map model. *Journal of materials process*ing technology, 130-131:608-617.
- [108] Sarma, R. 2000. An assessment of geometric methods in trajectory synthesis for shape-creating manufacturing operations. *Journal of Manu*facturing Systems, 19(1):59–72.
- [109] Siller, H., Rodriguez, C. A., and Ahuett, H. 2006. Cycle time prediction in high-speed milling operations for sculptured surface finishing. *Journal of Materials Processing Technology*, 174(1-3):355–362.
- [110] Suh, S. H. and Shin, Y. S. 1996. Neural network modeling for tool path planning of rough cut in complex pocket milling. *Journal of Manufacturing Systems*, 15(5):295–304.
- [111] Sun, Y.-W., Guoa, D.-M., and Jia, Z.-Y. 2006. Spiral cutting operation strategy for machining of sculptured surfaces by conformal map approach. *Journal of Materials Processing Technology*, 180(1-3):74–82.
- [112] Suresh, K. and Yang, D. C. H. 1994. Constant scallop-height machining of free-form surfaces. ASME Journal of Engineering for Industry, 116(2):253–259.
- [113] Takata, S. 1989. A cutting simulation system for machinability evaluation using a workpiece model. *Anals CIRP*, 38(1):417–420.
- [114] Takeuchi, Y., Shimizu, H., Idemura, T., Watanabe, T., and Ito, T. 1990.
  5-axis control machining based on solid model. *Journal of the Japan Society for Precision Engineering*, 56(1):111–116.
- [115] Tata, K., Fadel, G., Bagchi, A., and Aziz, N. 1998. Efficient slicing for layered manufacturing. *Rapid Prototyping Journal*, 4(4):151–167.

- [116] Vafaeesefa, A. and ElMaraghy, H. A. 1998. Accessibility analysis in 5-axis machining of sculptured surfaces. In *Proceedings of the 1998 IEEE International Conference on Robotics & Automation*, pages 2464–2469.
- [117] Vaněček, Jr., G. 1991. BRep-Index: a multidimensional space partitioning tree. In SMA '91: Proceedings of the first ACM symposium on Solid modeling foundations and CAD/CAM applications, pages 35–44.
- [118] Šír, Z., Feichtinger, R., and Jüttler, B. 2006. Approximating curves and their offsets using biarcs and Pythagorean hodograph quintics. Computer-Aided Design, 38(6):608–618.
- [119] Śír, Z. and Jüttler, B. 2005. Constructing acceleration continuous tool paths using Pythagorean hodograph curves. *Mechanism and Machine The*ory, 40(11):1258–1272.
- [120] Wallner, J. and Pottmann, H. 2000. On the geometry of sculptured surface machining. In Laurent, P.-J., Sablonnière, P., and Schumaker, L. L., editors, Curve and Surface Design. Vanderbilt University Press, Nashville, USA.
- [121] Wang, F.-C. and Wright, P. K. 1998. Open architecture controllers for machine tools, Part 2: A real time quintic spline interpolator. *Journal of manufacturing science and engineering*, 120(2):425–432.
- [122] Wang, F.-C. and Yang, D. C. H. 1993. Nearly arc-length parameterized quintic-spline interpolation for precision machining. *Computer-Aided Design*, 25(5):281–288.
- [123] Warkentin, A., Ismail, F., and Bedi, S. 1998. Intersection approach to multi-point machining of sculptured surfaces. *Computer Aided Geometric Design*, 15(6):567–584.
- [124] Warkentin, A., Ismail, F., and Bedi, S. 2000. Multi-point tool positioning strategy for 5-axis machining of sculptured surfaces. Computer Aided Geometric Design, 17(1):83–100.
- [125] Weck, M., Meylahn, A., and Hardebusch, C. 1999. Innovative algorithms for spline-based CNC controller, production engineering research and development in germany. *Annals of the German Academic Society for Production Engineering*, VI(1):83–86.
- [126] Weck, M. and Ye, G. H. 1990. Sharp corner tracking using the IKF control strategy. Annals CIRP, 39(1):437–441.
- [127] Woo, T. C. 1994. Visibility maps and spherical algorithms. *Computer-Aided Design*, 26(1):6–16.
- [128] Xu, X. J., Bradley, C., Zhang, Y. F., Loh, H. T., and Wong, Y. S. 2002. Tool-path generation for five-axis machining of free-form surfaces based on accessibility analysis. *International Journal of Production Research*, 40(14):3253-3274.
- [129] Y-S Lee, T.-C. C. 1996. Automatic cutter selection for five-axis sculptured surface machining. *International Journal of Production Research*, 34(4):977–998.

- [130] Yoon, J.-H. 1997. Tool tip gouging avoidance and optimal tool positioning for 5-axis sculptured surface machining. *International Journal of Production Research*, 41(10):2125–2142.
- [131] Yoon, J.-H., Pottmann, H., and Lee, Y.-S. 2003. Locally optimal cutting positions for 5-axis sculptured surface machining. *Computer-Aided Design*, 35(1):69–81.
- [132] Young, H.-T., Chuang, L.-C., Gerschwiler, K., and Kamps, S. 2004. A five-axis rough machining approach for a centrifugal impeller. *International Journal of Advanced Manufacturing Technology*, 23(3-4):233–239.
- [133] Zhang, Q. G. and Greenway, R. B. 1998. Development and implementation of a NURBS curve motion interpolator. *Robotics and Computer-Integrated Manufacturing*, 14(1):27–36.

# Introduction to Five-Axis NC Machining

# 2.1 Five-Axis NC Machining Concepts

Numerical control or numerically controlled (NC) machines are automatically operated by commands received by their processing units. The NC machines were first developed soon after World War II and made it possible for a precise and efficient production of large quantities of the desired components in a reliable repetitive manner. Early NC machines were often fed with instructions which were punched onto paper tape or punch cards. In the 1960s, NC machines largely gave way to computer numerical control (CNC) machines which refers specifically to a computer controller that reads G-code instructions (see Sect. 2.2) and drives the machine tool.

Five-axis milling machines are NC machines which characterized by three translational and two rotary axes. A five-axis milling machine with two rotary axes on the table is depicted in Fig. 2.1. A block of a raw material called the workpiece is fixed to the *machine table* by means of *clamps* (*clumping device*) (see Fig. 2.1b). The material is then removed from the workpiece by a rotating *cutter* attached to the *spindle* through the *tool holder*. The process of material removal with the goal to produce a required industrial part is called *milling*, *machining* or *cutting*.

The NC machines are programmed by means of a special code called the NC program or the part program composed of commands represented by letters, numbers and special symbols. The part program consists of instructions to control the machine movements following a certain manufacturing technology and methodology. For example, the program tells the machine what is the required shape and size of the tool, at what speed and feedrate and at what orientation relative to the workpiece this tool should be used. The part program also prescribes a set of cutter location (CL) points assigned to cut the desired part.

<sup>&</sup>lt;sup>1</sup> A cutter location refers to the position at which an NC milling machine has been instructed to hold the milling cutter.

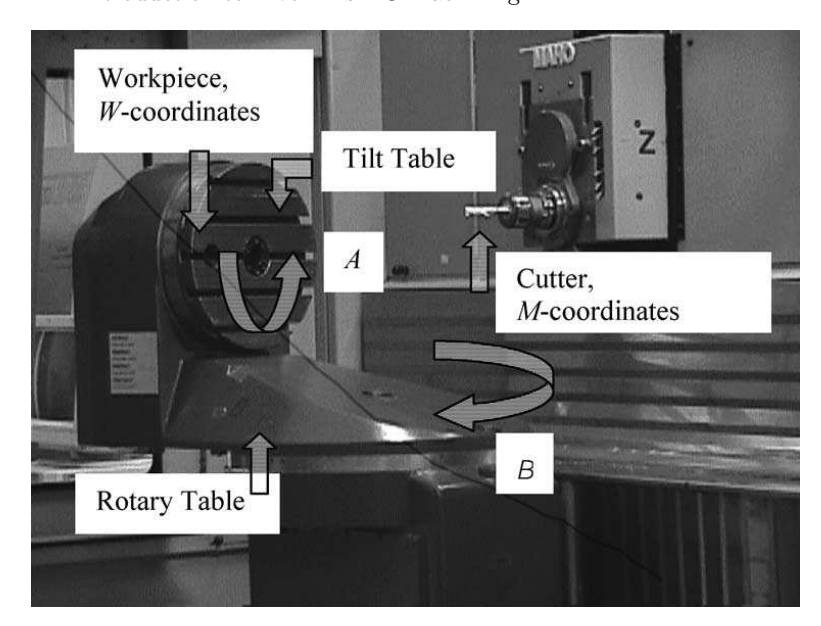
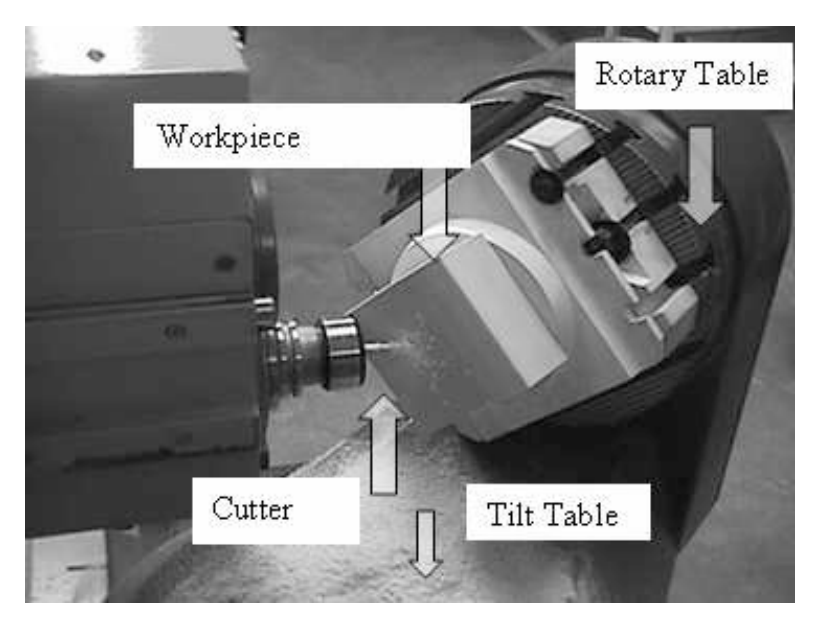


Fig. 2.1a. MAHO 600E milling machine



 $\textbf{Fig. 2.1b.} \ \ \text{Workpiece, clumping device, and rotary tables of MAHO 600E}$ 

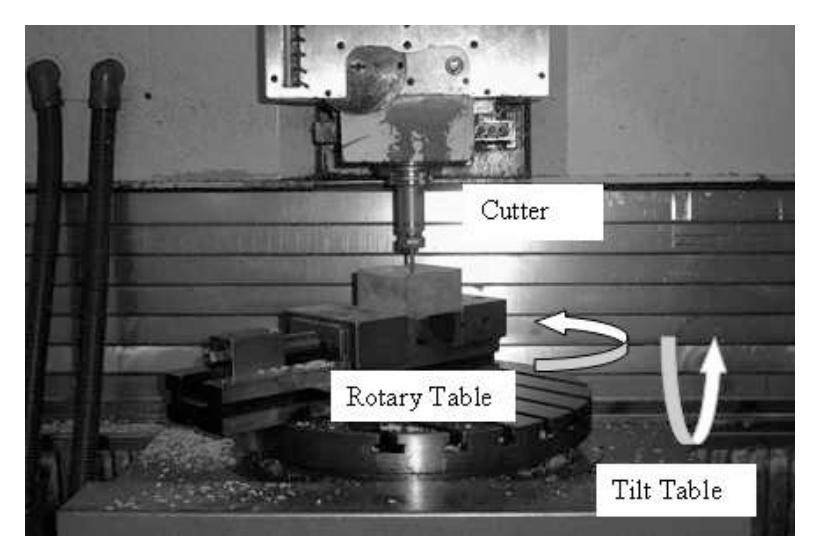


Fig. 2.1c. HERMLE UWF902H milling machine

The design of the part program takes into account the specific part geometry, the cutting process, the machine parameters and the cutting tools used. The program is fed to the machine controller that drives servomotors of the machine to move the table or the spindle by specified amounts in X, Y or Z and to tilt the cutter relative to the workpiece in one or two rotary axes. The part is machined by moving the cutter along a pre-computed path in space called the  $tool\ path$ . Generation of a part program to cut a specific part typically involves the following steps:

- Generation of the tool path in the workpiece coordinate system. Usually this step requires that a successive set of coordinates  $W = (x_w, y_w, z_w)$  called cutter contact<sup>2</sup> (CC) points and the tool orientations  $I = (I_x, I_y, I_z)$  in the workpiece coordinate system are distributed along a set of curves following a specified pattern such as the zigzag or the spiral curves (Fig. 2.2).
- The CL data are then computed from the set of CC points. The method for CC-CL data conversion must include the geometry of the cutting tool and the orientation of the tool relative to the workpiece. Various optimization techniques could be used at this step to generate optimal cutter location data (see, for instance, [2]).
- Each CL point is then transformed into the machine axial command  $\Pi = (M, \mathfrak{R}) \in \mathbb{R}^5$ , carrying three Cartesian coordinates  $M = (x_m, y_m, z_m)$  of the tool tip in the machine coordinate system and two rotation angles  $\mathfrak{R} = (a, b)$ . Converting coordinates of the CL points from the workpiece

<sup>&</sup>lt;sup>2</sup> A cutter contact point refers to the coordinates where the tool cutting edge makes contact with the surface.

coordinate system to the machine coordinate system is called postprocessing. The postprocessor requires knowledge of the machine kinematics and the machine configuration.

• The axial commands are then converted into an NC part program following the format understood by the machine controller.

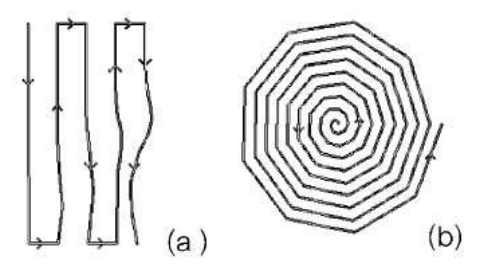


Fig. 2.2. Zigzag (a) and spiral (b) tool paths

The above sequence may or may not include an optimization and verification steps. The optimization step involves a cost function representing a certain type of error or a combination of several types of errors. The tool path is then modified or reconstructed entirely in such a way that the cost function is minimized or at least decreased.

The verification stage includes an actual machining or computer modeling of the material removal which produces the output as a solid model. The solid model can then be compared with the desired part and the efficiency of the optimization strategies can be evaluated.

## 2.2 NC Part Programming

The NC part program is a detailed plan (program) of manufacturing consisting of instructions called the NC blocks. The syntax of each instruction follows a specified format standardized by the ISO. This standard is maintained by many machine control units (MCU) manufacturers with some minor variations. When the machine is operated, the NC program is executed sequentially, one command or NC block at a time. An NC block is made up of words which consist of characters and digits. Each word begins with an address code which is a single letter character (A-Z) that defines what the computer should do with the numerical data that follows. This command structure is called the word address code. For example, the block

N20 G01 X100 Y-150 Z10.5 A30 B-10 F100 M03 S600

consists of 10 words: N20, G01, X100, Y-150, Z10.5, A30, B-10, F100, M03, and S600. The block N20 instructs the machine to move the tool from its current position to position  $(x_m, y_m, z_m) = (100, -150, 10.5)$  linearly (G01) and to rotate the A-axis by 30 degrees and the B-axis by -10 degrees with a feedrate of 100 mm/min (F100) and with the spindle rotating clockwise (M03) at 600 rpm (S600).

The NC part program is usually written in a high level language such as APT (Automatic Programmed Tools) [7], UNIAPT<sup>3</sup>, etc. It is then converted into the word address codes. Some commercial CAD/CAM systems such as Unigraphics, Pro Engineer, etc. include functions that can generate the word address codes directly from the tool paths.

A complete NC part program starts with a percent sign (%) followed by NC blocks represented in the ISO word address format. Each NC block starts with the block number indicated by an N word address. The block can contain one word address or a sequence of word addresses. The standardization of the English alphabet used to code the word addresses is given in Table 2.1.

Each letter other than G and M has a unique function and is followed by a parameter which is either an integer or a floating point number. The format of the ISO word address block is as follows:

N5 G2 X
$$\pm$$
53 Y $\pm$ 53 Z $\pm$ 53 U..V..W..I..J..K.. F5 S4 T4 M2 \*

All word addresses except N are optional and the block format is order-sensitive. The numerical value after each word address indicates the maximum number of digits allowed for that particular word address. A single digit indicates an integer value and two digits indicate a real value. The first and the second digit indicate the maximum number of digits before and after the decimal point, respectively. For example, N5 means the block sequence number starts with the letter N followed by at most 5 digits (N0-N99999). X±53 means that the primary X motion dimension starts with the letter X followed by plus or minus sign and a real value written with at most 5 digits before the decimal point and at most 3 digits after the decimal point. The block ends with the symbol "\*" or ";" or "carriage return" or "line feed". The usage of the word addresses for performing machine operation is given below.

### **Preparatory Functions**

A pre-set function which assigns a type of the tool movement is indicated by a G word address followed by a two digit integer ranging from 00 to 99. Examples of machine tool action instructed by the G-codes are:

- Rapid move.
- Controlled feed move in straight line or arc.

<sup>&</sup>lt;sup>3</sup> UNIAPT is a minicomputer-based version of an Automatic Programmed Tool (APT) developed by a software company called United Computing to compute tool paths.

Table 2.1. List of word address codes

Character	r Address for
A	Angular dimension around X axis
В	Angular dimension around Y axis
$^{\mathrm{C}}$	Angular dimension around Z axis
D	Angular dimension around special axis or third feed function*
${f E}$	Angular dimension around special axis or second feed function*
$\mathbf{F}$	Feed function
G	Preparatory function
H	Unassigned
I	Distance to arc center or thread lead parallel to X
J	Distance to arc center or thread lead parallel to Y
K	Distance to arc center or thread lead parallel to Z
${ m L}$	Unassigned
${ m M}$	Miscellaneous function
N	Sequence number
O	Reference rewind stop
P	Third rapid traverse or tertiary motion dimension parallel to X*
Q	Third rapid traverse or tertiary motion dimension parallel to Y*
R	Third rapid traverse or tertiary motion dimension parallel to Z*
S	Spindle speed function
${ m T}$	Tool function
$\mathbf{U}$	Secondary motion dimension parallel to X*
V	Secondary motion dimension parallel to Y*
$\mathbf{W}$	Secondary motion dimension parallel to Z*
X	Primary X motion dimension
Y	Primary Y motion dimension
$\mathbf{Z}$	Primary Z motion dimension
* The lett	ton many ha wood for other amountions

<sup>\*</sup> The letter may be used for other operations

- Series of controlled feed moves that would result in a hole being bored, a workpiece cut (routed) to a specific dimension, or a decorative profile shape added to the edge of a workpiece.
- Set tool information such as offset.

The ISO standardized G-codes are given in Table 2.2.

## **Coordinate Functions**

The coordinate of the tool tip are specified using a word address such as X, Y, Z, U, V, W, I, J, K, etc. These word addresses are normally signed real values.

## Feed Functions

The feedrate is specified by an F word address. The feedrate units are set by using an appropriate G-code (G94 or G95). The feed function is modal which

Table 2.2. List of G-code functions

Code	Function
G00	Point-to-point positioning, rapid traverse
G01	Line interpolation
G02	Circular interpolation, clockwise (WC)
G03	Circular interpolation, anti-clockwise (CCW)
G04	Dwell
G05	Hold/Delay
G06	Parabolic interpolation
G07	Unassigned
G08	Acceleration of feedrate
G09	Deceleration of feedrate
G10	Linear interpolation for "long dimensions" (10 inches-100 inches)
G11	Linear interpolation for "short dimensions" (up to 10 inches)
G12	Unassigned
G13-G16	Axis designation
G17	XY plane designation
G18	ZX plane designation
G19	YZ plane designation
G20	Circular interpolation, CW for "long dimensions"
G21	Circular interpolation, CW for "short dimensions"
G22-G29	Unassigned
G30	Circular interpolation, CCW for "long dimensions"
G31	Circular interpolation, CCW for "short dimensions"
G32	Unassigned
G33	Thread cutting, constant lead
G34	Thread cutting, linearly increasing lead
G35	Thread cutting, linearly decreasing lead
G36-G39	Unassigned
G40	Cutter compensation-cancels to zero
G41	Cutter radius compensation-offset left
G42	Cutter radius compensation-offset right
G43	Cutter compensation-positive
G44	Cutter compensation-negative
G45-G52	Unassigned
G53	Deletion of zero offset
G54-G59	Datum point/zero shift
G60	Target value, positioning tolerance 1
G61	Target value, positioning tolerance 2 or loop cycle
G62	Rapid traverse positioning
G63	Tapping cycle
G64	Change in feedrate or speed
G65-G69	Unassigned
G70	Dimensioning in inch units
G71	Dimensioning in metric units
G72-G79	Unassigned
G80	Canned cycle cancelled
G81-G89	Canned drilling and boring cycles

Table 2.2. List of G-code functions (cont.)

Code	Function
G90	Specifies absolute input dimensions
G91	Specifies incremental input dimensions
G92	Programmed reference point shift
G93	Unassigned
G94	feedrate/min (inch units when combined with G70)
G95	feedrate/rev (metric units when combined with G71)
G96	Spindle feedrate for constant surface feed
G97	Spindle speed in revolution per minute
G98-G99	Unassigned

means that once the feedrate is set it affects all the subsequent blocks until it is replaced by another F value.

## **Speed Function**

The spindle speed is assigned by an S word address given in revolutions per minute (rpm) when used with the preparatory code G97. For a constant surface speed (G96) the spindle speed is given in meters per minute or feet per minute.

#### **Tool Function**

For the NC machines equipped with tool magazines and automatic tool changers, the tool selection is performed by a T word address followed by a number indicating the position of the tool in the magazine. For example T19 mean the tool stored in position 19 in the magazine is to be used. If the tool change is to be done manually, the T word address would signal the machine to stop.

#### Miscellaneous Function

Control of the clumping device, spindle, coolant and some other global operations is performed by an M word address. The standard M-codes are given in Table 2.3.

It must be noted that M80-M99 are unassigned which means that the MCU manufacturers can use those remaining for other purposes such as to accommodate new CNC programming capabilities, for example, real-time surface interpolation [6] or Pythagorean-hodograph curves [3–5].

# Example of a simple NC milling program

We conclude this section with a simple NC program to cut a small rectangle  $2~\mathrm{cm} \times 4~\mathrm{cm}$ .

Table 2.3. List of M-code functions

	Table 2.3. List of M-code functions
Code	Function
M00	Program stop, spindle and coolant off
M01	Optional programmable stop
M02	End of program-often interchangeable with M30
M03	Spindle on, CW
M04	Spindle on, CCW
M05	Spindle stop
M06	Tool change
M07	Coolant supply No. 1 on
M08	Coolant supply No. 2 on
M09	Coolant off
M10	Clamp
M11	Unclamp
M12	Unassigned
M13	Spindle on, $CW + coolant$ on
M14	Spindle on, $CCW + coolant$ on
M15	Rapid traverse in + direction
M16	Rapid traverse in - direction
M17-M18	Unassigned
M19	Spindle stop at specified angular position
M20-M29	Unassigned
M30	Program stop at end of tape + tape rewind
M31	Interlock by-pass
M32-M35	Constant cutting velocity
	Unassigned
M40-M45	Gear changes; otherwise unassigned
M46-M49	Unassigned
M50	Coolant supply No. 3 on
M51	Coolant supply No. 4 on
M52-M54	Unassigned
M55	Linear cutter offset No. 1 shift
M56	Linear cutter offset No. 2 shift
M57-M59	Unassigned
M60	Piece part change
M61	Linear piece part shift, location 1
M62	Linear piece part shift, location 2
M63-M67	Unassigned
M68	Clamp piece part
M69	Unclamp piece part
M70	Unassigned
M71	Angular piece part shift, location 1
M72	Angular piece part shift, location 2
M73-M77	Unassigned
M78	Clamp non-activated machine bed-ways
M79	Unclamp non-activated machine bed-ways
M80-M99	Unassigned

```
N1 X0 Y0 T01
N2 X0 Y40
N3 X20 Y40
N4 X20 Y0
N5 X0 Y0
N6 M00
```

Line 1 (N1) tells the machine to traverse to grid point (X,Y) = (0,0) and to use tool #1.

```
Line 2 tells the machine to traverse to grid point (X, Y) = (0, 40).
```

```
Line 3 tells the machine to travel to grid point (X,Y) = (20,40).
```

Line 4 tells the machine to travel to grid point (X, Y) = (20, 0).

Line 5 returns the machine to origin (X, Y) = (0, 0).

Line 6 stops the machine.

#### 2.3 Classification of Five-Axis Machines

A typical five-axis machine has three translational axes and two rotary axes. The five degrees of freedom is the minimum needed for establishing an arbitrary position and orientation of the cutting tool relative to the workpiece [1].

Five-axis machines can be classified into four groups based on the number of translational and rotary axes: (i) three translational axes and two rotary axes; (ii) two translational axes and three rotary axes; (iii) one translational axes and four rotary axes and (iv) five rotary axes. However, the majority of existing five-axis machine tools falls in the first group and all methods presented in this book are developed for this type of five-axis machines.

The machine axes can be assigned to the tool and to the machine tables using a variety of combinations. The kinematics chain diagram of the machine gives an idea of how this assignment has been done. For example, the kinematics chain diagram in Fig. 2.3 corresponds to the five-axis machine in Fig. 2.1a. The diagram tells us that the table (actually, the table is composed of two smaller connected tables) is carried by four axes including the both rotary axes and the tool is carried by only one axis.

Another useful classification of five-axis machines is based on the number of table and tool carrying axes. Finally, the machines can be also classified by the location of the rotary axes (on the tool or the table).

The above classifications of the five-axis machines are given below:

# Classification of five-axis machines based on the number of workpiece and tool carrying axes

1. 5/0 machine. All axes carry the table and the tool is fixed in space. Since the tool is fixed, it is best used when the size of the workpiece is small.

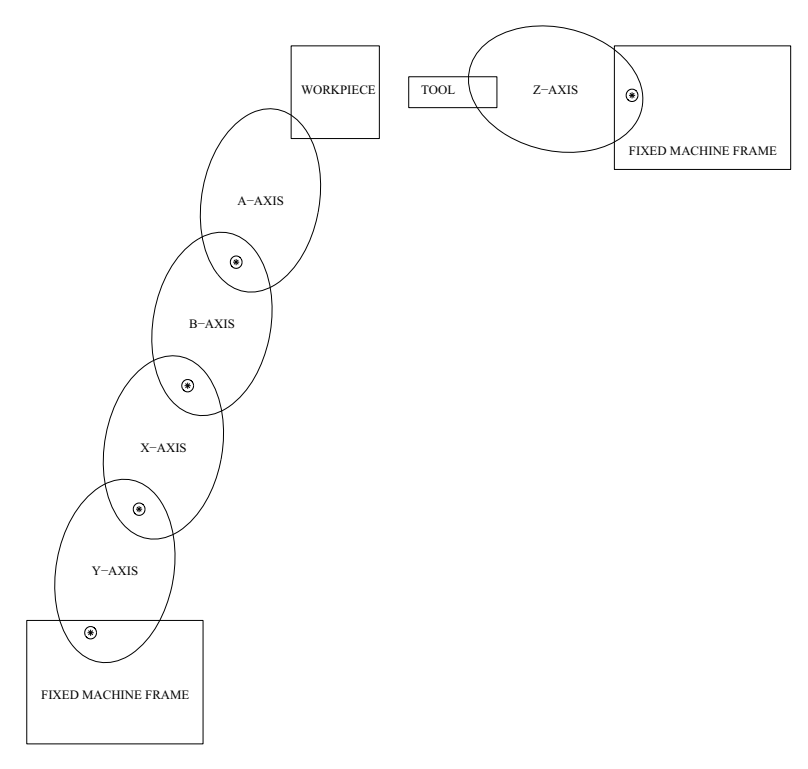


Fig. 2.3. Kinematic chain diagram of machine in Fig. 2.1a

- 2. 4/1 machine. There are four table carrying axes and one tool carrying axis (Fig. 2.4).
- 3. 3/2 machine. There are three table carrying axes and two tool carrying axes (Fig. 2.5).
- 4. 2/3 machine. There are two table carrying axes and three tool carrying axes (Fig. 2.6). This configuration allows machining of large workpieces.
- 5. 1/4 machine. There are one table carrying axis and four tool carrying axes.
- 6. 0/5 machine. All axes carry the tool and the table is fixed in space. The configuration was designed to handle very heavy workpieces. However, a large number of links in the tool carrying kinematics chain could result in a considerable error due to elastic deformations in the axis slides.

# Classification of five-axis machines based on the location of the two rotary axes

- 1. 2-0 machine. The two rotary axes carry the table (Fig. 2.4).
- 2. 1-1 machine. One rotary axis carries the table and one carries the tool (Fig. 2.5).

3. 0-2 machine. The two rotary axes carry the tool (Fig. 2.6).

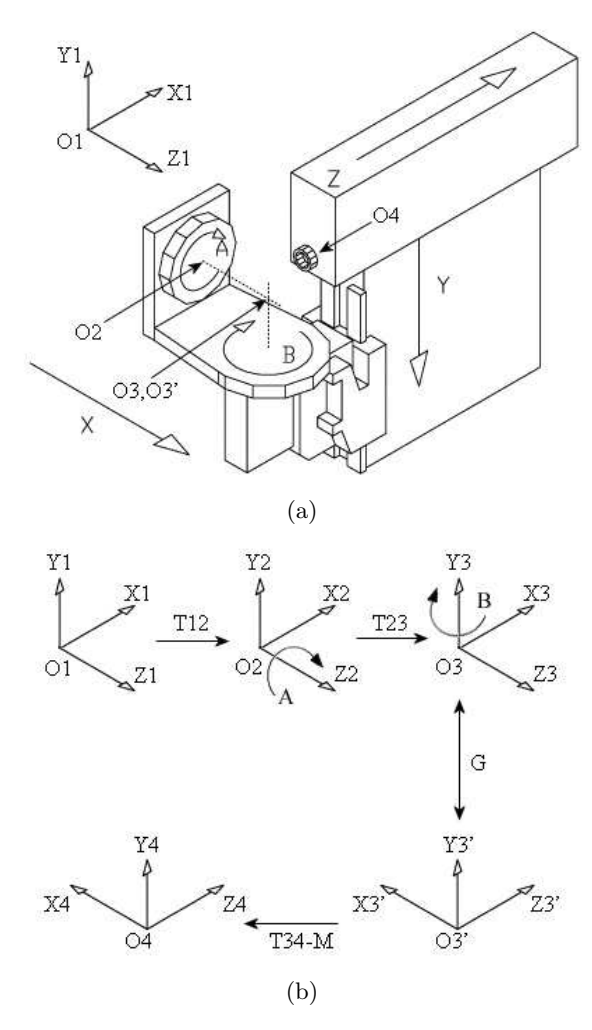


Fig. 2.4. (a) example of 2-0 machine and (b) the reference coordinate systems

Selection of a five-axis machine for a certain application is not an easy task. It can be done by analyzing characteristics of the workpiece such as the weight and the size. For example, a very heavy workpiece requires a machine with a horizontal table which makes it more convenient to fix and to handle the workpiece. Also, the machine should have a short workpiece kinematics chain since a heavy workpiece could result in an elastic deformations in the axis slides that carry the table [1]. The suitability of the machine can be also

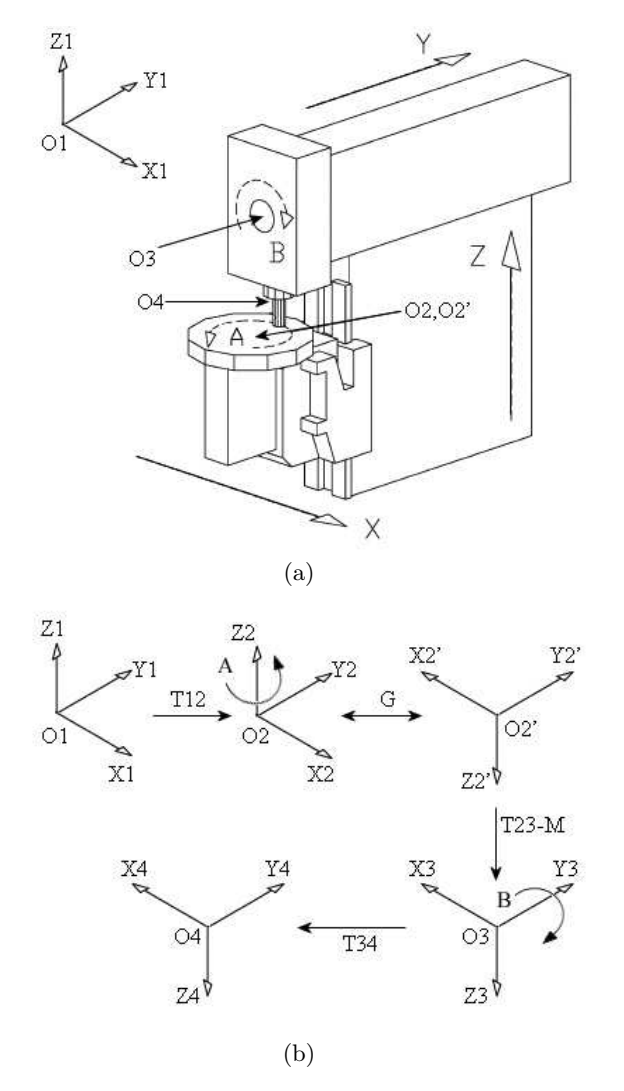


Fig. 2.5. (a) example of 1-1 machine and (b) the reference coordinate systems

analyzed in the framework of the kinematics error theory. The theoretical background for such analysis is given in Chap. 7 of this book.

# 2.4 Five-Axis Machine Kinematics

Five-axis machines offer five degrees of freedom which allow the cutting tool to incline or to tilt with regard to the workpiece while traveling from one point to another. Consequently, the tool tip affected by the machine kinematics travels

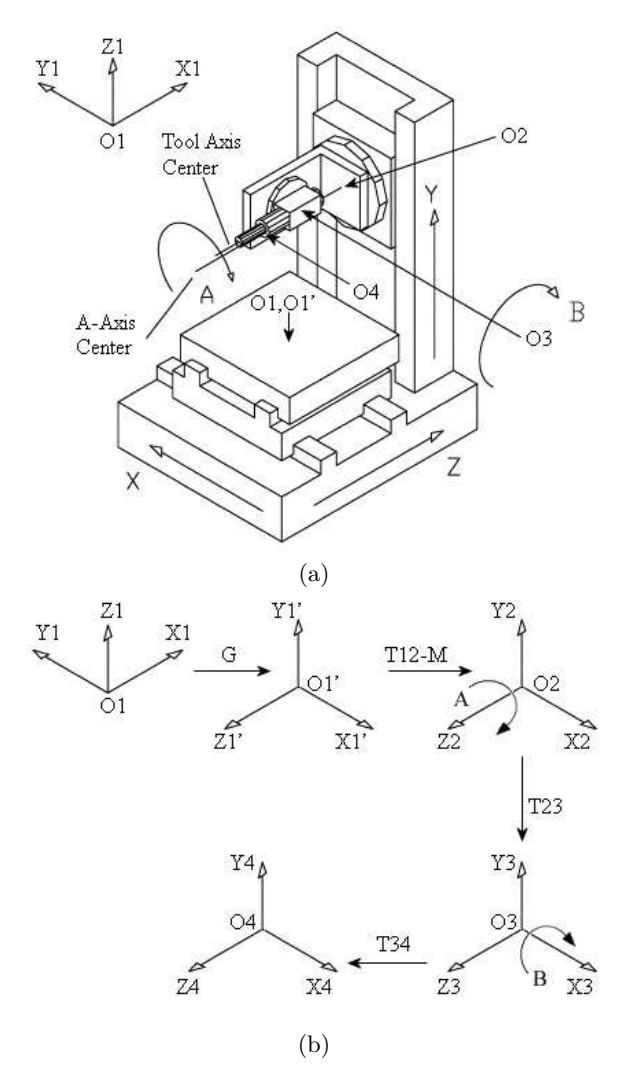


Fig. 2.6. (a) example of 0-2 machine and (b) the reference coordinate systems

in the workpiece coordinate system along a nonlinear trajectory. While this nonlinearity of the machine tools allows for complex surface parts to be milled it can also result in undercuts or overcuts or even in collisions between the cutting device and other parts of the machine.

The generation of NC part program that specifies the traveling path of the cutting device usually starts with the distribution of CC points on the surface. In five-axis machining, each CC point is also associated with a tool vector positioned in a right-handed, rectangular coordinate system. CC points are then converted into CL points which specify the coordinates of the tool tip in

the workpiece coordinate systems. Finally, the CL points are transformed into the machine coordinates (or G-Codes) to control the motions of the machine and finally into the NC program.

The conversion from a CC point to a CL point depends on the tool geometry and inclination (see an example given in Chap. 3). The transformation of the CL points from the workpiece coordinate system to the machine coordinate system for a particular five-axis machine requires information regarding the kinematics of that machine.

The kinematics  $\mathfrak{K} \equiv \mathfrak{K}(\mathfrak{R}, M)$  of a machine is a transformation from a point  $M = (x_m, y_m, z_m)$  in the machine coordinates to a point  $W = (x_w, y_w, x_w)$  in the workpiece coordinates where  $\mathfrak{R} = (a, b)$  is a pair of rotation angles. For simplicity, the transformation will be denoted  $\mathfrak{K}(M)$  when possible. Also, let  $I = (I_x, I_y, I_z)$  denote the tool vector orientation specified in the workpiece coordinate system.

To derive an equation of the machine kinematics, the following coordinate systems are introduced: the workpiece coordinate system  $O_1$ , the coordinate system of the first rotary part  $O_2$ , the coordinate system of the second rotary part  $O_3$ , and the coordinate system of the spindle  $O_4$  (see Figs. 2.4-2.6). The first rotary axis is called the A-axis, whereas the second rotary axis is called the B-axis. When an NC machine is powered up, the machine's measuring system is initialized by traveling the tool of the machine to the reference point in the machine coordinate system so that the machine control knows the absolute position of each slide.

Consider a five-axis machine displayed in Fig. 2.1a. The machine is of the 2-0 type. The two rotary axes A and B carry the table. The motions of the machine slides from reference position in machine coordinate system are as follows (the onlooker standing in front of the machine looking in the positive Z machine direction):

- $x_m$  plus: the table moves to the right
- $y_m$  plus: the table moves downwards
- $z_m$  plus: the tool moves away from the viewer
- a plus: the table carrying workpiece rotates clockwise around the A-axis
- b plus: the table swings from right to left around the B-axis

The positive direction of each Cartesian axis slide is selected such that the cutting device appears to move away from the workpiece in the positive direction of the corresponding axis in the spindle coordinate system  $O_4$  (see Fig. 2.4). In other words, the positive direction of an axis slide that carries the table is in the opposite direction of the positive direction of the corresponding axis in  $O_4$  and the positive direction of an axis slide that carries the tool is in the same direction of the positive direction of the corresponding axis in  $O_4$ . For example, the slides X and Y of the 2-0 machine in Fig. 2.4 which carry the table have positive directions that are in opposite direction of positive  $X_4$  and  $Y_4$ , respectively, while slide Z which carries the tool has positive direction that is in the same direction of positive  $Z_4$ .

The transformation from the workpiece to the machine coordinates consists of three types of transformations: coordinate transformation to another reference system without motions and transformation corresponding to actual machine rotations, and actual translations. The 2-0 machine (Fig. 2.4) kinematics equations are derived as follows:

Step 1: Coordinate transformation  $O_1 \rightarrow O_2$ 

Point W in  $O_1$  is transformed into point  $P_2$  in  $O_2$ .

$$P_2 = W + T_{12},$$

where  $T_{12}$  is the coordinate of the center of  $O_1$  in  $O_2$ .

Step 2: Rotation around A-axis in  $O_2$  by a

Point  $P_2$  is rotated around A-axis in  $O_2$  by a to a new location  $P_{2A}$ .

$$P_{2A} = A[a]P_2 = A[a](W + T_{12}),$$

where  $A[a] = \begin{bmatrix} \cos a & \sin a & 0 \\ -\sin a & \cos a & 0 \\ 0 & 0 & 1 \end{bmatrix}$  is the rotation matrix around A-axis.

Step 3: Coordinate transformation  $O_2 \rightarrow O_3$ 

Point  $P_{2A}$  in  $O_2$  is transformed into point  $P_3$  in  $O_3$ .

$$P_3 = P_{2A} + T_{23} = A[a](W + T_{12}) + T_{23},$$

where  $T_{23}$  is the coordinate of the center of  $O_2$  in  $O_3$ .

Step 4: Rotation around B-axis in  $O_3$  by b

Point  $P_3$  is rotated around B-axis in  $O_3$  by b to a new location  $P_{3B}$ .

$$P_{3B} = B[b]P_3 = B[b](A[a](W + T_{12}) + T_{23}),$$

$$P_{3B} = B[b]P_3 = B[b](A[a](W + T_{12}) + T_{23}),$$
where  $B[b] = \begin{bmatrix} \cos b & 0 - \sin b \\ 0 & 1 & 0 \\ \sin b & 0 & \cos b \end{bmatrix}$  is the rotation matrix around  $B$ -axis.

Step 5: Coordinate rotation (axis alignment)  $O_3 \rightarrow O_3'$ 

We now perform axis alignment for  $O_3$  (the last reference coordinate system on the table) to  $O_4$  (the first reference coordinate system on the tool).

$$P_3' = GP_{3B} = GB[b](A[a](W + T_{12}) + T_{23}),$$

where 
$$G = \begin{bmatrix} 0 & 0 & -1 \\ 0 & 1 & 0 \\ 1 & 0 & 0 \end{bmatrix}$$
 is the axis alignment matrix.

Point  $P'_3$  is now given in the coordinate system  $O'_3$  where each direction of the three Cartesian coordinate axes lies in the same direction of the corresponding Cartesian coordinate axis of  $O_4$ 

Step 6: Coordinate transformation  $O'_3 \to O_4$  with machine slide translation

Point  $P_3'$  in  $O_3'$  is transformed to point  $P_4$  in  $O_4$ . Recall that the workpiece attached to the table will appear to move away from the spindle in the negative directions in  $O_4$  for positive value of machine slide translation M. Thus for machines slide translation M, the center of  $O_3'$  will be at location  $T_{34} - M$  in  $O_4$  where  $T_{34}$  is the coordinate of  $O'_3$  in  $O_4$  with respect to the machine zero point M = (0,0,0). Finally, the transformation of the point  $P'_3$  in  $O'_3$  to point  $P_4$  in  $O_4$  is given as follows:

$$P_4 = P_3' + T_{34} - M = GB[b](A[a](W + T_{12}) + T_{23}) + T_{34} - M.$$

Let  $T_4 = (0, 0, -L)$  denote the coordinate of the tool tip in coordinate system  $O_4$  where L is the tool lenght. Equating  $P_4$  and  $T_4$  yields

$$T_4 = P_4 = GB[b] (A[a] (W + T_{12}) + T_{23}) + T_{34} - M.$$
 (2.1)

After rearrangement,

$$M = GB[b] (A[a] (W + T_{12}) + T_{23}) + T_{34} - T_4,$$
  

$$W = A^{-1}[a] (B^{-1}[b]G^{-1} (M - T_{34} + T_4) - T_{23}) - T_{12},$$
(2.2)

The equation relating the two rotation angles a and b and the tool vector orientation  $I = (I_x, I_y, I_z)$  can be derived as follows. Let  $T'_1$  be the coordinate of  $T'_4 = (0, 0, -L + 1)$  in  $O_1$  and is given by

$$T_1' = A^{-1}[a] \left( B^{-1}[b]G^{-1} \left( M - T_{34} + T_4' \right) - T_{23} \right) - T_{12}. \tag{2.3}$$

The unit vector  $T'_4 - T_4 = (0, 0, 1)$  is equivalent to the tool vector orientation and is expressed in  $O_1$  coordinate system as follows:

$$I = T_1' - W = A^{-1}[a]B^{-1}[b]G^{-1}(T_4' - T_4) = \begin{bmatrix} \cos(a)\cos(b)\\ \sin(a)\cos(b)\\ -\sin(b) \end{bmatrix}.$$
 (2.4)

Inverting with regard to a and b yields

$$a = \begin{cases} \tan^{-1} \left( \frac{I_y}{I_x} \right) & \text{if } I_x > 0 \text{ and } I_y \ge 0, \\ \tan^{-1} \left( \frac{I_y}{I_x} \right) + \pi & \text{if } I_x < 0, \\ \tan^{-1} \left( \frac{I_y}{I_x} \right) + 2\pi \text{ otherwise,} \end{cases}$$

$$b = -\sin I.$$
(2.5)

Derivations of machine kinematics equations for arbitrary configurations of five-axis machines can be done in a similar fashion. For the 1-1 machine shown in Fig. 2.5, the coordinate of the tool tip in  $O_4$  is given by

$$T_4 = B[b] (GA[a] (W + T_{12}) + T_{23} - M) + T_{34}.$$
 (2.6)

Clearly,

$$M = GA[a] (W + T_{12}) + T_{23} + B^{-1}[b] (T_{34} - T_4),$$

$$W = A^{-1}[a]G^{-1} (M - T_{23} - B^{-1}[b] (T_{34} - T_4)) - T_{12},$$

$$I = T'_1 - W = A^{-1}[a]G^{-1}B^{-1}[b] (T'_4 - T_4) = \begin{bmatrix} \cos(a)\sin(b) \\ -\sin(a)\sin(b) \\ \cos(b) \end{bmatrix},$$

$$Cos(b)$$

$$a = \begin{cases} -\tan^{-1} \left(\frac{I_y}{I_x}\right) & \text{if } I_x > 0 \text{ and } I_y \le 0, \\ -\tan^{-1} \left(\frac{I_y}{I_x}\right) + \pi & \text{if } I_x < 0, \\ -\tan^{-1} \left(\frac{I_y}{I_x}\right) + 2\pi & \text{otherwise,} \end{cases}$$

$$b = \cos^{-1} I_z.$$

$$(2.7)$$

where

$$A[a] = \begin{bmatrix} \cos a - \sin a & 0 \\ \sin a & \cos a & 0 \\ 0 & 0 & 1 \end{bmatrix},$$

$$B[b] = \begin{bmatrix} \cos b & 0 - \sin b \\ 0 & 1 & 0 \\ \sin b & 0 & \cos b \end{bmatrix},$$

$$G = \begin{bmatrix} -1 & 0 & 0 \\ 0 & 1 & 0 \\ 0 & 0 & -1 \end{bmatrix},$$

$$T_4 = (0, 0, L).$$

$$(2.8)$$

For the 0-2 machine shown in Fig. 2.6, the coordinate of the tool tip  $T_4$  in  $O_4$  is given by

$$T_4 = B[b] (A[a] (GW + T_{12} - M) + T_{23}) + T_{34}.$$
 (2.9)

Clearly,

$$M = GW + T_{12} + A^{-1}[a] \left( T_{23} + B^{-1}[b] \left( T_{34} - T_4 \right) \right),$$

$$W = G^{-1} \left( M - T_{12} - A^{-1}[a] \left( T_{23} + B^{-1}[b] \left( T_{34} - T_4 \right) \right) \right),$$

$$I = T_1' - W = G^{-1}A^{-1}[a]B^{-1}[b] \left( T_4' - T_4 \right) = \begin{bmatrix} \cos(b) \\ \sin(a)\sin(b) \\ -\cos(a)\sin(b) \end{bmatrix},$$

$$a = \begin{cases} -\tan^{-1} \left( \frac{I_y}{I_z} \right) & \text{if } I_y \le 0 \text{ and } I_z > 0, \\ -\tan^{-1} \left( \frac{I_y}{I_z} \right) + \pi & \text{if } I_z < 0, \\ -\tan^{-1} \left( \frac{I_y}{I_z} \right) + 2\pi & \text{otherwise,} \end{cases}$$

$$b = -\cos^{-1} I_x.$$

$$(2.10)$$

where

$$A[a] = \begin{bmatrix} \cos a - \sin a & 0 \\ \sin a & \cos a & 0 \\ 0 & 0 & 1 \end{bmatrix},$$

$$B[b] = \begin{bmatrix} 1 & 0 & 0 \\ 0 & \cos b - \sin b \\ 0 & \sin b & \cos b \end{bmatrix},$$

$$G = \begin{bmatrix} 0 & -1 & 0 \\ 0 & 0 & 1 \\ -1 & 0 & 0 \end{bmatrix},$$

$$T_4 = (0, 0, L).$$

$$(2.11)$$

# 2.5 Five-Axis Machining Example

Creating objects such as industrial molds and dies by five-axis machines requires a computer program that instructs the machine to move the cutting device through a block of a raw material in such a way that it removes all the excess material, leaving behind the desired shape. The path of the tool tip is called the tool path and the process of creating the tool path is called the tool path generation.

Consider a surface S(u, v) = (x(u, v), y(u, v), z(u, v)) described by a set of parametric equations given by

$$x = 100u - 50,$$
  

$$y = 100v - 50,$$
  

$$z = 10((u + 0.5)^{2} + v^{2}) - 50,$$
(2.12)

where  $0 \le u \le 1$  and  $0 \le v \le 1$ . The surface plot is shown in Fig. 2.7.

A simple way to generate the tool path for five-axis machining of this surface is the zigzag pattern shown in Fig. 2.2a. There are 10 tool tracks equally spaced in the v-direction. In turn, each track contains 10 CC points equally spaced in the u-direction Each CC point is associated with a tool vector aligned with the surface normal vector. The method of calculating the surface normal vector can be found in Sect. 3.1. The plot of the CC points along with the tool vector orientations is shown in Fig. 2.8. Since the tool vector orientation is aligned with the surface normal vector, the cutter contact point is assumed to coincide with the tool tip. Thus, the CL points are set to have the same location as the CC points.

Next, CL points are converted into the machine commands or the G-codes. For MAHO machine shown in Fig. 2.1a, (2.2) and (2.5) are used to compute the machine coordinates M and the two rotation angles, a and b. The machine parameters are given below:

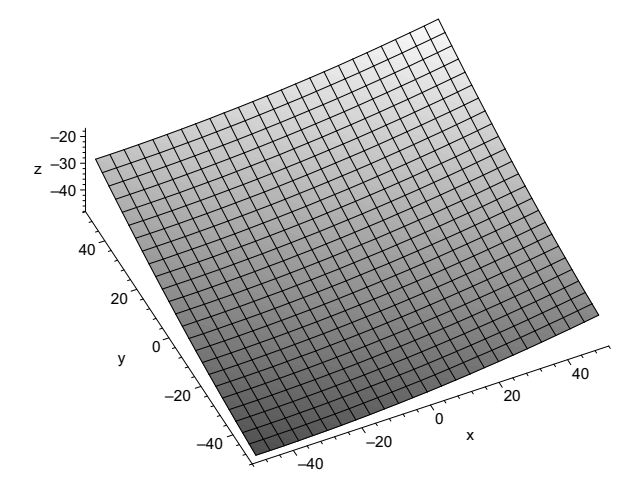


Fig. 2.7. Simple shape parametric surface

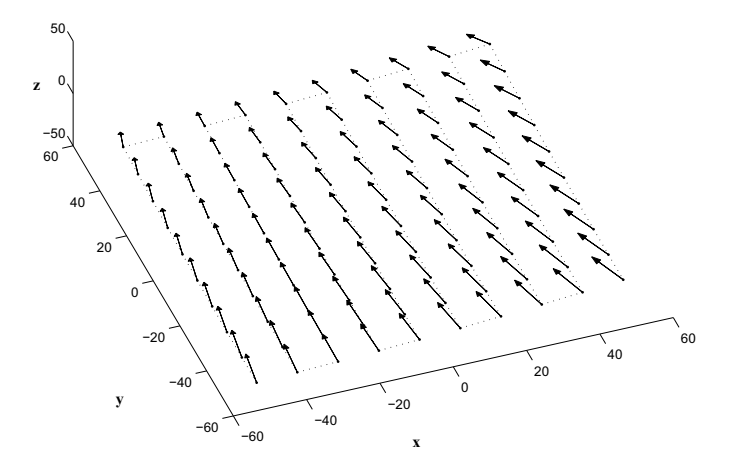


Fig. 2.8. Zigzag tool path for surface (2.12) (Fig. 2.7)

$$\begin{split} T_{12} &= (0.0, 0.0, 213.58), \\ T_{23} &= (0.08, 0.0, -250.314), \\ T_{34} &= (0.0, 0.0, -350.0), \\ L &= 177.651. \end{split}$$

The coordinates of the CL points in the workpiece and the machine coordinate systems are partially listed in Table 2.4. The G-codes are straightforwardly derived from the machine coordinates.  $x_m$ ,  $y_m$  and  $z_m$  are prefixed with the address words X, Y and Z, respectively. Likewise, the two rotation

angles are prefixed with the address words A and B. Each CL point constitutes one block of the G-code. The G-code begins with the word address N followed by the block number. The G-codes are given in Table 2.5.

Table 2.4. List of CL points for tool path in Fig. 2.8

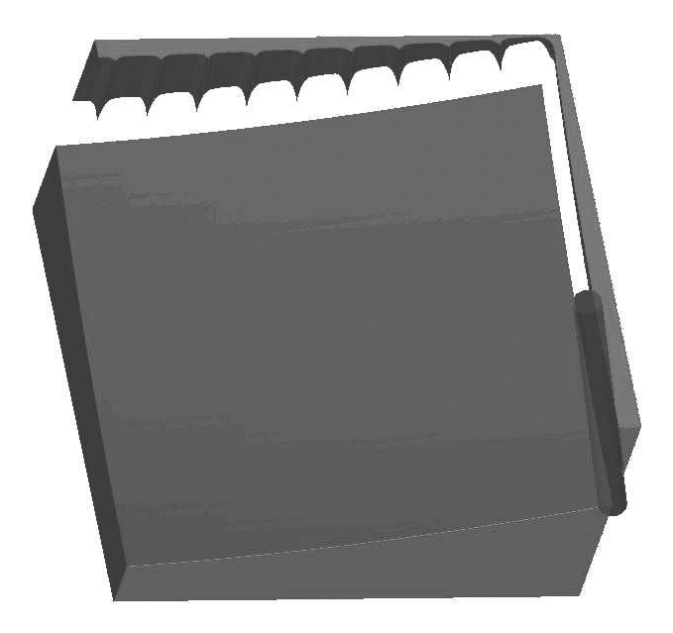
Point Number	$x_w$	$y_w$	$z_w$	$I_x$	$I_y$	$I_z$
1	-50.000	-50.000	-47.500	-0.100	0.000	0.995
2	-50.000	-38.889	-47.377	-0.099	-0.022	0.995
3	-50.000	-27.778	-47.006	-0.099	-0.044	0.994
4	-50.000	-16.667	-46.389	-0.099	-0.066	0.993
5	-50.000	-5.556	-45.525	-0.099	-0.088	0.991
6	-50.000	5.556	-44.414	-0.099	-0.110	0.989
7	-50.000	16.667	-43.056	-0.099	-0.132	0.986
8	-50.000	27.778	-41.451	-0.098	-0.153	0.983
9	-50.000	38.889	-39.599	-0.098	-0.174	0.980
10	-50.000	50.000	-37.500	-0.098	-0.195	0.976
11	-38.889	50.000	-36.265	-0.119	-0.195	0.974
12	-38.889	38.889	-38.364	-0.119	-0.174	0.978
13	-38.889	27.778	-40.216	-0.120	-0.153	0.981
14	-38.889	16.667	-41.821	-0.120	-0.131	0.984
15	-38.889	5.556	-43.179	-0.121	-0.110	0.987
16	-38.889	-5.556	-44.290	-0.121	-0.088	0.989
17	-38.889	-16.667	-45.154	-0.121	-0.066	0.990
18	-38.889	-27.778	-45.772	-0.121	-0.044	0.992
19	-38.889	-38.889	-46.142	-0.121	-0.022	0.992
20	-38.889	-50.000	-46.265	-0.121	0.000	0.993
		:				
91	50.000	50.000	-17.500	-0.282	-0.188	0.941
92	50.000		-19.599			
93	50.000	27.778	-21.451	-0.284	-0.147	0.947
94	50.000	16.667	-23.056	-0.285	-0.127	0.950
95	50.000	5.556	-24.414	-0.286	-0.106	0.952
96	50.000	-5.556	-25.525	-0.286	-0.085	0.954
97	50.000	-16.667	-26.389	-0.287	-0.064	0.956
98	50.000	-27.778	-27.006	-0.287	-0.043	0.957
99	50.000	-38.889	-27.377	-0.287	-0.021	0.958
100	50.000	-50.000	-27.500	-0.287	0.000	0.958

Figure 2.9 shows the result of cutting surface (2.12) (Fig. 2.7) using the  $10\times10$  tool path. The simulation is done with Unigraphics 18. Clearly, the tool path contains insufficient number of CL points and left a great amount of an excess material.

Figure 2.10 displays the result of cutting using a  $20\times20$  zigzag tool path. The tool now removes most of the excess material and produces a reasonable model of the desired surface.



**Fig. 2.9.** Cutting simulation of surface (2.12) (Fig. 2.7) with  $10 \times 10$  tool path



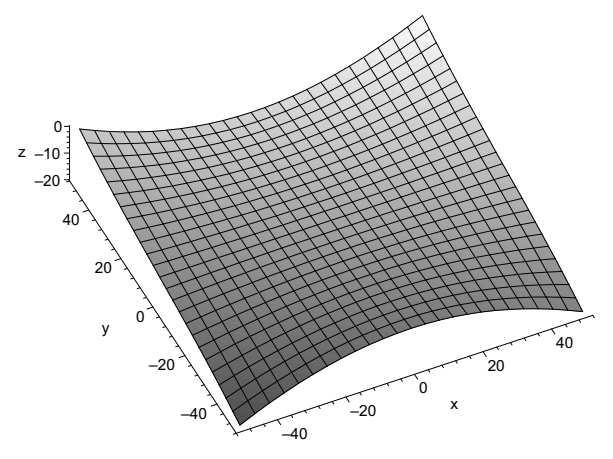
**Fig. 2.10.** Cutting simulation of surface (2.12) (Fig. 2.7) with  $20 \times 20$  tool path

Table 2.5. G-codes for tool path in Fig. 2.8

Point Number	G-Code							
1	N10	G01	X58.213	Y50.000	Z-251.183	A180.000	B-84.289 F100	
2	N11	G01	X65.599	Y27.116	Z-250.181	A192.529	B-84.151 F100	
3	N12	G01	X65.823	Y5.077	Z-249.387	A203.962	B-83.755 F100	
4	N13	G01	X60.483	Y-13.868	Z-248.802	A213.690	B-83.147 F100	
5	N14	G01	X51.687	Y-29.066	Z-248.426	A221.634	B-82.379 F100	
6	N15	G01	X41.073	Y-40.881	Z-248.259	A228.013	B-81.498 F100	
7	N16	G01	X29.636	Y-50.000	Z-248.301	A233.130	B-80.538 F100	
8	N17	G01	X17.907	Y-57.080	Z-248.549	A237.265	B-79.523 F100	
9	N18	G01	X6.142	Y-62.644	Z-249.002	A240.642	B-78.471 F100	
10	N19	G01	X-5.544	Y-67.082	Z-249.657	A243.435	B-77.396 F100	
11	N20	G01	X-5.058	Y-59.256	Z-248.513	A238.570	B-76.809 F100	
12	N21	G01	X6.126	Y-54.078	Z-247.854	A235.491	B-77.826 F100	
13	N22	G01	X17.155	Y-47.741	Z-247.398	A231.843	B-78.810 F100	
14	N23	G01	X27.830	Y-39.929	Z-247.146	A227.490	B-79.747 F100	
15	N24	G01	X37.806	Y-30.270	Z-247.101	A222.274	B-80.621 F100	
16	N25	G01	X46.515	Y-18.380	Z-247.264	A216.027	B-81.406 F100	
17	N26	G01	X53.090	Y-3.990	Z-247.637	A208.610	B-82.074 F100	
18	N27	G01	X56.376	Y12.815	Z-248.219	A199.983	$B\text{-}82.590~\mathrm{F}100$	
19	N28	G01	X55.170	Y31.305	Z-249.010	A190.305	B-82.919 F100	
20	N29	G01	X48.751	Y50.000	Z-250.009	A180.000	B-83.032 F100	
				:				
91	N100	G01	X-46.756	Y-13.868	Z-246.860	A213.690	B-70.173 F100	
92	N101	G01	X-40.711	Y-7.966	Z-246.207	A210.651	B-70.775 F100	
93	N102	G01	X-35.461	Y-1.644	Z-245.751	A207.408	B-71.328 F100	
94	N103	G01	X-31.117	Y5.077	Z-245.495	A203.962	B-71.825 F100	
95	N104	G01	X-27.787	Y12.156	Z-245.440	A200.323	B-72.260 F100	
96	N105	G01	X-25.578	Y19.531	Z-245.588	A196.504	B-72.626 F100	
97	N106	G01	X-24.580	Y27.116	Z-245.940	A192.529	B-72.917 F100	
98	N107	G01	X-24.860	Y34.805	Z-246.496	A188.427	B-73.129 F100	
99	N108	G01	X-26.453	Y42.476	Z-247.256	A184.236	$B\text{-}73.258~\mathrm{F}100$	
100	N109	G01	X-29.357	Y50.000	Z-248.219	A180.000	B-73.301 F100	

The above method for tool path generation works fine for simple surfaces. However, for complex surfaces such as the one shown in Fig. 2.11, the method could produce, overcuts, undercuts at the CC points as well as nonlinear trajectory loops between the points which could destroy the workpiece or even damage the machine itself (see Figs. 2.12 and 2.13).

Furthermore, for the concave surfaces, the cutting tool needs to be inclined to avoid curvature interference. Besides, the distance between the tool tracks is fixed. Therefore, if the distance is too large, the tool leaves behind ridges of unremoved material which called cusps or scallops. On the other hand, a too small distance results in a redundant path when the tool makes unnecessary cuts in the same areas between the tracks.



 ${\bf Fig.~2.11.~Bezier~surface}$ 

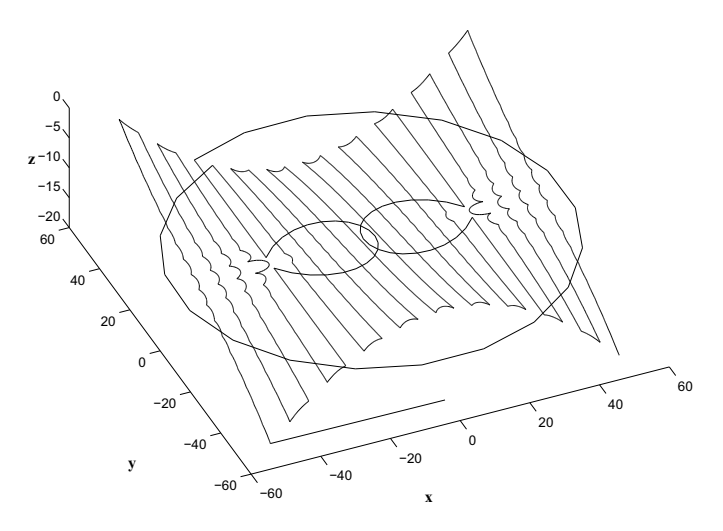


Fig. 2.12. Tool trajectories with loops of 20×20 tool path for surface in Fig. 2.11

#### References

- [1] Bohez, E. L. J. 2002. Five-axis milling machine tool kinematic chain design and analysis. *International Journal of Machine Tools and Manufacture*, 42(4):505–520.
- [2] Choi, B. K., Park, J. W., and Jun, C. S. 1993. Cutter-location data optimization in 5-axis surface machining. Computer-Aided Design, 25(6):377–386.
- [3] Farouki, R. T., Manjunathaiah, J., Nicholas, D., Yuan, G.-F., and Jee, S. 1998. Variable-feedrate CNC interpolators for constant material re-



Fig. 2.13. Cutting simulation of surface in Fig. 2.11 with 20×20 tool path

moval rates along Pythagorean-hodograph curves.  $Computer-Aided\ Design,$  30(8):631–640.

- [4] Farouki, R. T., Manjunathaiah, J., and Yuan, G.-F. 1999. G codes for the specification of Pythagorean-hodograph tool paths and associated feedrate functions on open-architecture CNC machines. *International Journal of Machine Tools and Manufacture*, 39(1):123–142.
- [5] Farouki, R. T. and Shah, S. 1996. Real-time CNC interpolators for Pythagorean-hodograph curves. Computer Aided Geometric Design, 13(7):583– 600.
- [6] Lin, R.-S. 2000. Real-time surface interpolator for 3-D parametric surface machining on 3-axis machine tools. *International Journal of Machine Tools* and Manufacture, 40(10):1513–1526.
- [7] Ross, D. T. 1978. Origins of the APT language for automatically programmed tools. In *HOPL-1: The first ACM SIGPLAN conference on History of programming languages*, pages 61–99.

## Fundamental Issues in Tool Path Planning

There are a number of issues involved in tool path planning for five-axis NC machining. Four fundamental issues are discussed in this chapter, namely, surface representation, machining strip width estimation, optimal tool orientation and forward step (kinematics) error.

#### 3.1 Surface Representation

Five-axis NC machines are widely used to machine dies, molds, turbine blades, aerospace and automotive parts, etc. These parts usually have complex geometry and are represented by parametric surfaces. Representation of surface by parametric equations allows the simple evaluation of differential properties of the surface. Many tool path generation techniques require calculation of certain surface properties such as the surface normal vector and the normal curvature. The close-form formula for commonly used surface properties are given below.

Let  $S \equiv S(u, v)$  be the required parametric surface, the *unit normal vector*,  $\mathbf{n}$ , is computed from the relation

$$\mathbf{n} = \frac{S_u \times S_v}{|S_u \times S_v|}.\tag{3.1}$$

The first fundamental form (or line element),  $\mathbf{I}$ , is defined by

$$\mathbf{I} = dS \cdot dS, 
= (S_u du + S_v dv) \cdot (S_u du + S_v dv), 
= S_u \cdot S_u du^2 + 2S_u \cdot S_v du dv + S_v \cdot S_v dv^2, 
= E du^2 + 2F du dv + G dv^2,$$
(3.2)

where

$$E = S_u \cdot S_u, \tag{3.3}$$

$$F = S_u \cdot S_v, \tag{3.4}$$

$$G = S_v \cdot S_v. \tag{3.5}$$

The second fundamental form, II, is defined by

$$\mathbf{II} = -d\mathbf{n} \cdot dS, 
= -(\mathbf{n}_{u}du + \mathbf{n}_{v}dv) \cdot (S_{u}du + S_{v}dv), 
= -\mathbf{n}_{u} \cdot S_{u}du^{2} - (\mathbf{n}_{u} \cdot S_{v} + \mathbf{n}_{v} \cdot S_{u})dudv - \mathbf{n}_{v} \cdot S_{v}dv^{2}, 
= \mathbf{n} \cdot S_{uu}du^{2} + (\mathbf{n} \cdot S_{vu} + \mathbf{n} \cdot S_{uv})dudv + \mathbf{n} \cdot S_{vv}dv^{2}, 
= \mathbf{n} \cdot S_{uu}du^{2} + 2\mathbf{n} \cdot S_{uv}dudv + \mathbf{n} \cdot S_{vv}dv^{2}, 
= edu^{2} + 2fdudv + qdv^{2},$$
(3.6)

where

$$e = \mathbf{n} \cdot S_{uu},\tag{3.7}$$

$$f = \mathbf{n} \cdot S_{uv},\tag{3.8}$$

$$g = \mathbf{n} \cdot S_{vv}. \tag{3.9}$$

The normal curvature of S in the direction  $\mathbf{v} = aS_u + bS_v$ , is given by

$$k(\mathbf{v}) = \frac{ea^2 + 2fab + gb^2}{Ea^2 + 2Fab + Gb^2}.$$
 (3.10)

The *principal curvatures*, which are the maximum and minimum of the normal curvature, are given by

$$k_{\text{max}} = H + \sqrt{H^2 - K},$$
 (3.11)

$$k_{\min} = H - \sqrt{H^2 - K},$$
 (3.12)

where K and H are the Gaussian curvature and the mean curvature, respectively. They are given by

$$K = \frac{eg - f^2}{EG - F^2} = k_{\min}k_{\max},$$
(3.13)

$$H = \frac{eG - 2fF + gE}{2(EG - F^2)} = \frac{1}{2}(k_{\min} + k_{\max}).$$
 (3.14)

The direction  $\mathbf{v} = aS_u + bS_v$  associated with a principal curvature, k, is computed using the relations

$$(e - kE)a + (f - kF)b = 0, (3.15)$$

$$(f - kF)a + (g - kG)b = 0. (3.16)$$

The surface points are classified into six different types, depending on the values of K and H as follows.

- Concave elliptic point If K > 0 and H > 0, the surface lies entirely on the surface normal side (**n**) of the tangent plane in its neighborhood. Both the principal curvatures are positive.
- Convex elliptic point If K > 0 and H < 0, the surface lies entirely on the opposite side  $(-\mathbf{n})$  of the tangent plane in its neighborhood. Both the principal curvatures are negative.
- Hyperbolic point If K < 0, the surface lies entirely on both sides of the tangent plane in its neighborhood. The principal curvatures have different signs.
- Concave parabolic point If K = 0 and H > 0, the surface lies entirely on the surface normal side (**n**) of the tangent plane in its neighborhood. One of the principal curvatures is positive and one is zero.
- Convex parabolic point If K = 0 and H < 0, the surface lies entirely on the opposite side  $(-\mathbf{n})$  of the tangent plane in its neighborhood. One of the principal curvatures is negative and one is zero.
- Planar umbilic point If K = 0 and H = 0, the surface lies entirely in the tangent plane in the neighborhood of the umbilic point.

#### 3.2 Machining Strip Width Estimation

In five-axis NC machining, several types of cutters can be used to mill the surface. The bottom of the cutter may be flat or rounded, as shown in Fig. 3.1. A ball-end cutter has rounded bottom where the filleted portion is the same size as the cutter radius. A rounded tool with a slight corner radius is called a toroidal cutter. A flat-end cutter has flat bottom. It can be used to remove the material much more effectively than the ball-end cutter but is more difficult to position relative to a sculptured surface. No matter which type of the milling tools is used, only a few shapes of surface can be cut exactly. This is because the shape of the tool almost never matches the shape of the surface. Irregular scallops between finishing tool passes are inevitably generated on the machined surface. The term scallop refers to ridges, cusps and other surface protrusions left between adjacent overlapping tool passes that extend above the design surface profile. In five-axis NC machining, controlling scallop height is a significant factor since a small scallop height significantly reduces the manual surface grinding and smoothing. Given the maximum scallop height h, the next adjacent tool path offset is found by computing the machining strip width at the current cutter contact point. Calculation of the machining strip width for various type of machining tools can be found in the literature (see, for instance, [2, 11, 12]). A simple but efficient algorithm for estimating the machining strip width of a flat-end cutter is presented here.

#### Machining strip width estimation for flat-end cutter

Let us first introduce a local coordinate system  $(O_l, \mathbf{x}_l, \mathbf{y}_l, \mathbf{z}_l)$  at the cutter contact point  $O_l$  as shown in Fig. 3.2.  $\mathbf{x}_l$  denotes the normalized projection of

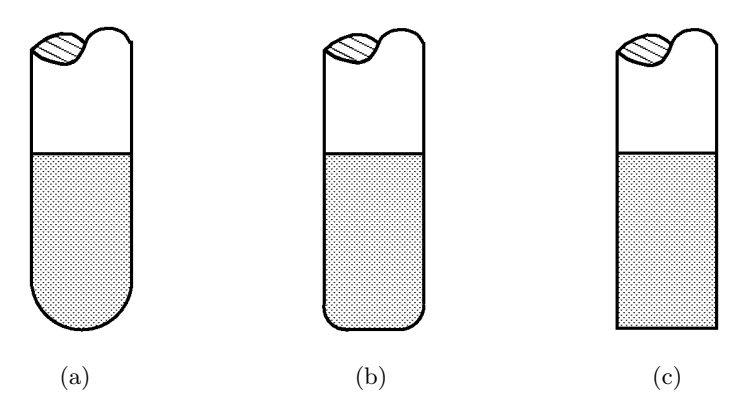


**Fig. 3.1.** Examples of cutting tools: (a) a ball-end cutter, (b) a toroidal cutter, (c) a flat-end cutter

the tool cutting direction<sup>1</sup> onto the tangent plane,  $\mathbf{z}_l$  denotes the unit normal vector of the surface, and  $\mathbf{y}_l = \mathbf{z}_l \times \mathbf{x}_l$ . In order to avoid gouging, the tool is first rotated by an inclination angle  $\lambda$  about the  $\mathbf{y}_l$  axis vector, then by a tilt angle  $\omega$  about the  $\mathbf{z}_l$  axis vector. The projected bottom edge of a flat-end cutter with radius r onto the  $\mathbf{y}_l$ - $\mathbf{z}_l$  plane becomes an ellipse, which is called the effective cutting shape.

A point P on the bottom edge of a flat-end cutter with radius r is represented in the cutter coordinate system  $(O_c, \mathbf{x}_c, \mathbf{y}_c, \mathbf{z}_c)$  by (see Fig. 3.2)

$$P_c = \begin{bmatrix} r \sin \theta \\ -r \sin \theta \\ 0 \end{bmatrix}, \tag{3.17}$$

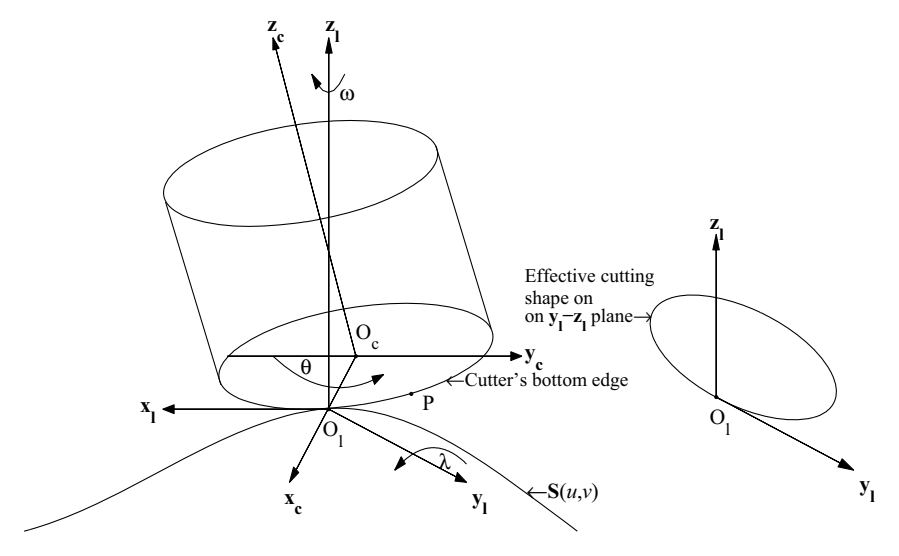
where  $\theta$  denotes the angle from the negative  $\mathbf{y}_c$  axis vector to the point P on the cutter's bottom edge (see Fig. 3.2).

For the flat-end tool, the center of the cutter coordinate system,  $\mathcal{O}_c$ , is the coordinate of the cutter location point. Calculation of the CL point from CC data for flat-end cutter is straightforward. Initially, the CL point is represented in the local coordinate system as

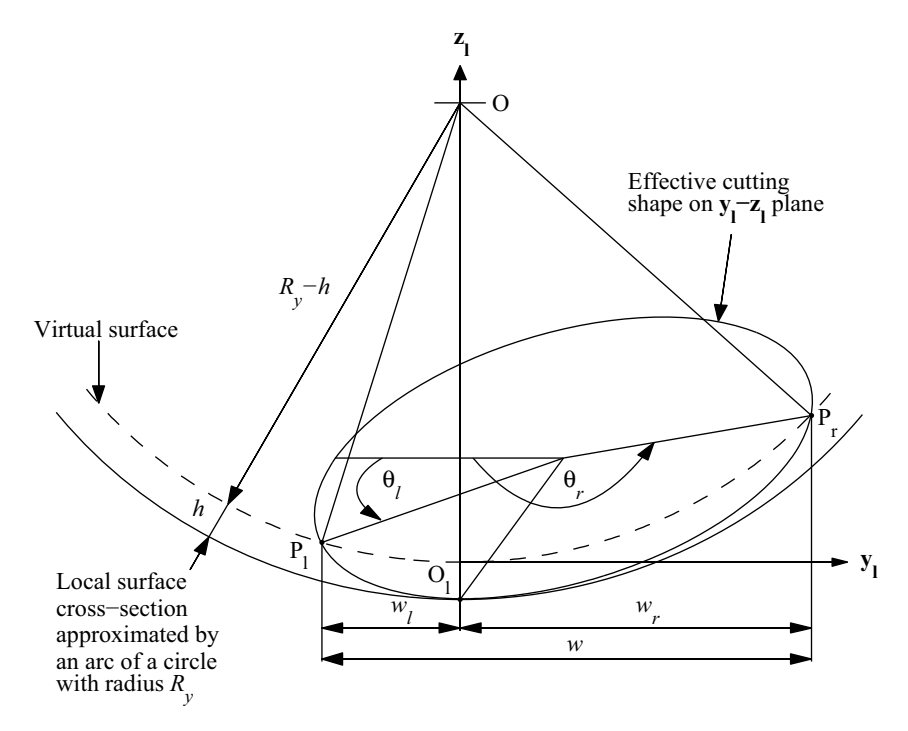
$$CL = \begin{bmatrix} -r \\ 0 \\ 0 \end{bmatrix}. \tag{3.18}$$

Then the tool is inclined by  $\lambda$  around the  $\mathbf{y}_l$ -axis. The CL point is now expressed as

<sup>&</sup>lt;sup>1</sup> The tool cutting direction is the direction from the current CC point to the next CC point.



 ${\bf Fig.~3.2.}$  Geometric analysis of the cutting operations



 ${\bf Fig.~3.3.}$  Machining strip width estimation

$$CL = \begin{bmatrix} \cos \lambda & 0 \sin \lambda \\ 0 & 1 & 0 \\ -\sin \lambda & 0 \cos \lambda \end{bmatrix} \begin{bmatrix} -r \\ 0 \\ 0 \end{bmatrix} = \begin{bmatrix} -r \cos \lambda \\ 0 \\ r \sin \lambda \end{bmatrix}. \tag{3.19}$$

Finally, tilting the tool by  $\omega$  around  $\mathbf{z}_l$  yields

$$CL = \begin{bmatrix} \cos \omega & \sin \omega & 0 \\ -\sin \omega & \cos \omega & 0 \\ 0 & 0 & 1 \end{bmatrix} \begin{bmatrix} -r\cos \lambda \\ 0 \\ r\sin \lambda \end{bmatrix} = \begin{bmatrix} -r\cos \lambda \cos \omega \\ r\cos \lambda \sin \omega \\ r\sin \lambda \end{bmatrix}.$$
(3.20)

CL point is then expressed in workpiece coordinate system as

$$CL = CC + (-r\cos\lambda\cos\omega)\mathbf{x}_l + (r\cos\lambda\sin\omega)\mathbf{y}_l + (r\sin\lambda)\mathbf{z}_l.$$
 (3.21)

Similarly, point P on the bottom edge of a flat-end cutter is represented in the local coordinate system  $(O_l, \mathbf{x}_l, \mathbf{y}_l, \mathbf{z}_l)$  by

$$P = \begin{bmatrix} x_{l} \\ y_{l} \\ z_{l} \end{bmatrix}$$

$$= \begin{bmatrix} \cos \omega & \sin \omega & 0 \\ -\sin \omega & \cos \omega & 0 \\ 0 & 0 & 1 \end{bmatrix} \begin{bmatrix} \cos \lambda & 0 \sin \lambda \\ 0 & 1 & 0 \\ -\sin \lambda & 0 \cos \lambda \end{bmatrix} (O_{c} + P_{c}),$$

$$= \begin{bmatrix} \cos \omega & \sin \omega & 0 \\ -\sin \omega & \cos \omega & 0 \\ 0 & 0 & 1 \end{bmatrix} \begin{bmatrix} \cos \lambda & 0 \sin \lambda \\ 0 & 1 & 0 \\ -\sin \lambda & 0 \cos \lambda \end{bmatrix} (\begin{bmatrix} -r \\ 0 \\ 0 \end{bmatrix} + \begin{bmatrix} r \sin \theta \\ -r \sin \theta \\ 0 \end{bmatrix}),$$

$$= \begin{bmatrix} -r(\cos \lambda \cos \omega (1 - \sin \theta) + \sin \omega \cos \theta) \\ r(\cos \lambda \sin \omega (1 - \sin \theta) - \cos \omega \cos \theta) \end{bmatrix}.$$

$$(3.22)$$

To evaluate the machining strip width, the surface cross-section perpendicular to the tool cutting direction  $\mathbf{x}_l$  is approximated by a circular arc, for which the radius  $R_y$  is equal to the radius of normal curvature<sup>2</sup> of the surface in the  $\mathbf{y}_l$  direction as shown in Fig. 3.3. Given the maximum scallop height h, the maximum machined surface error is represented by a virtual circular arc of radius  $R_y - h$  concentric with the first circular arc as shown in Fig. 3.3. The machining strip width is then obtained by locating the intersections of the effective cutting shape with this virtual circular arc.

The equation of the effective cutting shape is found by projecting (3.22) onto the  $\mathbf{y}_l$ - $\mathbf{z}_l$  plane, i.e., by setting  $x_l$  component of point P to zero. The equation of the virtual circular arc with radius  $R_y - h$  as shown in Fig. 3.3 is given by

$$y_l^2 + (z_l - R_y)^2 = (R_y - h)^2.$$
 (3.23)

<sup>&</sup>lt;sup>2</sup> The radius of normal curvature is positive for concave surface and negative for convex surface.

Substituting (3.22) into (3.23) yields

$$c_1 \sin^2 \theta + c_2 \sin \theta + c_3 \sin 2\theta - 2c_3 \cos \theta + c_4 = 0, \tag{3.24}$$

where

$$c_1 = r^2(\cos^2\lambda\sin^2\omega + \sin^2\lambda - \cos^2\omega),$$
 
$$c_2 = -2r^2(\cos^2\lambda\sin^2\omega + \sin^2\lambda) + 2rR_y\sin\lambda,$$
 
$$c_3 = \frac{r^2\cos\lambda\sin2\omega}{2},$$
 
$$c_4 = r^2\sin^2\lambda\cos^2\omega - 2rR_y\sin\lambda + r^2 + 2hR_y - h^2.$$

The values of  $\theta_l$  and  $\theta_r$  corresponding to the left and right intersection points  $P_l$  and  $P_r$  (see Fig. 3.3) are found by solving (3.24).

When  $\omega = 0$ , (3.24) has a closed form solution given by

$$\theta_{l} = \sin^{-1} \left( \frac{-c_{2} - \sqrt{c_{2}^{2} - 4c_{1}c_{4}}}{2c_{1}} \right), \ 0 \le \theta_{l} \le \frac{\pi}{2},$$

$$\theta_{r} = \pi - \theta_{l}.$$
(3.25)

We are interested in the solutions  $\theta_l$  and  $\theta_r$  close to the CC point, i.e., the intersection points on the lower edge of an ellipse. When the inclination angle  $\lambda$  is small or the maximum scallop height h is large, (3.24) and (3.25) might exhibit no solutions or the intersection points lie on the upper edge of an ellipse. In such case,  $\theta_l$  and  $\theta_r$  are set to  $\theta_{P_l}$  and  $\theta_{P_r}$  corresponding to the left-most point and the right-most point on the effective cutting shape, respectively. The left-most and right-most points on the effective cutting shape are found by solving  $dy_l(\theta)/d\theta = 0$ . Differentiating  $y_l$  in (3.22) yields

$$r\cos\lambda\sin\omega\cos\theta - r\cos\omega\sin\theta = 0. \tag{3.26}$$

Therefore,

$$\theta_{P_l} = \tan^{-1}(\cos \lambda \tan \omega),$$
  

$$\theta_{P_r} = \tan^{-1}(\cos \lambda \tan \omega) + \pi.$$
(3.27)

The left and the right machining strip widths  $w_l$  and  $w_r$  at the current CC point  $\mathcal{O}_l$  are then expressed as

$$w_l = |r(\cos \omega \cos \theta_l - \cos \lambda \sin \omega (1 - \sin \theta_l))|,$$
  

$$w_r = |r(\cos \omega \cos \theta_r - \cos \lambda \sin \omega (1 - \sin \theta_r))|.$$
(3.28)

The entire machining strip width is then defined by

$$w = w_l + w_r. (3.29)$$

The machining strip width estimation method presented above is similar to the method used by Lee and Ji [11] but with two modifications. First, the local surface cross-section at the CC point is approximated by a circular arc instead of the quadratic equation (see Fig. 3.4(a)) for consistency with the subsequent calculation for optimal tool orientation and gouging avoidance presented in Sect. 3.3. Second, by approximating the surface cross-section by circular arc, the offset curve corresponding to the maximum allowable machined surface error h, can be easily computed by using a virtual circular arc of radius R-h as shown in Fig. 3.3. In contrast, the machined surface error or scallop height, h, is underestimated when using the method of Lee and Ji where the offset curve is computed by shifting the approximated local surface cross-section in the normal direction  $\mathbf{z}_l$  by h as shown in Fig. 3.4(a). The difference  $\Delta h = h - \hat{h}$  is, however, negligible for small values of h (see Fig. 3.4(b)).

#### Machining strip width estimation for ball-end cutter

The calculation of the machining strip width of a ball-end cutter can be considered as a special case of the method presented above when  $\lambda = \pi/2$  and  $\omega = 0$ . In this case (3.24) becomes

$$(-2r^2 + 2rR_y)\sin\theta + (2r^2 - 2rR_y) + 2hR_y - h^2 = 0, (3.30)$$

$$\sin \theta = 1 - \frac{2hR_y - h^2}{2rR_y - 2r^2}.$$
 (3.31)

Using the trigonometric identity  $\cos^2 \alpha + \sin^2 \alpha = 1$ , the machine strip width of (3.28) becomes

$$w_l = w_r = r\cos\theta,$$
  
=  $r\sqrt{1-\sin^2\theta}$ . (3.32)

The entire machining strip width is then given by

$$w = w_l + w_r = 2r\sqrt{\frac{2hR_y - h^2}{rR_y - r^2} - \left(\frac{2hR_y - h^2}{2rR_y - 2r^2}\right)^2}.$$
 (3.33)

Since in practice  $|R_y| \gg h$ , the terms consisting of  $h^2$ ,  $h^3$ , and  $h^4$  in (3.33) can be disregarded. The maching strip width is then approximated by

$$w = \sqrt{\frac{8hrR_y}{R_y - r}},\tag{3.34}$$

which is the same approximation presented in [12]. Equation (3.34) is also used in [13] to calculate the machining strip width for a flat-end tool where the tool radius r is replaced by the effective cutter radius  $r_e$  (see Sect. 3.3).

The machining strip width calculation of the toroidal cutter can be found in [2].

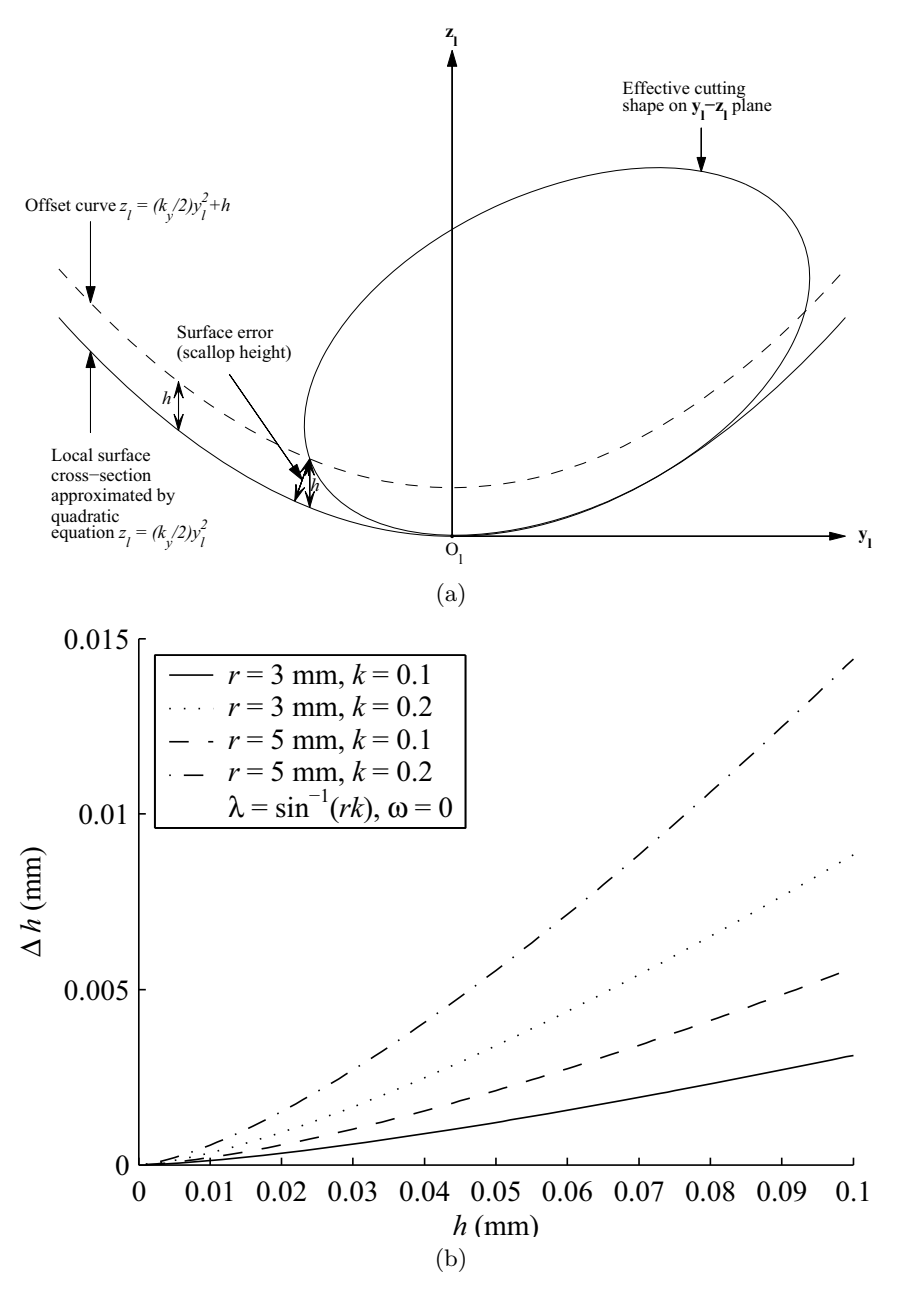


Fig. 3.4. (a) machining strip width estimation method of Lee and Ji, (b) plot of the difference between the maximum allowable error h, and the estimated machined surface error  $\hat{h}$ , with normal curvature k, tool radius r, and tool orientation  $(\lambda, \omega) = (\sin^{-1}(rk), 0)$ 

#### 3.3 Optimal Tool Orientation and Gouging Avoidance

In five-axis machining, the effective cutting shape is determined by the tool orientation  $(\lambda, \omega)$ . The effective cutter radius  $r_e$  of a flat-end cutter is given by [13]

$$r_e = ra^2 \left(\frac{1+b^2}{a^2+b^2}\right)^{3/2},$$
 (3.35)

where

 $a = \sin \lambda \cos \omega$ ,

 $b = \tan \lambda \sin \omega$ ,

which is simplified to

$$r_e = \frac{r\cos^2\omega}{\sin\lambda}. (3.36)$$

To optimize the machining strip width,  $\lambda$  and  $\omega$  are usually set so that  $r_e$  is best matched to the radius of curvature at the CC point. For convex or planar surfaces (see Sect. 3.1), the tool inclination angle  $\lambda$  is normally set to a small default angle or zero and the tilt angle  $\omega$  is set to zero. If the surface is non-convex, a non-zero tool inclination angle  $\lambda$  is needed to avoid gouging.

Lee and Ji [11] presents a simple and fast algorithm suitable for being incorporated into the tool path generation strategies. The algorithm finds a minimum inclination angle to eliminate overcutting in both the  $\mathbf{x}_l$ - $\mathbf{z}_l$  and  $\mathbf{y}_l$ - $\mathbf{z}_l$  planes, as follows:

$$\lambda_{\min} = \max(\lambda_x, \lambda_y),$$

$$\lambda_x = \sin^{-1}\left(\frac{r}{R_x}\right), \text{ if } (r \le R_x) \text{ and } (R_x > 0),$$

$$\lambda_y = \sin^{-1}\left(\frac{r}{R_y}\right), \text{ if } (r \le R_y) \text{ and } (R_y > 0),$$
(3.37)

where  $R_x$  and  $R_y$  are the radius of normal curvature in the  $\mathbf{x}_l$  and  $\mathbf{y}_l$  directions, respectively.

Unfortunately, the method is not applicable to the non-convex surfaces when  $R_x$  and  $R_y$  are both negative but the maximum principle curvature is positive. Clearly, in this case, the method outputs  $\lambda_{\min} = 0$ . This "bug" often leads to local gouging. Lo [13] solves this problem by continuously checking for gouging in all directions. Furthermore, a modification of these techniques is presented in this book.

Consider a flat-end cutter as shown in Fig. 3.2. Gouging occurs when any point on the circle touches or goes inside the surface. Let G be a gouging point, which is another point on the circle that touches the surface (as shown in Fig. 3.5(a)). The line connecting the two points,  $O_l$  and G, forms a chord on the circle and has an angle of  $\phi$  with respect to  $O_lO_c$  (see Fig. 3.5(a)). Let  $\lambda_{\phi}$  be the tool inclination angle that corresponds to a specific value of  $\phi$ 

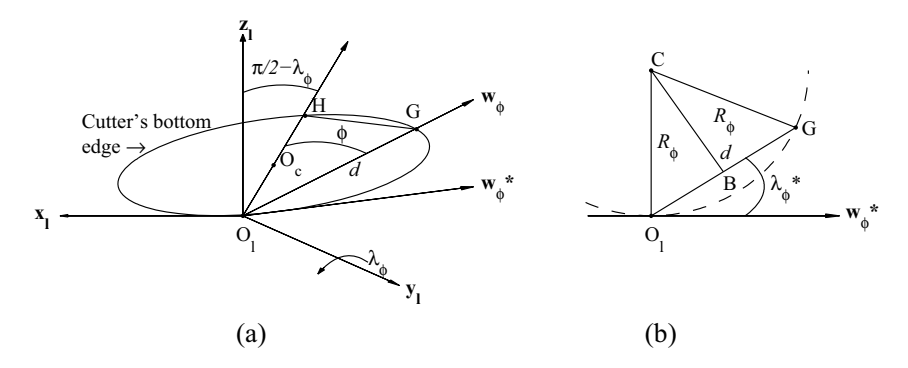


Fig. 3.5. Tool gouging

for a gouging point G, the minimum tool inclination angle to avoid gouging is formulated as the following optimization problem:

$$\lambda_{\min} = \max_{-\pi/2 \le \phi \le \pi/2} \lambda_{\phi}. \tag{3.38}$$

Lo [13] solved this problem numerically by utilizing the gradient method. However, it can be shown that the solution of (3.38) for a non-convex surface can be expressed in a closed-form formula.

Consider a gouging point G, the chord  $\overline{O_lG}$  has a length of d and an angle of  $\phi$  with respect to  $\overline{O_lO_c}$  (see Fig. 3.5(a)). Since  $O_lGH$  is a right-angled triangle having the angle  $O_lGH$  right, the length d can be calculated by

$$d = 2r\cos\phi. \tag{3.39}$$

Let  $\mathbf{w}_{\phi}$  be a unit vector in the direction of  $\overline{\mathbf{O}_{l}G}$  and  $\mathbf{w}_{\phi}^{*}$  be a unit vector tangent to the surface which is obtained by projecting  $\mathbf{w}_{\phi}$  onto the  $\mathbf{x}_{l}$ - $\mathbf{y}_{l}$  plane as shown in Fig. 3.5(a). Since  $\mathbf{O}_{l}$  and G are both located on the surface, they can be connected by a circular arc whose radius  $R_{\phi}$  is equal to the radius of curvature in the  $\mathbf{w}_{\phi}^{*}$  direction (see Fig. 3.5(b)). Let  $\lambda_{\phi}$  be the inclination angle of the tool that corresponds to a specific value of  $\phi$  for a gouging point G,  $\mathbf{w}_{\phi}$  can be obtained by rotating the unit vector [-1,0,0] by  $\phi$  around the  $\mathbf{z}_{l}$ -axis and then by  $\lambda_{\phi}$  around the  $\mathbf{y}_{l}$ -axis. Thus, we have

$$\mathbf{w}_{\phi} = \begin{bmatrix} \cos \lambda_{\phi} & 0 \sin \lambda_{\phi} \\ 0 & 1 & 0 \\ -\sin \lambda_{\phi} & 0 \cos \lambda_{\phi} \end{bmatrix} \begin{bmatrix} \cos \phi & \sin \phi & 0 \\ -\sin \phi & \cos \phi & 0 \\ 0 & 0 & 1 \end{bmatrix} \begin{bmatrix} -1 \\ 0 \\ 0 \end{bmatrix},$$

$$= \begin{bmatrix} -\cos \phi \cos \lambda_{\phi} \\ \sin \phi \\ \cos \phi \sin \lambda_{\phi} \end{bmatrix}. \tag{3.40}$$

 $\mathbf{w}_{\phi}^{*}$  is expressed as

$$\mathbf{w}_{\phi}^{*} = \begin{bmatrix} \frac{-\cos\phi\cos\lambda_{\phi}}{\sqrt{\cos^{2}\phi\cos^{2}\lambda_{\phi} + \sin^{2}\phi}} \\ \frac{\sin\phi}{\sqrt{\cos^{2}\phi\cos^{2}\lambda_{\phi} + \sin^{2}\phi}} \end{bmatrix}.$$
 (3.41)

Let  $\lambda_{\phi}^*$  be the angle by which  $\overline{O_lG}$  is inclined with respect to the  $\mathbf{x}_l$ - $\mathbf{y}_l$  plane as shown in Fig. 3.5(b). From (3.40) and (3.41), we have

$$\cos \lambda_{\phi}^* = \mathbf{w}_{\phi} \cdot \mathbf{w}_{\phi}^* = \sqrt{\cos^2 \phi \cos^2 \lambda_{\phi} + \sin^2 \phi}.$$
 (3.42)

Since  $\overline{\mathrm{CO}_l}$  is perpendicular to the  $\mathbf{x}_l$ - $\mathbf{y}_l$  plane and  $\mathrm{O}_l\mathrm{BC}$  is a right-angled triangle having the angle  $\mathrm{O}_l\mathrm{BC}$  right, the angle  $\mathrm{O}_l\mathrm{CB}$  is, therefore, equal to  $\lambda_{\phi}^*$ . The length of  $\overline{\mathrm{O}_lG}$  is then given by

$$d = 2R_{\phi} \sin \lambda_{\phi}^*,$$
  
=  $2R_{\phi} \sqrt{1 - \cos^2 \lambda_{\phi}^*},$  (3.43)

where the value of  $\sin \lambda_{\phi}^*$  is obtained using the trigonometric identity  $\sin^2 \alpha + \cos^2 \alpha = 1$ . Substituting (3.42) into (3.43) yields

$$d = 2R_{\phi}\sqrt{1 - \sin^2 \phi - \cos^2 \phi \cos^2 \lambda_{\phi}},$$

$$= 2R_{\phi}\sqrt{\cos^2 \phi - \cos^2 \phi \cos^2 \lambda_{\phi}},$$

$$= 2R_{\phi}\cos \phi \sqrt{1 - \cos^2 \lambda_{\phi}},$$

$$= 2R_{\phi}\cos \phi \sin \lambda_{\phi}.$$
(3.44)

Equating (3.39) to (3.44), we have

$$\lambda_{\phi} = \sin^{-1}(r/R_{\phi}) = \sin^{-1}(rk_{\phi}).$$
 (3.45)

The minimum inclination angle  $\lambda$  for gouging avoidance is then expressed as

$$\lambda_{\min} = \max_{-\pi/2 \le \phi \le \pi/2} \lambda_{\phi} = \max_{-\pi/2 \le \phi \le \pi/2} \sin^{-1}(rk_{\phi}) = \sin^{-1}(rk_{\max}), \quad (3.46)$$

where  $k_{\text{max}}$  is the maximum surface curvature at the CC point.

In the case when gouging can not be eliminated by inclining the tool alone or the inclination angle  $\lambda$  exceeds the limit of the machine, searching for the tilt angle  $\omega$  is needed or a smaller tool size must be used [7]. An algorithm for setting the tilt angle  $\omega$  can be found in [11].

Remark 3.1. The surface cross-section is approximated by a circular arc in the  $\mathbf{y}_{l}$ - $\mathbf{z}_{l}$  plane corresponding to an osculating circle having the radius  $R_{u}$ . The

osculating circle represents the best approximating curve having the constant curvature. The approach has been used in many practical applications (see, for instance, [12, 13]). However, the approximation is accurate only in the vicinity of the CC point. Therefore, the estimate of the machining strip is accurate when the machining strip itself is sufficiently small. The applicability of the approximation can be verified by comparing the approximating arcs with the actual curves on the surface in an appropriate norm. If the accuracy is insufficient then a high order approximation must be used.

Remark 3.2. The accuracy of the above model based on a single contact point may be insufficient. In this case multipoint strategies [20–22] could also be applied to further enhance the accuracy of the tool positioning.

#### 3.4 Kinematics Error

Besides controlling the size of the scallop left between two successive tool paths, the forward step (kinematics) error due to nonlinearity of the machine kinematics needs to be minimized as well. The kinematics error between two CC points is defined as the difference between the desired and the actual trajectory of the tool tip. The mathematical representation of the tool tip trajectory can be derived as follows:

Let  $\mathfrak{K}$  be the transformation such that  $\forall W, M, \mathfrak{R}, \mathfrak{K}^{-1}(\mathfrak{K}(\mathfrak{R}, M)) = M$  and  $\mathfrak{K}(\mathfrak{K}^{-1}(\mathfrak{R}, W)) = W$ . Let  $\Pi_p \equiv (M_p, \mathfrak{R}_p), \ \Pi_{p+1} \equiv (M_{p+1}, \mathfrak{R}_{p+1})$  be two successive coordinates of the tool path in  $\mathbb{R}^5$ .  $M_p$  and  $W_p$  denote spatial positions of the tool tip in machine and workpiece coordinate systems, respectively, and  $\mathfrak{R}_p$  the corresponding pair of rotation angles.

Let us invoke the inverse kinematics to transform workpiece coordinates  $W_p$  into machine coordinates  $M_p \equiv (x_p, y_p, z_p)$  as follows:  $M_p \equiv \mathfrak{K}^{-1}(\mathfrak{R}_p, W_p)$ . The rotation angles  $\mathfrak{R} \equiv \mathfrak{R}(t) = (a(t), b(t))$  and the machine coordinates of the tool tip  $M \equiv M(t)$  are assumed to change linearly between the prescribed points, namely,  $M(t) = tM_{p+1} + (1-t)M_p$ ,  $\mathfrak{R}(t) = t\mathfrak{R}_{p+1} + (1-t)\mathfrak{R}_p$ , where t is a fictitious time coordinate  $(0 \le t \le 1)$ . Transforming machine coordinates M back to workpiece coordinates W for every t yields

$$\begin{split} W_{p,p+1}(t) &= \mathfrak{K}(\mathfrak{R}(t), M(t)), \\ &= \mathfrak{K}(t\mathfrak{R}_{p+1} + (1-t)\mathfrak{R}_p, tM_{p+1} + (1-t)M_p). \end{split} \tag{3.47}$$

Now the machine coordinates  $M_p$  and  $M_{p+1}$  must be eliminated so that the resulting trajectory depends only on the workpiece coordinates and orientation of the tool.  $M_p$ ,  $M_{p+1}$  are eliminated by using the inverse transformation  $M_p = \mathfrak{K}^{-1}(\mathfrak{R}_p, W_p)$ . Substituting  $M_p$ ,  $M_{p+1}$  into (3.47) yields

$$\begin{split} W_{p,p+1}(t) &= \mathfrak{K}(\underline{t}\mathfrak{R}_{p+1} + (1-t)\mathfrak{R}_{\underline{p}}, \\ & t\mathfrak{K}^{-1}(\mathfrak{R}_{p+1}, W_{p+1}) + (1-t)\mathfrak{K}^{-1}(\mathfrak{R}_p, W_p)). \end{split} \tag{3.48}$$

Let  $W_{p,p+1}^D(t) \equiv (x_{p,p+1}^D(t), y_{p,p+1}^D(t), z_{p,p+1}^D(t)) \in S(u,v)$  be a curve between  $W_p$  and  $W_{p+1}$  extracted from the surface in such a way that it represents the desired tool trajectory. The kinematics error is represented as a maximum deviation between  $W_{p,p+1}^D(t)$  and  $W_{p,p+1}(t) \equiv (x_{p,p+1}(t), y_{p,p+1}(t), z_{p,p+1}(t))$  (see Fig. 3.6), namely,

$$\epsilon_{p,p+1} = \max_{0 \le t \le 1} |W_{p,p+1}^{D}(t) - W_{p,p+1}(t)|,$$

$$= \max_{0 \le t \le 1} \left[ \left( x_{p,p+1}^{D}(t) - x_{p,p+1}(t) \right)^{2} + \left( y_{p,p+1}^{D}(t) - y_{p,p+1}(t) \right)^{2} + \left( z_{p,p+1}^{D}(t) - z_{p,p+1}(t) \right)^{2} \right]^{\frac{1}{2}}.$$
(3.49)

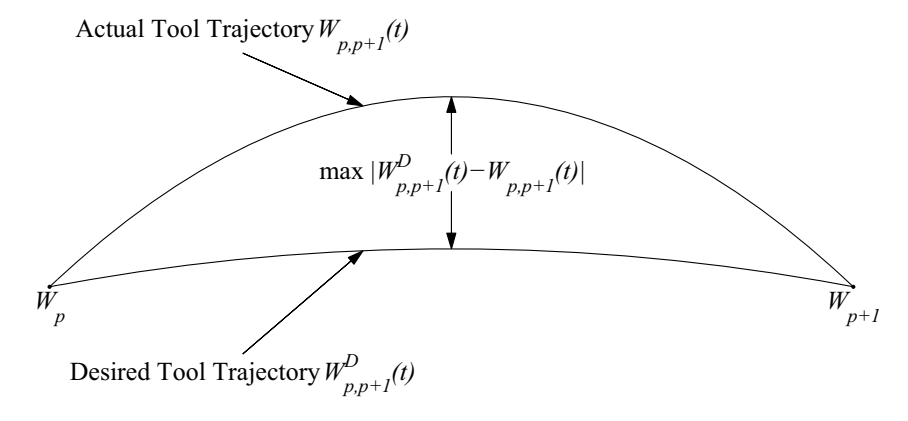


Fig. 3.6. Kinematics error between two cutter contact points  $W_p$  and  $W_{p+1}$ 

The kinematics error depends not only on the characteristics of the surface versus the tool orientation but on the previous rotations as well [15]. Consider the machine kinematics given in (2.2) and (2.5) for the 2-0 machine. If the size of angular jump of rotation angle a between any two points is larger than  $\pi$ , then the subsequence value of a should be adjusted in order to minimize the difference eliminating unexpected motion and collision due to sharp variations of the rotation angle a. As an example, angle adjustment for the 2-0 machine can be performed without effecting the desired tool orientation by using one of the following rules (see Fig. 3.7 and [15]).

(1) 
$$a_{\text{new}} = a_{\text{old}} \pm \pi,$$
  
 $b_{\text{new}} = -\pi - b_{\text{old}},$   
(2)  $a_{\text{new}} = a_{\text{old}} \pm 2\pi,$   
 $b_{\text{new}} = b_{\text{old}},$   
(3.50)

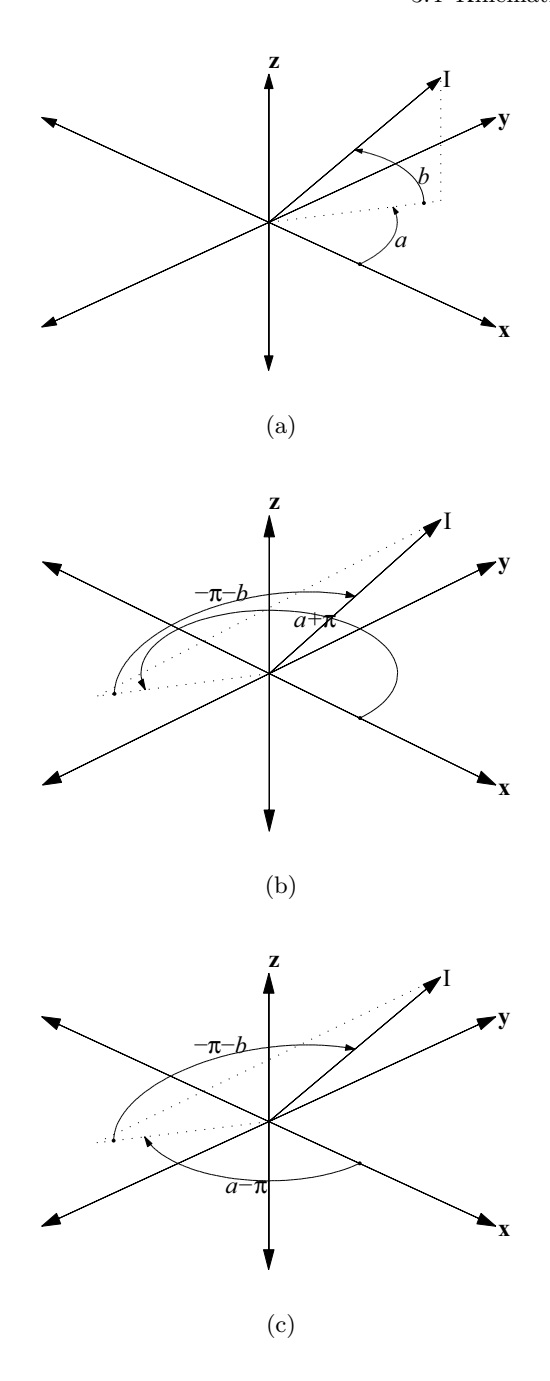


Fig. 3.7. Angle adjustment for the 2-0 machine

The above rules can be interpreted as follows. For the 2-0 machine, the tool orientation relative to the workpiece can be described by two angles, a and b. The tool which is initially aligned with the **x**-axis is first rotated around **y**-axis by b and then around **z**-axis by a (see Fig. 3.7(a)). The same tool orientation can also be achieved by first rotating the tool around **y**-axis by  $-\pi - b$  and then around **z**-axis by  $a + \pi$  (see Fig. 3.7(b)). Likewise, the same tool orientation can also be achieved by first rotating the tool around **y**-axis by  $-\pi - b$  and then around **z**-axis by  $a - \pi$  (see Fig. 3.7(c)).

Figure 3.8 demonstrates the minimization of kinematics error by the angle adjustment rules. Consider two CC points,  $W_1$  and  $W_2$ , and the associated tool orientations  $I_1$  and  $I_2$  given by

$$W_{1} = [-50.0, -50.0, -40.0],$$

$$I_{1} = [0, -0.625, 0.781],$$

$$W_{2} = [-50.0, 10.0, -20.8],$$

$$I_{2} = [0, 0.158, 0.987].$$
(3.51)

The machine rotation angles are calculated using (2.5).

$$(a_1, b_1) = (4.7122, -0.896),$$
  
 $(a_2, b_2) = (1.571, -1.412).$  (3.52)

The tool trajectory is shown in Fig. 3.8(a). To reduce the error,  $a_2$  and  $b_2$  are adjusted as follows:

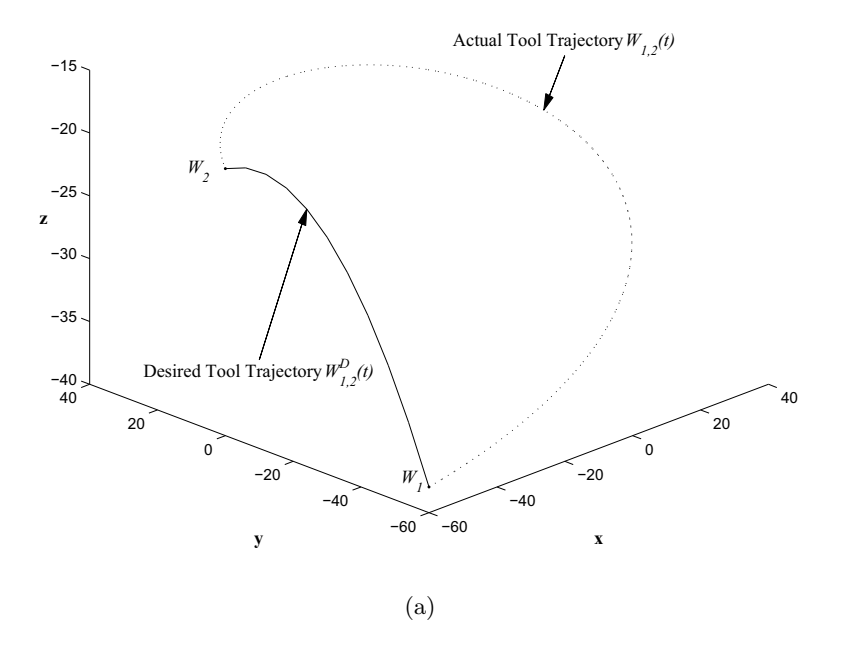
$$a_2^{\text{new}} = a_2 + \pi = 4.7126,$$
  
 $b_2^{\text{new}} = -\pi - b_2 = -1.7296.$  (3.53)

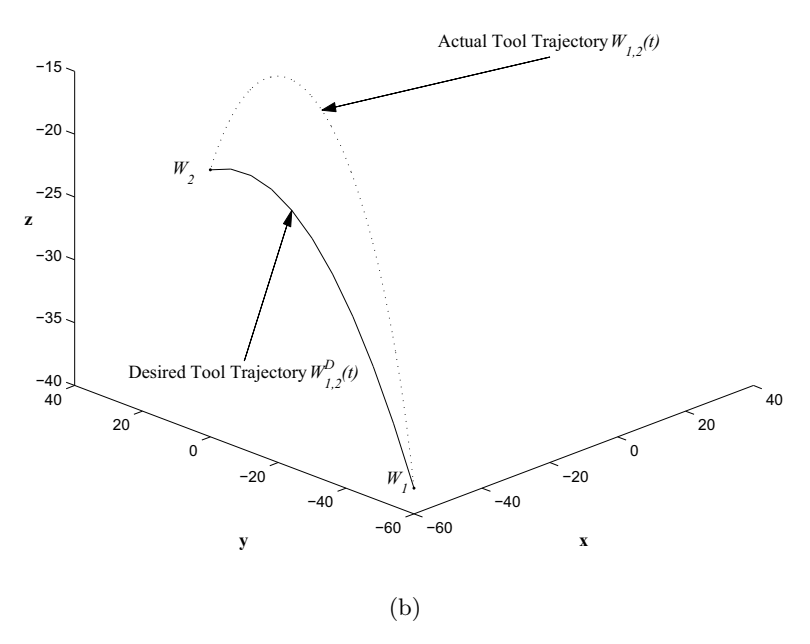
The tool trajectory after angle adjustment is shown in Fig. 3.8(b). Angle adjustment can be simultaneously applied to a set of successive points on the tool path (see Chap. 6). However, if the kinematics error between the two points still exceeds a prescribed tolerance, a new point is inserted between the two (see Chap. 6).

#### 3.5 Tool Path Generation

Sections 3.1 to 3.4 provide necessary information needed for tool path generation. There exists a large number of tool path generation techniques presented in the literature (see surveys by Dragomatz and Mann [3] and Sarma [17]). Tool path generation techniques can be classified into two main groups: isoparametric tool path (see, for examples, [1, 4, 19]) and non-isoparametric tool paths (see, for examples, [5, 6, 10, 12, 14]).

The isoparametric method is popular for tool path generation due to ease of computation. However, the machining efficiency and surface smoothness





 ${\bf Fig.~3.8.}$  Kinematics error reduction by angle adjustment

can be quite poor due to the redundant machining and an unpredictable scallop height, especially when the parametric increment is too small or large. Isoparametric tool paths are generated by calculating the smallest tool path interval and using it as a constant offset to the next tool path. The tool path interval depends on the local surface shape, cutter shape and size, and the allowable scallop height (see Sect. 3.2). Besides, the machining strip widths of the two adjacent cutter paths (Fig. 3.9) have to overlap to ensure that the machined surface error (scallop height) is within the tolerance. The incremental values  $\Delta u$  and  $\Delta v$  in the parametric domain corresponding to the machining strip width w can be found by solving the following equation.

$$\Delta u S_u + \Delta v S_v = w \mathbf{y}_l. \tag{3.54}$$

Example of isoparametric tool path is shown in Fig. 3.10.

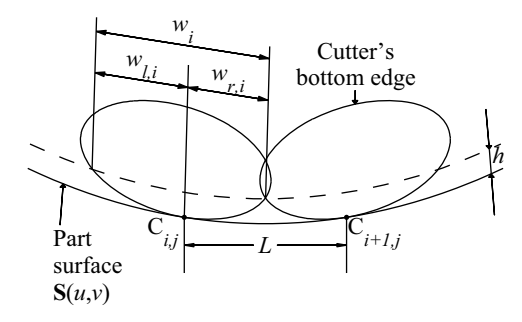


Fig. 3.9. Overlapping of machining strips on adjacent tool paths

Optimization of the tool path of a five-axis NC machine presents a considerable challenge. Recent papers have displayed a number of sophisticated methods to optimize the conventional isoparametric tool path. Besides, a variety of methods is available to generate unconventional patterns, for instance: the neural network approach [18], the Voronoi diagram technique [8], the monotone chain method [16], the distance map method [9], etc. The next two chapters present two techniques for tool path generation and optimization, namely, the adaptive space-filling curves and the grid generation method. Each technique can be used to optimize the conventional isoparametric tool path. Furthermore, when combining the two techniques together, an efficient tool path can be generated for surfaces with complicated boundaries, cuts off, pockets, islands, etc.

#### References

[1] Bobrow, J. E. 1985. NC machine tool path generation from CSG part representations. *Computer Aided Design*, 17(2):69–76.

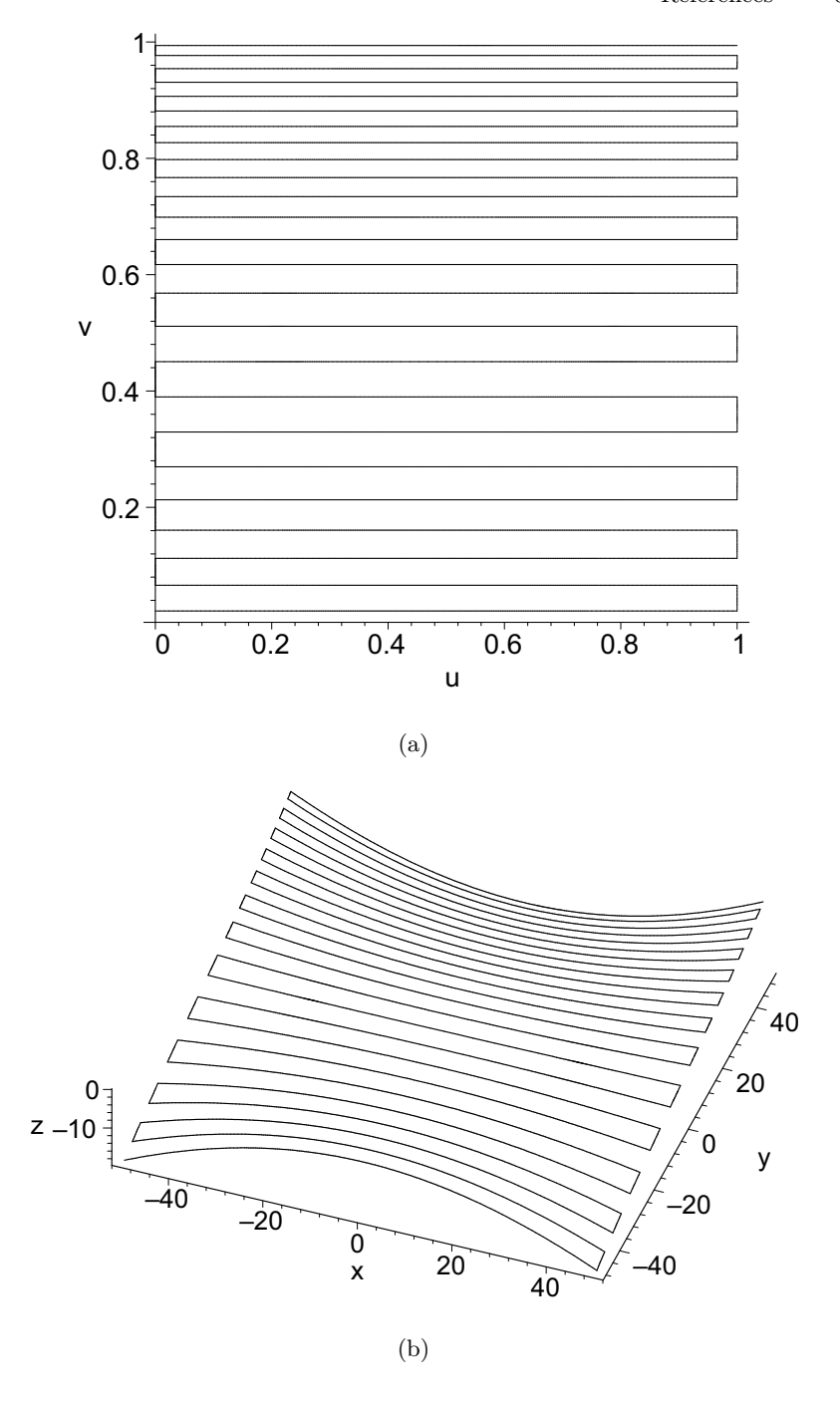


Fig. 3.10. Example of isoparametric tool path

- [2] Chiou, C.-J. and Lee, Y.-S. 2002. A machining potential field approach to tool path generation for multi-axis sculptured surface machining. *Computer-Aided Design*, 34(5):357–371.
- [3] Dragomatz, D. and Mann, S. 1997. A classified bibliography of literature on NC milling path generation. *Computer-Aided Design*, 29(3):239–247.
- [4] Elber, G. and Cohen, E. 1994. Toolpath generation for freeform surface models. *Computer-Aided Design*, 26(6):490–496.
- [5] Griffiths, J. G. 1994. Toolpath based on Hilbert's curve. Computer-Aided Design, 26(11):839–844.
- [6] Hatna, A. and Grieve, B. 2000. Cartesian machining versus parametric machining: a comparative study. *International Journal of Production Re*search, 38(13):3043–3065.
- [7] Jensen, C. G., Red, W. E., and Pi, J. 2002. Tool selection for five-axis curvature matched machining. *Computer-Aided Design*, 34(3):251–266.
- [8] Jeong, J. and Kim, K. 1999a. Generating tool paths for free-form pocket machining using z-buffer-based Voronoi diagrams. *International Journal of Advanced Manufacturing Technology*, 15(3):182–187.
- [9] Jeong, J. and Kim, K. 1999b. Generation of tool paths for machining free-form pockets with islands using distance maps. *International Journal of Advanced Manufacturing Technology*, 15(5):311–316.
- [10] Lee, Y.-S. 1998. Non-isoparametric tool path planning by machining strip evaluation for 5-axis sculptured surface machining. *Computer-Aided Design*, 30(7):559–570.
- [11] Lee, Y.-S. and Ji, H. 1997. Surface interrogation and machining strip evaluation for 5-axis CNC die and mold machining. *International Journal* of Production Research, 35(1):225–252.
- [12] Lin, R.-S. and Koren, Y. 1996. Efficient tool-path planning for machining free-form surfaces. ASME Journal of Engineering for Industry, 118(1):20– 28.
- [13] Lo, C. C. 1999. Efficient cutter-path planning for five-axis surface machining with a flat-end cutter. *Computer-Aided Design*, 31(9):557–566.
- [14] Makhanov, S. S., Batanov, D., Bohez, E., Sonthipaumpoon, K., Anotaipaiboon, W., and Tabucanon, M. 2002. On the tool-path optimization of a milling robot. *Computers & Industrial Engineering*, 43(3):455–472.
- [15] Munlin, M.-A., Makhanov, S. S., and Bohez, E. L. J. 2004. Optimization of rotations of a five-axis milling machine near stationary points. *Computer-Aided Design*, 36(12):1117–1128.
- [16] Park, S. C. and Choi, B. K. 2000. Tool-path planning for direction-parallel area milling. *Computer-Aided Design*, 32(1):17–25.
- [17] Sarma, R. 2000. An assessment of geometric methods in trajectory synthesis for shape-creating manufacturing operations. *Journal of Manufacturing Systems*, 19(1):59–72.
- [18] Suh, S. H. and Shin, Y. S. 1996. Neural network modeling for tool path planning of rough cut in complex pocket milling. *Journal of Manufacturing Systems*, 15(5):295–304.

- [19] Wang, Y. and Tang, X. 1999. Five-axis NC machining of sculptured surfaces. *International Journal of Advanced Manufacturing Technology*, 15(1):7–14.
- [20] Warkentin, A., Ismail, F., and Bedi, S. 1998. Intersection approach to multi-point machining of sculptured surfaces. Computer Aided Geometric Design, 15(6):567–584.
- [21] Warkentin, A., Ismail, F., and Bedi, S. 2000. Multi-point tool positioning strategy for 5-axis machining of sculptured surfaces. *Computer Aided Geometric Design*, 17(1):83–100.
- [22] Yoon, J.-H. 1997. Tool tip gouging avoidance and optimal tool positioning for 5-axis sculptured surface machining. *International Journal of Production Research*, 41(10):2125–2142.

### Space-Filling Curve Tool Paths

# 4.1 A Brief History of Space-Filling Curves and Their Applications

An N-dimensional space-filling curve (SFC) is a continuous, surjective (onto) function from the unit interval [0,1] to the N-dimensional unit hypercube  $[0,1]^N$ . In particular, a 2-dimensional space-filling curve is a continuous curve that passes through every point of the unit square  $[0,1]^2$ .

The history of space-filling curves started in 1878 when George Cantor (1845–1918) demonstrated that any two smooth manifolds of arbitrarily finite dimensions have the same cardinality. Cantor's finding implies that the unit line segment [0, 1] can be mapped bijectively<sup>2</sup> onto the unit square [0, 1]<sup>2</sup>. In 1879, Eugen Netto (1848–1919), however, demonstrated that such mapping is necessary discontinuous and cannot be called a curve. If the condition of bijectivity were dropped, Giuseppe Peano (1858–1932) found a continuous map from the interval onto the square in 1890. This was the first example of a space-filling curve (see Fig. 4.1). Furthers examples were introduced by D. Hilbert (in 1891, see Fig. 4.2), E.H. Moore (in 1900), H. Lebesgue (in 1904), W. Sierpiński (in 1912), G. Pólya (in 1913), etc [23].

SFCs are encountered in different fields of computer science, especially where it is important to linearize multidimensional data. Examples of multidimensional data are matrices, images, tables and computational grids resulting from the discretization of partial differential equations (PDEs). Typical applications of SFCs are data indexing [14, 20], data storing and retrieving [25], image processing [26, 28], image scanning and coding [5, 7, 27], mesh partitioning and reordering [24], etc.

<sup>&</sup>lt;sup>1</sup> A function f from a domain X to a codomain Y is said to be surjective if its values span its whole codomain; that is, for every y in Y, there is at least one x in X such that f(x) = y.

<sup>&</sup>lt;sup>2</sup> A function f from a domain X to a codomain Y is said to be bijective if for every y in Y there is exactly one x in X such that f(x) = y.

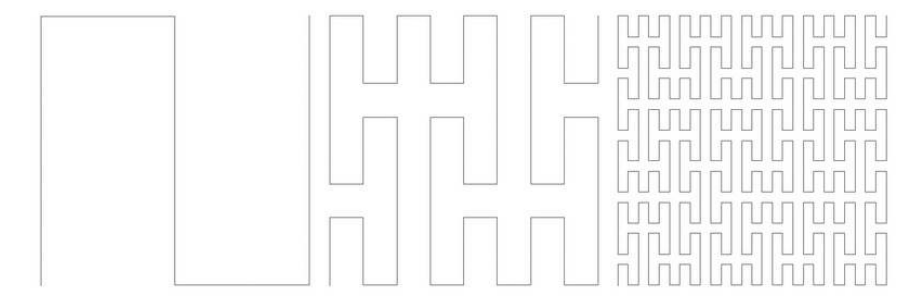


Fig. 4.1. 3 iterations of the Peano's space-filling curve

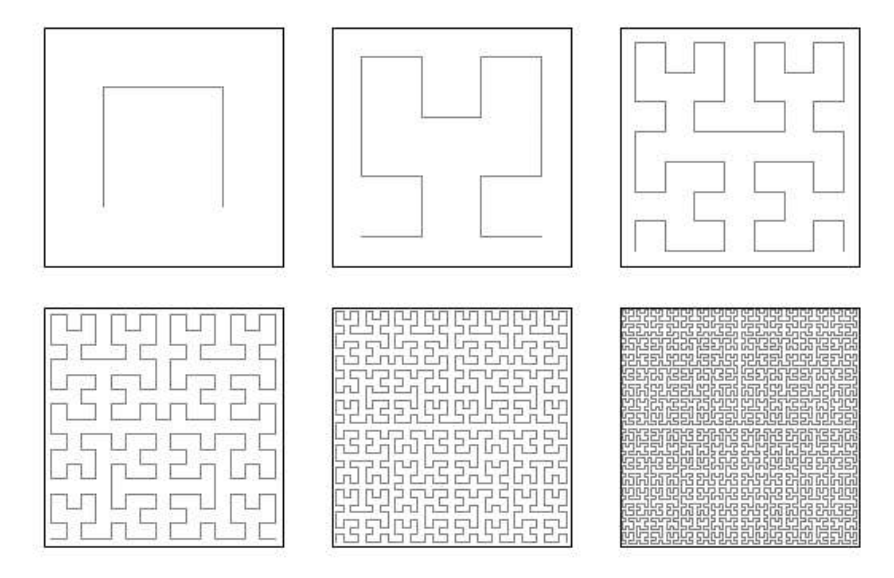


Fig. 4.2. 6 iterations of the Hilbert's space-filling curve

With the variety of space-filling curves and the wide spread of multidimensional applications, the selection of the appropriate space-filling curve for a certain application is not a trivial task. According to the classification in [1], space-filling curves are classified into two categories: recursive and nonrecursive space-filling curves. Examples of recursive SFCs are the Peano's curve (Fig. 4.1) and the Hilbert's curve (Fig. 4.2). Most existing applications of SFCs employ recursive SFCs. The recursive behavior of SFCs allows for the linearization of recursive hierarchical data structures.

One of the most favorable properties of SFCs is their locality and the fact that the linearization is easily computable. Locality means that an SFC never leaves a region at any level of refinement before traversing all points of that region. Thus neighboring data in a multidimensional space remain neighboring after linearization.

In this chapter, we present the use of space-filling curves as tool paths. Given a set of CC data distributed on the surface, a space-filling curve tool path can be thought of as a curve that visits each CC point on the surface once and only once. We also consider the use of non-recursive SFC to allow the curve to travel in the optimal cutting directions.

#### 4.2 Tool Path Optimization

Programming a five-axis NC machine requires consideration of a number of important issues, such as optimizing tool paths, avoiding interferences, and improving the cutting efficiency. Tool path optimization could be performed with regard to the cutting time, scallop heights, length of the tool path, width of the machining strip, volume of the removed material, etc. A complete optimization scheme involves specifying 1) a model of cutting operations, 2) topologies of the prescribed tool path patterns, 3) a set of constraints, and 4) an optimization procedure (see, for instance, [18]).

Let  $S \equiv S(u,v)$  be the required surface,  $\mathfrak{M}$  be a set of parameters related to the workpiece setup and the machine configuration, and  $\mathfrak{T}$  be the parameters of the tool such as the tool length, diameter, shape. A model of the cutting operations, taking as input S,  $\mathfrak{T}$ ,  $\mathfrak{M}$  and  $\Pi$  produces a machining result, the output surface  $T \equiv T(u,v)$ . The general optimization problem is then formulated by

$$\min_{\Pi, \mathfrak{T}, \mathfrak{M}} \epsilon, \tag{4.1}$$

where  $\epsilon = ||S - T||$  represents the error in an appropriate norm. The optimization is performed with respect to the following constraints:

- 1. Scallop height: the scallop between the successive tool tracks must not exceed a prescribed tolerance [16, 18].
- 2. Local accessibility: excess material must not be removed when the tool comes in contact with the desired surface. The excess removal commonly occurs due to *curvature interference* and *surface interference* [10, 11, 21].
- 3. Global accessibility: the tool must not come into contact with either machine parts or unwanted parts of the desired surface [13]. This means collision detection must be incorporated into the optimization procedure.

The set of independent variables comprises the tool spatial positions and orientations, rotations of the machine parts, the shape and the size of the tool. Usually, the tool visits the prescribed positions following the zigzag or spiral patterns. However, the optimization could also utilize complicated patterns adapted in such a way that a certain criteria is minimized or at least decreased.

We present the use of space-filling curves as tool paths for five-axis NC machining of sculptured surfaces. Application of the SFC to NC tool path generation has been first reported in [8] and [6]. Griffiths [8] proposed the use

of the Hilbert curve as a tool path while Cox et al. [6] used various forms of space-filling curves such as the Moore curve. Both tool path generation methods have been developed for three-axis NC machining with the ball-end cutter. However, the space-filling curves have not been particularly popular in the five-axis machining community due to large inaccuracies produced by sharp angular turns which characterize the standard SFC patterns.

Nonetheless, tool path generation based on the SFC has a number of attractive features such as the possibility to locally adapt the curve (without changing the global structure) in such a way that the cutting device travels along the optimal direction. In addition, the entire surface is cut in one path eliminating the need of tool retractions.

The use of adaptive SFC as tool paths is presented in this book to overcome the above mentioned drawbacks while keeping the above mentioned advantages. The adaptive SFC is a better candidate for creating tool path than the Hilbert's curve. First, the Hilbert's curve is only applicable to a grid  $2^n$  by  $2^n$  while the adaptive SFC can be used for any rectangular grid as well as block structured grid (the generation of SFC tool paths on block structured grid is presented in Chap. 5). Second, as opposed to the Hilbert's curve having the ratio of three-quarters turn per point [12], the adaptive SFC turns only when necessary, in other words, only when the optimal cutting direction changes. Since the sharp turns usually produce large kinematics errors [19], it is anticipated that the adaptive SFC performs better than a conventional SFC (see also the forthcoming discussion in Sect. 4.3).

The SFC tool path generation method requires three steps: (1) the grid construction, (2) the generation of the adaptive space-filling curve, and (3) the tool path correction. The simplest rectangular grid can be constructed by overlaying two zigzag tool paths generated by the traditional isoparametric scheme. The grid is then filled by an SFC generated by the Hamiltonian path algorithm. Finally, the tool path and the orientation of the tool are adjusted at the turns to eliminate sharp variations in the orientation of the cutting device which result in large kinematics errors.

Consider the following optimization with regard to the length of the tool path,

$$\min_{\Pi} L, \text{ subject to } h < h_{\text{max}}, \epsilon < \epsilon_{\text{max}},$$
(4.2)

where  $\Pi$  is the tool path represented by a structured set of the positions and orientations (the so-called CL data, see Sect. 2.1), h is the scallop height and  $h_{\rm max}$  is the maximum allowed scallop height. If the machining strips do not overlap, the remaining areas are considered as scallops as well. Therefore, the first constraint controls the scallops and provides that the machining strips cover the entire surface. The second constraint requires that the difference  $\epsilon$  between the actual and the desired trajectory does not exceed a prescribed tolerance  $\epsilon_{\rm max}$ . The above two conditions are nothing else than an approximation of a more general requirement that the machined surface does not deviate from the actual surface by more than  $(h_{\rm max}, \epsilon_{\rm max})$ . The minimization of L

is performed in such a way that  $\Pi$  maximizes the machining strip width. In turn, increasing the machining strip width combined with the SFC strategies makes it possible to cut the surface by traveling along a shorter path.

The scallop height constraint is satisfied by constructing two overlaying isoparametric zigzag patterns. The patterns satisfy the scallop height constraints given the surface curvature, a shape and a size of the cutter. The second constraint is satisfied by removing sharp angular turns producing large error and adding additional cutter-contact points, if necessary.

## 4.3 Tool Path Generation using Adaptive Space-filling Curves

The most popular SFC is the recursive Hilbert's curve [12] considered for numerous applications including the tool path planning [8]. Hilbert's curve is particularly appealing in tool path planning as its refinement property can be used to adaptively increase the density of the path. However, each refinement of the tool path based on the Hilbert's curve increases the tool path density in the refined region by a factor of 2 resulting in lower machining efficiency due to the increased total path length. Besides, the Hilbert's curve has an undesirable property that it leads to a path where the tool is constantly changing directions which slows down the machining process and produces large kinematics errors.

To overcome these drawbacks, adaptive SFC is used for tool path generation. It is characterized by the following useful features. First of all the adaptive SFC always follows the local optimal direction. Second, as opposed to the conventional SFC, the adaptive SFC turns only when necessary, in other words, only when the optimal direction changes. Third, the adaptive SFC eliminates the large kinematics errors and the overcuts appearing due to the sharp angular turns. Finally, local refinement of the adaptive SFC is accomplished in exactly the same fashion that the conventional SFC is refined.

A problem of adaptive SFC generation is formulated in terms of a Hamiltonian path on a grid-like graph consisting of the CC points in the (u, v) plane. The algorithm comprises three steps: (1) the grid construction, (2) the space-filling curve generation, and (3) the tool path correction.

#### 4.3.1 Grid Construction

Consider a grid m by n obtained by overlaying two isoparametric tool paths as shown in Fig. 4.3(a-c). The isoparametric paths are generated by calculating the smallest tool path interval and using it as a constant offset to the next tool path (see Sect. 3.5). The tool path interval depends on the local surface shape, cutter shape and size, and the allowable scallop height. Besides, the machining strip widths of the two adjacent cutter paths (see Fig. 3.9) have to overlap to ensure that the machined surface error (scallop height) is within

the tolerance. Techniques for calculating the machining strip width are given in Sect. 3.2.

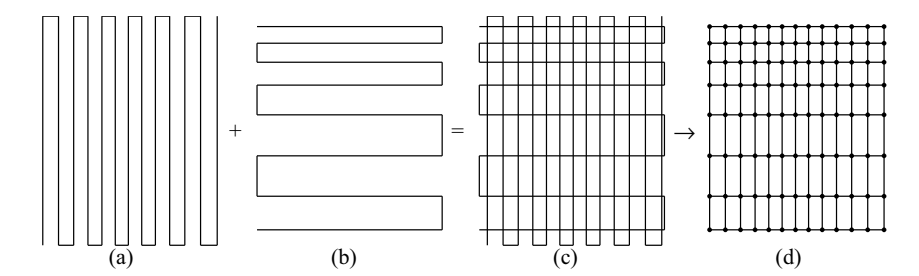


Fig. 4.3. (a) isoparametric tool path in the v-direction, (b) isoparametric tool path in the u-direction, (c) overlaying of two isoparametric tool paths, (d) the resulting grid

Furthermore, the grid is regarded as an undirected graph G where each two adjacent vertices are connected by an edge as shown in Fig. 4.3(d). The vertices of the graph correspond to initial set of CC points on the required surface whereas the distance between two connected vertices is the distance between the corresponding CC points in  $\mathbb{R}^3$ . Note that a cut along the path between any two connected vertices satisfies the scallop height constraint. This feature allows for the tool path optimization by means of the SFC. The SFC tool path generation algorithm is presented next.

#### 4.3.2 Space-Filling Curve Generation

The tool path generation on the grid-like graph constructed in Sect. 4.3.1 is formulated as the Hamiltonian path problem [22]. Finding a path with the minimal length is nothing else than the traveling salesman problem. Since the problem is NP-hard [9], the algorithms for finding the optimal solution are slow and inefficient.

In this book, a simple and computationally efficient Hamiltonian path algorithm is presented. The algorithm is based on the cover and merge algorithm developed by Dafner et al. [7] for 2-dimensional image scanning. The algorithm is extended to an arbitrary rectangular grid. In addition, a correction scheme designed for the SFC tool path generation is presented (see Sect. 4.3.3).

First, all vertices are covered by small disjoint circuits. The circuits are then merged into a single Hamiltonian circuit. The initial circuits are created by constructing small rectangular cyclic paths over every 4 adjacent vertices, i.e., by connecting the vertices on even rows and columns with the vertices on odd rows and columns, respectively, as shown in Fig. 4.4(a). Besides, if m or n is odd, the virtual circuits are constructed to cover the vertices along

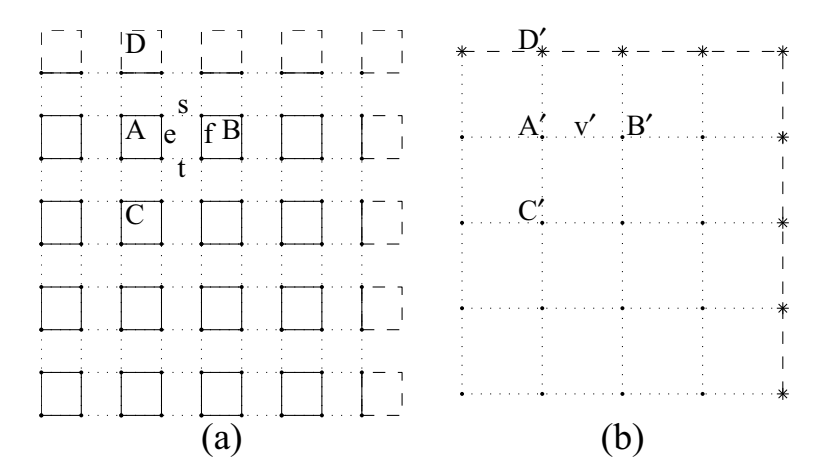


**Fig. 4.4.** (a) undirected graph G covered by initial small circuits, (b) dual graph G'

the boundaries as shown by the dashed lines in Fig. 4.4(a). Any two adjacent circuits can be merged into one bigger circuit. The cost of merging is defined by

$$Cost(A, B) = |s| + |t| - |e| - |f|, \tag{4.3}$$

where |e| denotes the distance in  $\mathbb{R}^3$  between two vertices connected by an edge e.

The cost of merging two virtual circuits is set to  $-\infty$ , i.e., all the virtual circuits are initially merged. This is to ensure that there is no discontinuity of the tool path after removing the virtual edges from the Hamiltonian path. Furthermore, a non-virtual circuit A can be merged with a virtual circuit D only if A is merged with a non-virtual circuit C located on the opposite side. To enforce this merging dependency, the cost of merging A and D is set equal to that of merging A and C. The merging dependency is used to eliminate a possibility of an inappropriate narrow zigzag tool path with a large number of turns along the boundaries (see Fig. 4.11).

To merge all small circuits, a dual graph G' is first constructed. Each small circuit in G defines a vertex in G' and two edges s and t connecting two small circuits A and B in G define an edge v' in G' as shown in Fig. 4.4(b). Then a minimum spanning tree is constructed by iteratively merging circuits according to the cost defined by (4.3). Figure 4.5 illustrates the merging algorithm along with the construction of the corresponding minimum spanning tree. After all the circuits are merged into a Hamiltonian circuit, the tool path is generated by removing all the virtual edges, if any (see Fig. 4.5(c)). Let T be a set of edges of the minimum spanning tree. The merging algorithm is then given below.

- 1. Set  $T = \emptyset$ . Order the edges of G' in the increasing order with regard to the merging cost. In case of a tie, order the edges connecting two non-virtual vertices first.
- 2. Consider the first non-visited edge. Include the edge in T if and only if it does not form a circuit (in the dual graph G') with other edges from T and if and only if it does not violate the merging dependency.
- 3. If the edge is added to T, merge the two circuits in G corresponding to the two vertices in G' connected by the recently added edge and go to step 4, otherwise goto step 2.
- 4. If T includes n-1 edges (where n is the number of vertices of G'), stop and output the resulting Hamiltonian circuit, otherwise go to step 2.

#### 4.3.3 Tool Path Correction

The tool path generated by the previous step requires two further modifications. First, the tool path trajectory should be modified to eliminate undercut areas. Second, the tool orientation needs to be carefully set when the tool is changing the direction.

The tool path adjustment is needed since the SFC tool path contains turns that cause the tool to miss some areas of the surface when the tool is changing the direction. At each turn, the machining strips of the two adjacent tool paths traveling in different directions might not overlap leaving an undercut or the overlap is insufficient and produces a large scallop height (see Fig. 4.6).

To eliminate this machined surface error, the tool path at the turn is modified so that the machining strip overlaps with the machining strip of the adjacent tool path. Figure 4.7 displays the two types of tool path alterations at the corner (left and right), and at the U turns. At these turns, the tool path is extended so that it overlaps with the machining strip of the adjacent tool path. The minimal extension length is

$$L_{\text{ext}} = L - w, \tag{4.4}$$

where L and w denote the tool path interval and the side machining strip width (left or right), respectively, as shown in Fig. 4.6.

The second modification is applied to the tool orientation. The tool orientation is usually set by rotating the tool about  $\mathbf{y}_l$  axis toward the  $\mathbf{x}_l$  axis (see the definition in Sect. 3.2) by an inclination angle  $\lambda$ . At sharp turns, the tool orientation changes abruptly creating large kinematics error. This kinematics error could not be reduced by merely inserting more points as usually done for tool path segmentation [2, 17]. Additionally, the tool orientation of the newly inserted CC point needs to be adjusted by interpolating the tool orientations at the two adjacent CC points. Care must be taken of when adjusting the tool orientation since changing the tool orientation could reduce the machining strip width leaving some areas undercut. Consider the sharp turn O-P-Q shown in Fig. 4.7. To make a correct turn, the  $\mathbf{x}_l$  axis at the turning point

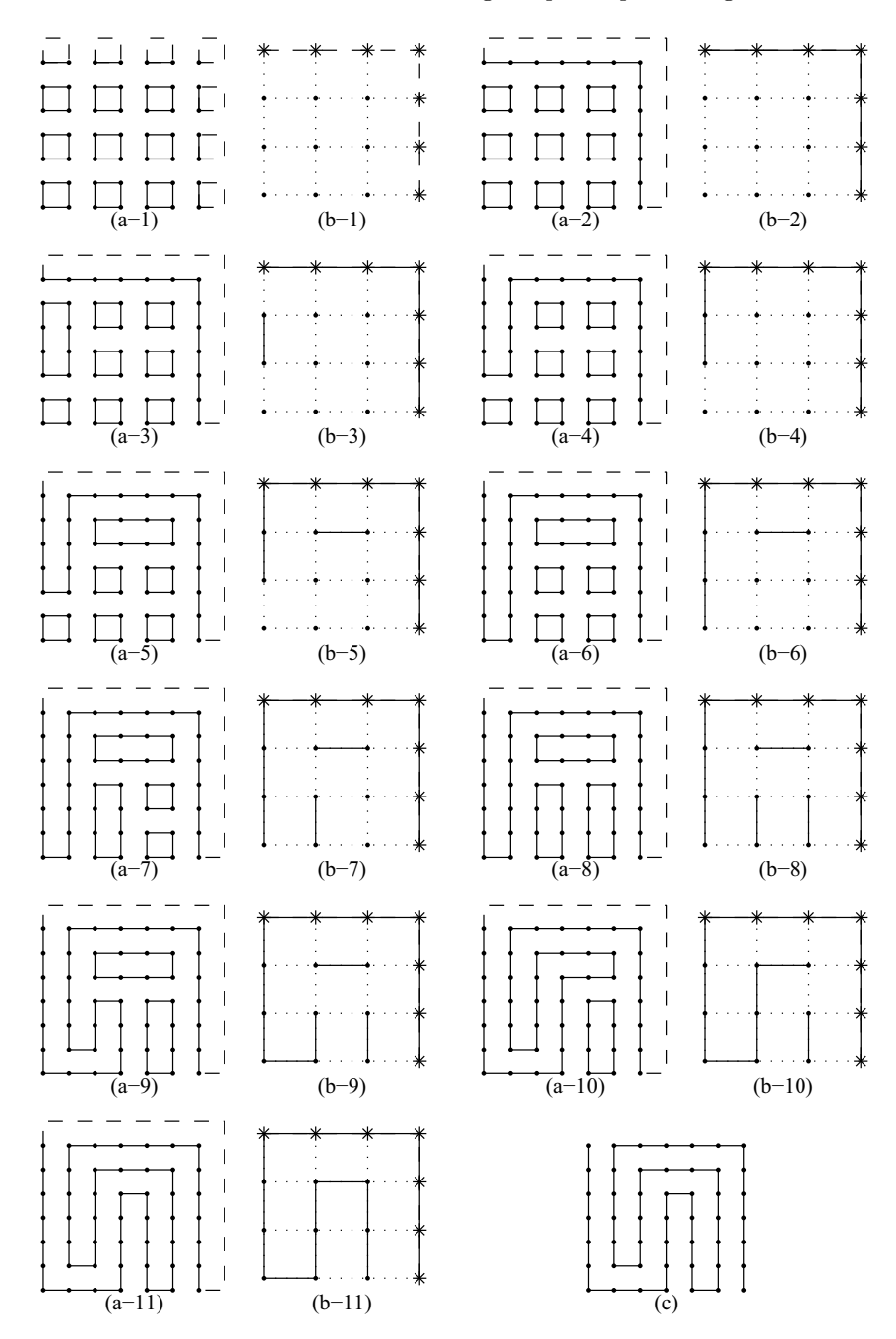
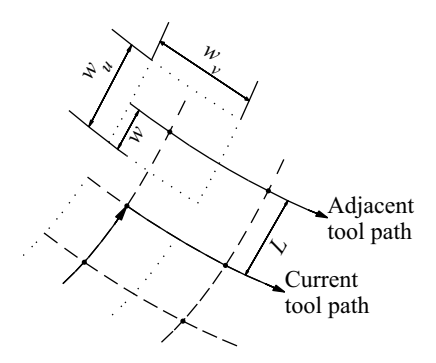


**Fig. 4.5.** (a) Hamiltonian circuit construction by merging of small circuits, (b) the corresponding minimum spanning tree construction, (c) the generated tool path



 ${\bf Fig.~4.6.}$  Machining strips ( dashed~lines) on adjacent tool paths generated by using space-filling curve

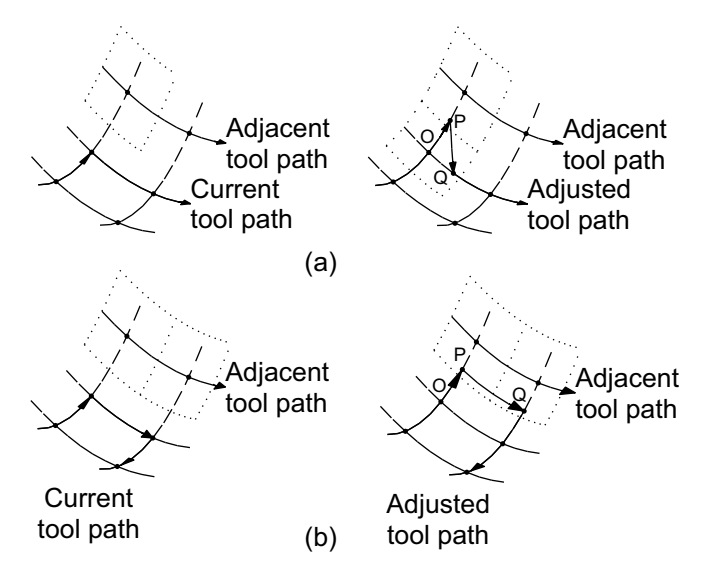


**Fig. 4.7.** Tool path trajectory alteration at corner turn (left or right) (a) and U turn (b)

P is redefined to be a unit surface tangent vector lying in the tool cutting direction at the previous CC point O. To reduce the kinematics error when going from point P to point Q, a new point P' is inserted and the  $\mathbf{x}_l$  axis at P' is interpolated using the two adjacent CC points, P and Q, i.e.,

$$\mathbf{x}_{l,P'}^* = \mathbf{x}_{l,P'} + \mathbf{x}_{l,Q'} \tag{4.5}$$

The  $\mathbf{x}_l$  axis at point P' is then found by computing the unit vector of the projection of  $\mathbf{x}_{l,\mathrm{P'}}^*$  on the surface tangent plane. This process is repeated until the kinematics error between any two adjacent CC points is within the tolerance.

Figure 4.8 shows the trajectories of the effective cutting edge of the tool projected onto the  $\mathbf{x}$ - $\mathbf{y}$  plane before and after applying the tool path correction.

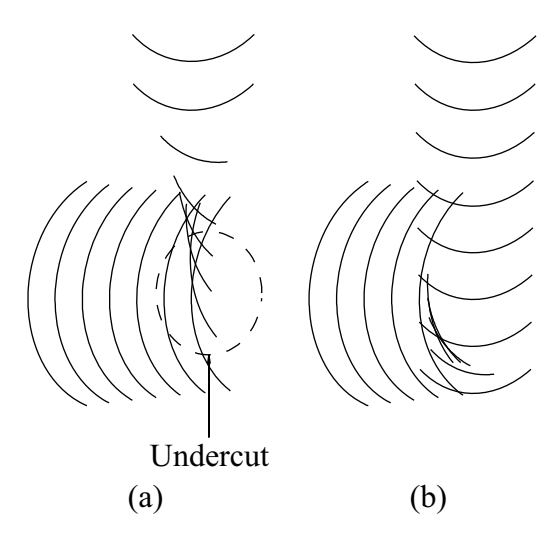


Fig. 4.8. Trajectories of the cutter's effective cutting edge (projected onto the x-y plane) before (a) and after (b) the tool path correction

Remark 4.1. The SFC tool path generation techniques are applicable to the generalized tool geometry (the so-called APT tool [3, 4]). In this case calculation of the effective cutting profile requires a numerical procedure. Once a relationship between the tool inclination and the effective cutting profile is established, the minimum tool inclination providing gouging free tool path can be computed for the generalized tool. Next, given the tool inclination, the isoparametric tool paths and hence the grid are computed. The proposed SFC generation algorithm is then executed without modifications.

## 4.4 Examples and Discussion

This section demonstrates the efficiency of the proposed tool path generation algorithm by examples and practical machining. In all examples, a flat-end cutter with radius r=3 mm is used and the machined surface tolerance h is set to 0.01 mm.

Example 4.1. Consider a cubic Bezier surface (Fig. 4.9) consisting of both convex and concave regions. The surface is characterized by

$$P_{x} = \begin{bmatrix} -50 - 50 - 50 - 50 \\ -15 - 15 - 15 - 15 \\ 15 & 15 & 15 & 15 \\ 50 & 50 & 50 & 50 \end{bmatrix},$$

$$P_{y} = \begin{bmatrix} -50 - 15 & 15 & 50 \\ -50 & -15 & 15 & 50 \\ -50 & -15 & 15 & 50 \\ -50 & -15 & 15 & 50 \end{bmatrix},$$

$$P_{z} = \begin{bmatrix} -20 - 10 - 10 & 0 \\ 0 & -10 - 10 - 20 \\ 0 & -10 - 10 - 20 \\ -20 - 10 - 10 & 0 \end{bmatrix},$$

$$(4.6)$$

where  $P_x$ ,  $P_y$  and  $P_z$  are the x, y and z coordinates of the 16 control points. The grid constructed by overlaying two isoparametric tool paths is depicted in Fig. 4.9. The resulting tool paths are depicted in Figs. 4.10 and 4.11. The practical machining, before and after applying tool path correction, is shown in Figs. 4.12 and 4.13, respectively. Clearly, the proposed method makes it possible to eliminate the areas where the material has not been removed while maintaining the required quality of the surface. Performance of the SFC generation method versus the isoparametric method is compared in Table 4.1.

**Table 4.1.** Performance of the SFC tool paths versus the isoparametric tool paths in terms of tool path length

	Total path length (mm)			
Tool path	Example 4.1	Example 4.2	Example 4.3	
Isoparametric in the $v$ direction	3917.31	9397.97	7831.70	
Isoparametric in the $u$ direction	2648.12	9397.97	9036.17	
SFC tool path	2637.54	7955.58	6780.84	

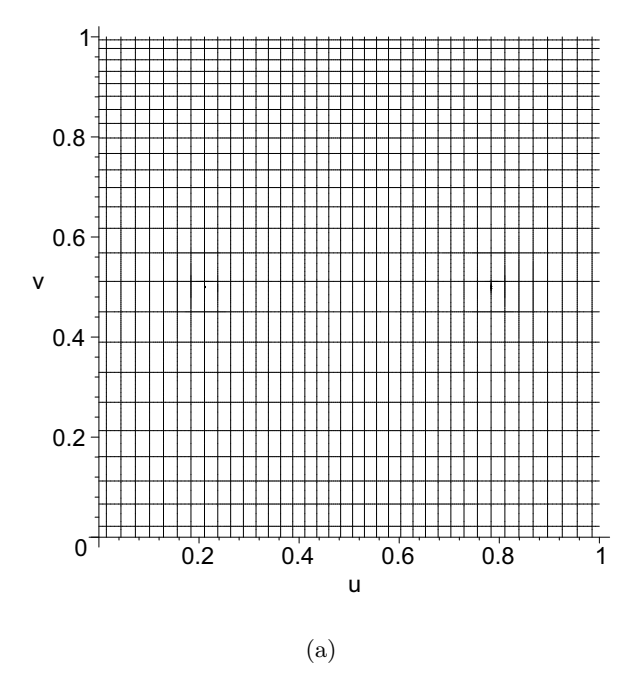
Example 4.2. The example demonstrates the SFC being adapted to high convexity of the surface at a stationary point. Consider a symmetric bell shaped parametric surface given by

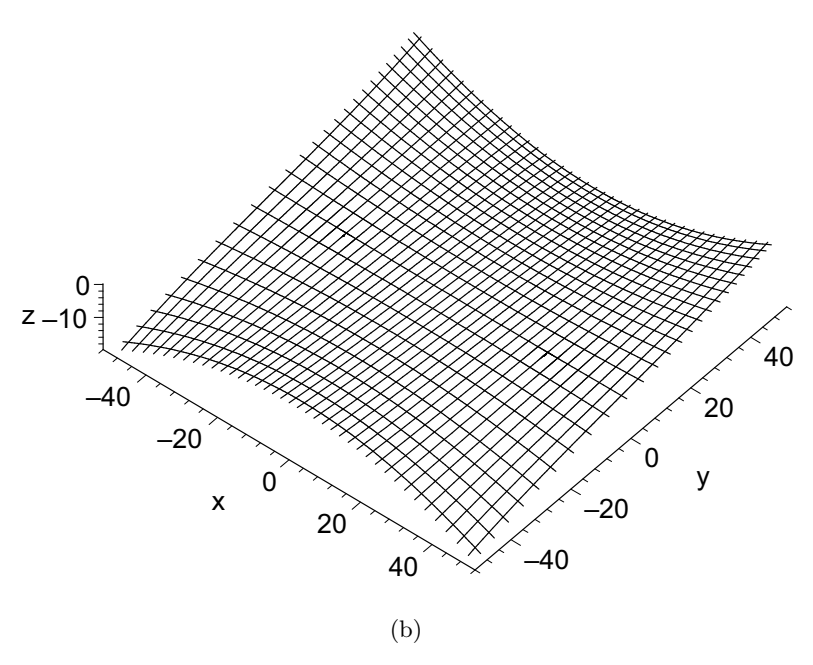
$$x = -50 + 105u - 15u^{2} + 10u^{3},$$
  

$$y = -50 + 105v - 15v^{2} + 10v^{3},$$
  

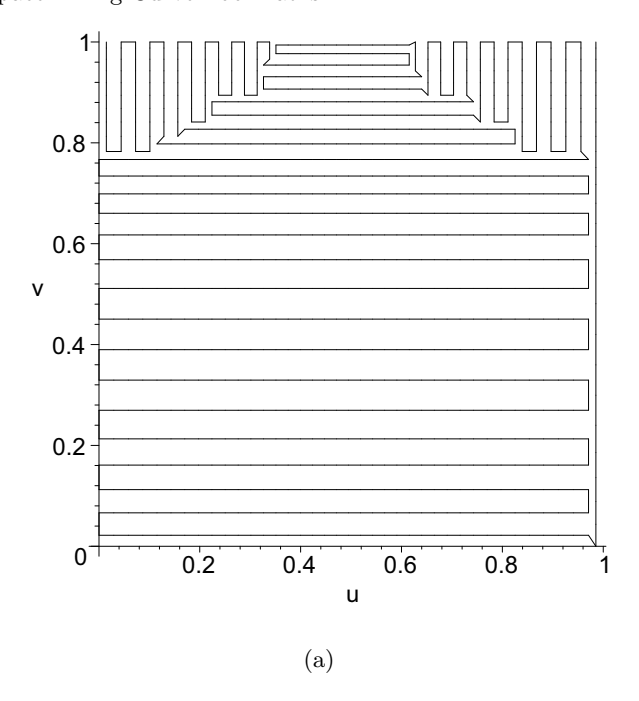
$$z = -100 + 900(uv - u^{2}v - uv^{2} + u^{2}v^{2}).$$
(4.7)

The grid constructed by overlaying two isoparametric tool paths is depicted in Fig. 4.14. The resulting tool path is shown in Fig. 4.15. Apparently, cutting across the top of the bell requires the longest distance and yields the narrowest





**Fig. 4.9.** Overlaying of two isoparametric tool paths for the surface in Example 4.1 in (u, v) domain (a) and in workpiece coordinate system (b)



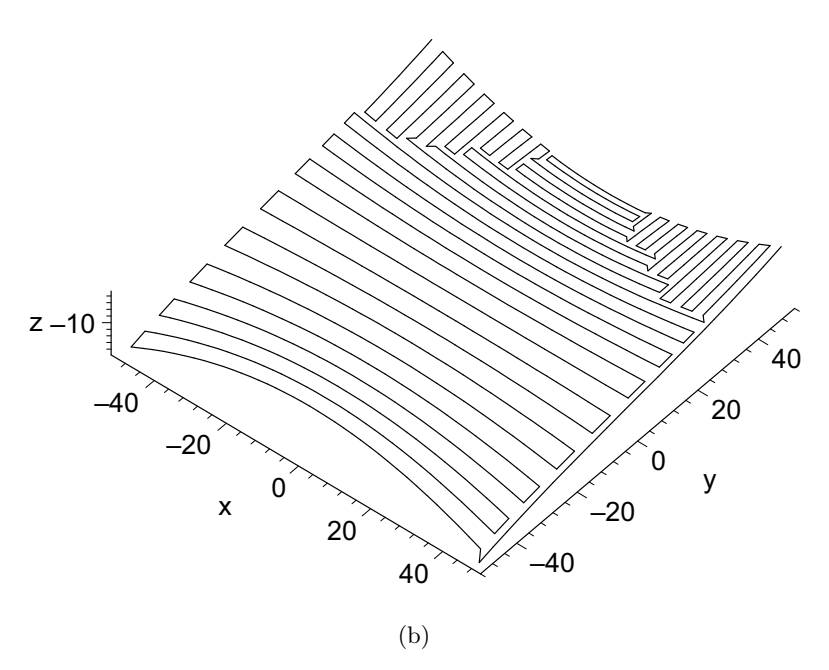


**Fig. 4.10.** SFC tool path for the surface in Example 4.1 in (u,v) domain  $(\mathbf{a})$  and in workpiece coordinate system  $(\mathbf{b})$ 

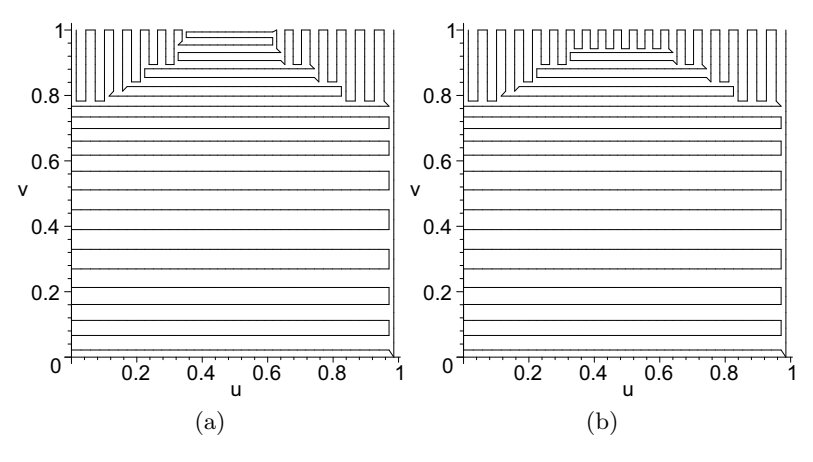


Fig. 4.11. SFC tool paths in Example 4.1 generated with (a) and without (b) merging dependency



Fig. 4.12. Practical machining using the SFC tool path without correction

machining strip width due to the high convexity of the surface at the top of the bell [15]. The generated SFC tool path shown in Fig. 4.15 is adapted to the optimal direction and avoids traversing across the top of the bell.

Example 4.3. The last example demonstrates the case when the proposed technique performs extremely well compared to the traditional isoparametric tool path method. Consider a double bell surface described by the following equations:



Fig. 4.13. Practical machining using the SFC tool path with correction

$$x = 100u - 50,$$
  

$$y = 100v - 50,$$
  

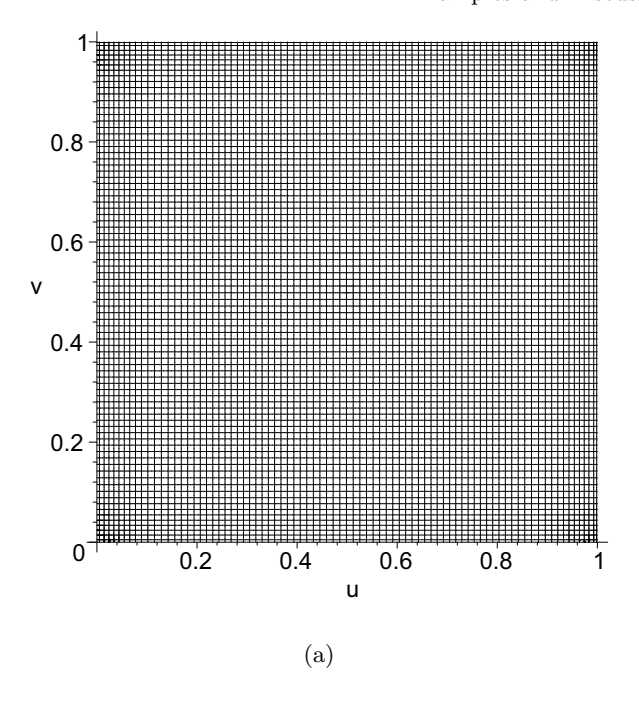
$$z = 400v(1 - v)(3.55u - 14.8u^{2} + 21.15u^{3} - 9.9u^{4}) - 28.$$
(4.8)

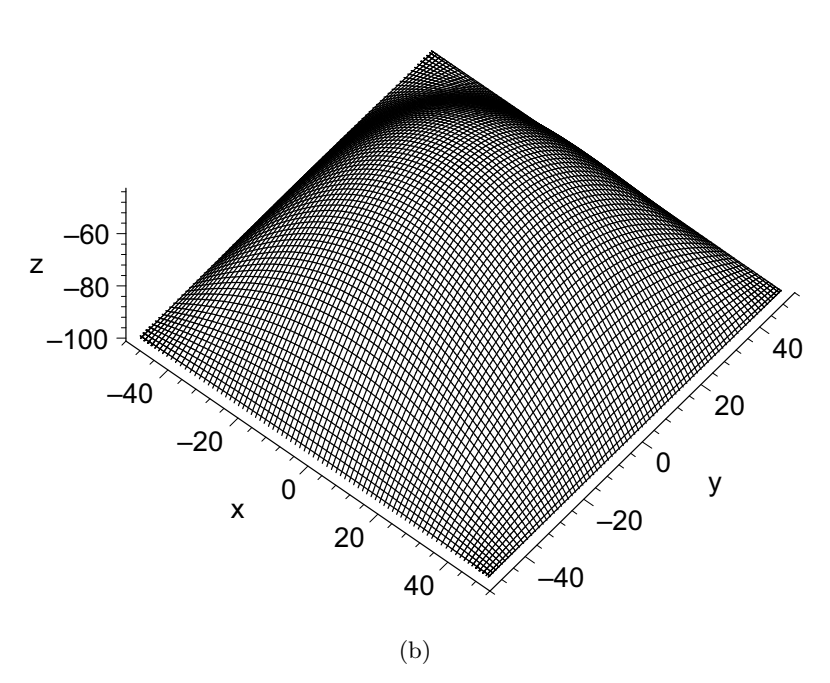
The grid constructed by overlaying two isoparametric tool paths is depicted in Fig. 4.16. The resulting tool path is shown in Fig. 4.17. The tool path verification is performed using Unigraphics 18 and the result of the simulation is shown in Fig. 4.18.

The comparison of the tool path generation method with the traditional isoparametric method in terms of the total path length is given in Table 4.1. As seen from the results, a substantial improvement of the SFC tool path as compared with the isoparametric tool paths (Examples 4.2 and 4.3) is achieved when the required surfaces contain comparable areas characterized by different optimal cutting directions (see Figs. 4.14 and 4.16). However, the SFC tool path constructed by the proposed cover and merge algorithm does not perform well when most of the optimal cutting is in a single direction (Example 4.1, see Fig. 4.9).

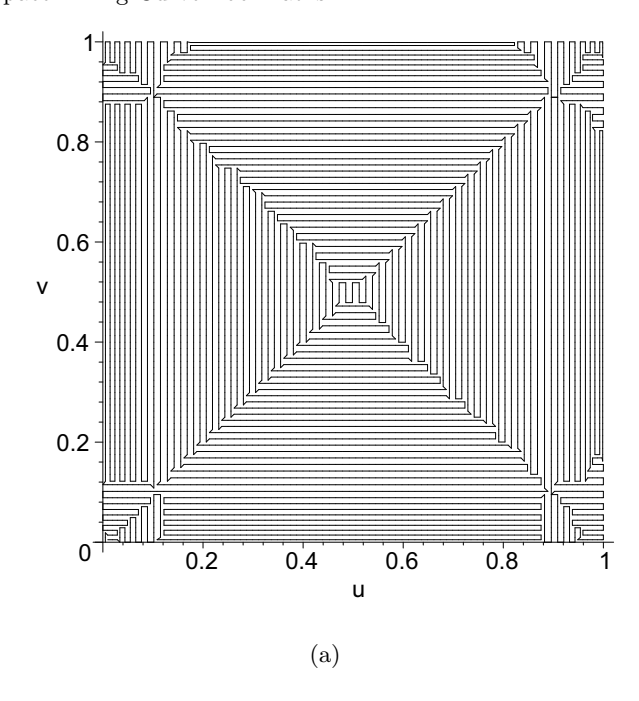
Remark 4.2. The SFC tool path optimization presented above focuses on minimization of the total tool path length. However, the tool path can also be optimized with regard to some other parameters such as the time required to machine the required surface, etc. Given the spatial and angular increments,  $\Delta x_m$ ,  $\Delta y_m$ ,  $\Delta z_m$ ,  $\Delta a$ ,  $\Delta b$ , between two CL points and the feedrate F, the machining time  $t_m$  is calculated as follows

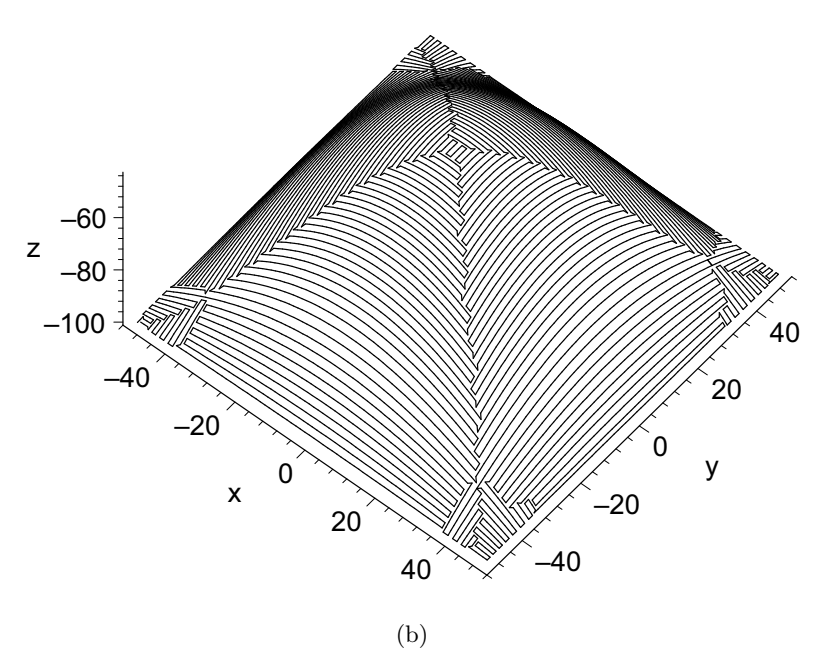
$$t_m = \max\{t_0, t_x, t_y, t_z, t_a, t_b\},\tag{4.9}$$



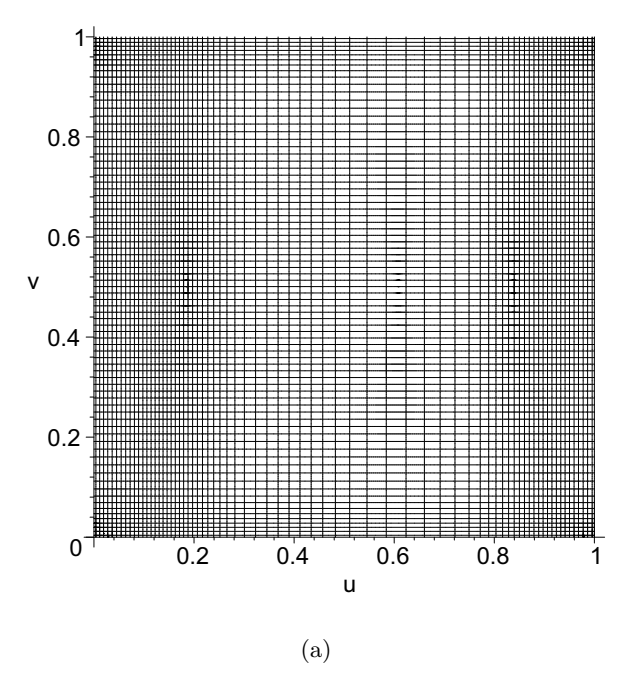


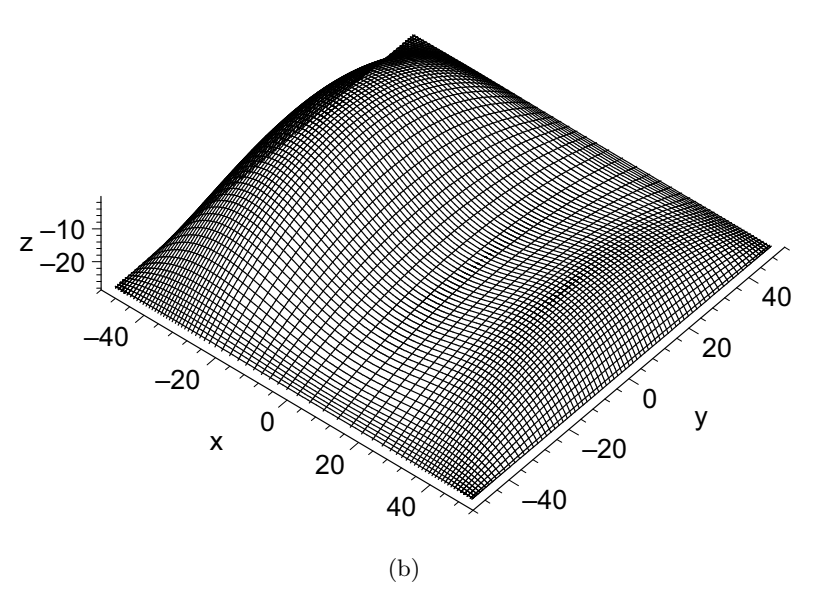
**Fig. 4.14.** Overlaying of two isoparametric tool paths for the surface in Example 4.2 in (u, v) domain (a) and in workpiece coordinate system (b)



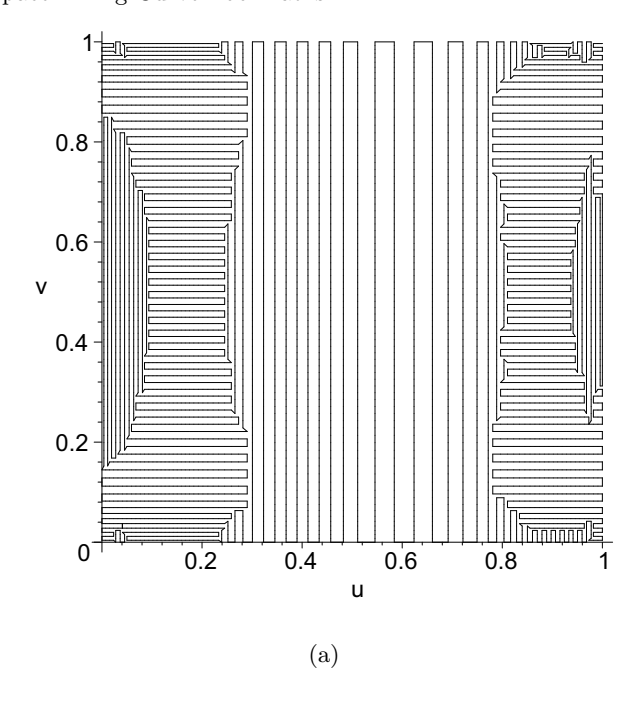


**Fig. 4.15.** SFC tool path for the surface in Example 4.2 in (u,v) (a) domain and in workpiece coordinate system (b)





**Fig. 4.16.** Overlaying of two isoparametric tool paths for the surface in Example 4.3 in (u, v) domain (a) and in workpiece coordinate system (b)



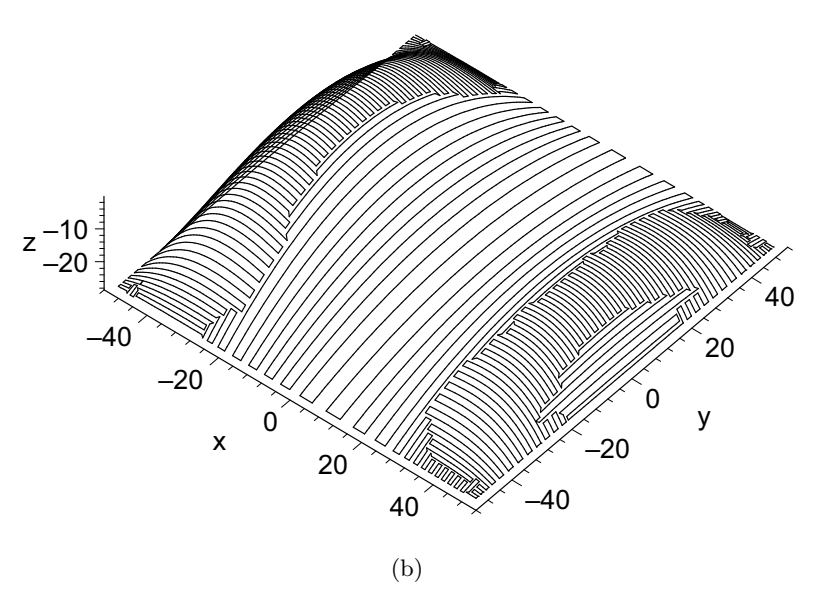


**Fig. 4.17.** SFC tool path for the surface in Example 4.3 in (u,v) domain (a) and in workpiece coordinate system (b)

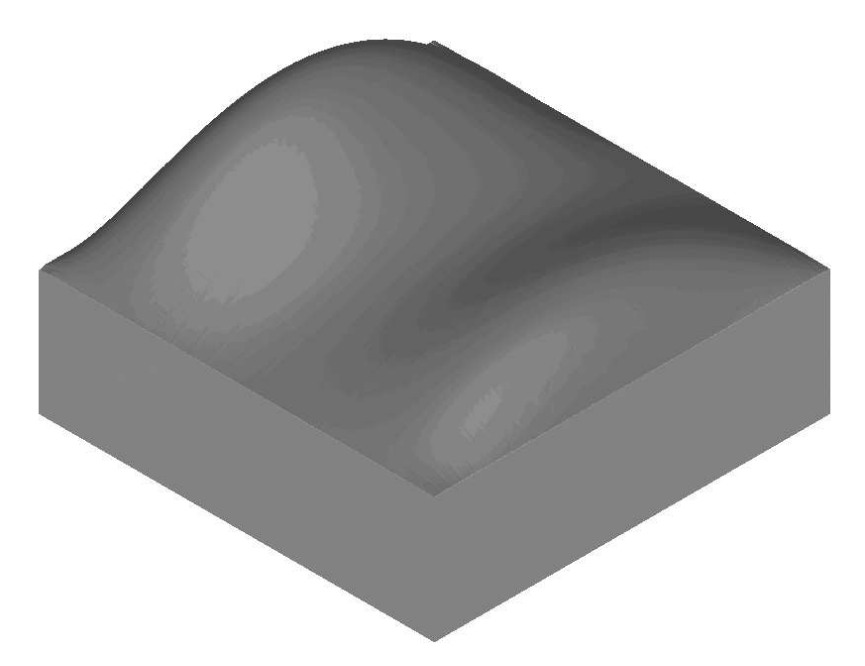


Fig. 4.18. Simulation result of five-axis machining with SFC tool path in Unigraphics 18

where 
$$t_0 = \frac{\Delta L}{F}$$
,  $\Delta L = \sqrt{(\Delta x_m)^2 + (\Delta y_m)^2 + (\Delta z_m)^2}$ ,  $t_x = \frac{\Delta x_m}{v_{x,\text{max}}}$ ,  $t_y = \frac{\Delta y_m}{v_{y,\text{max}}}$ ,  $t_z = \frac{\Delta z_m}{v_{z,\text{max}}}$ ,  $t_a = \frac{\Delta a}{v_{a,\text{max}}}$ ,  $t_b = \frac{\Delta b}{v_{b,\text{max}}}$ , and  $v_{\text{max}}$  denotes maximum velocitiy in the corresponding axis. In case of MAHO 600E, the maximum spatial and angular velocities are given by  $v_{x,\text{max}} = v_{y,\text{max}} = v_{z,\text{max}} = 4000$  mm/min.,  $v_{a,\text{max}} = 235^{\circ}/\text{sec.}$ ,  $v_{b,\text{max}} = 162^{\circ}/\text{sec.}$ 

The estimated machining time for each of the tool path in Table 4.1 is given in Table 4.2. Note that a shorter tool path with many turns may take longer time than a longer tool path with fewer turns. For example, machining a simple surface such as the surface in Example 4.1 does not require many turns with sharp angle variations. Consequently, the corresponding SFC tool path outperforms the conventional isoparametric tool path in terms of the tool path length as well as in terms of the machining time. However, for a complex shaped surface such as the surface in Example 4.3, sharp turns may slow down the machining process when the angular velocity constraints are violated. For such surfaces the SFC strategy works better on the milling machines with high-speed rotational axes.

**Table 4.2.** Performance of the SFC tool paths versus the isoparametric tool paths in terms of estimated machining time

	Estimated machining time (seconds)		
Tool path	Example 4.1	Example 4.2	Example 4.3
Isoparametric in the $v$ direction	4541	12342	10622
Isoparametric in the $u$ direction	4013	12342	16744
SFC tool path	3790	11750	16414

## References

- [1] Asano, T., Ranjan, D., Roos, T., Welzl, E., and Widmayer, P. 1997. Space-filling curves and their use in the design of geometric data structures. *Theoretical Computer Science*, 181(1):3–15.
- [2] Bohez, E. L. J. 2002. Five-axis milling machine tool kinematic chain design and analysis. *International Journal of Machine Tools and Manufacture*, 42(4):505–520.
- [3] Bohez, E. L. J., Makhanov, S. S., and Sonthipermpoon, K. 2000. Adaptive nonlinear tool path optimization for 5-axis machining. *International Journal of Production Research*, 38(17):4329–4343.
- [4] Chiou, C.-J. and Lee, Y.-S. 2002. A machining potential field approach to tool path generation for multi-axis sculptured surface machining. *Computer-Aided Design*, 34(5):357–371.
- [5] Cole, A. J. 1987. Compaction techniques for raster scan graphics using space-filling curves. *The Computer Journal*, 30(1):87–92.
- [6] Cox, J. J., Takezaki, Y., Ferguson, H. R. P., Kohkonen, K. E., and Mulkay, E. L. 1994. Space-filling curves in tool-path applications. *Computer-Aided Design*, 26(3):215–224.
- [7] Dafner, R., Cohen-Or, D., and Matias, Y. 2000. Context-based space filling curves. *Computer Graphics Forum*, 19(3):209–218.
- [8] Griffiths, J. G. 1994. Toolpath based on Hilbert's curve. Computer-Aided Design, 26(11):839–844.
- [9] Hopcroft, J. E. and Ullman, J. D. 1979. Introduction To Automata Theory, Languages, And Computation. Addison-Wesley Longman Publishing Co., Inc., Boston, MA, USA.
- [10] Kim, K. and Jeong, J. 1996. Finding tool approach directions for sculptured surface manufacture. *IIE Transactions on Design and Manufacturing*, 28(10):829–836.
- [11] Koren, Y. and Lin, R.-S. 1995. Five-axis surface interpolators. *Annals of CIRP*, 44(1):379–382.
- [12] Lam, W. M., Shapiro, J. M., and Sarnoff, D. 1994. A class of fast algorithms for the Peano-Hilbert space-filling curve. In *ICIP* (1), pages 638–641.
- [13] Lauwers, B., Dejonghe, P., and Kruth, J. P. 2003. Optimal and collision free tool posture in five-axis machining through the tight integration of

- tool path generation and machine simulation. Computer-Aided Design, 35(5):421-432.
- [14] Lawder, J. K. and King, P. J. H. 2001. Querying multi-dimensional data indexed using the hilbert space-filling curve. *ACM SIGMOD Record*, 30(1):19–24.
- [15] Lee, Y.-S. and Ji, H. 1997. Surface interrogation and machining strip evaluation for 5-axis CNC die and mold machining. *International Journal of Production Research*, 35(1):225–252.
- [16] Lin, R.-S. and Koren, Y. 1994. Real time interpolator for machining ruled surfaces. In *ASME Annual Meeting Proceedings*, pages 951–960.
- [17] Makhanov, S. S., Batanov, D., Bohez, E., Sonthipaumpoon, K., Anotaipaiboon, W., and Tabucanon, M. 2002. On the tool-path optimization of a milling robot. *Computers & Industrial Engineering*, 43(3):455–472.
- [18] Makhanov, S. S. and Ivanenko, S. A. 2003. Grid generation as applied to optimize cutting operations of the five-axis milling machine. Applied Numerical Mathematics, 46(3-4):331–351.
- [19] Munlin, M.-A., Makhanov, S. S., and Bohez, E. L. J. 2004. Optimization of rotations of a five-axis milling machine near stationary points. *Computer-Aided Design*, 36(12):1117–1128.
- [20] Pascucci, V. and Frank, R. J. 2001. Global static indexing for real-time exploration of very large regular grids. In *Supercomputing '01: Proceedings of the 2001 ACM/IEEE conference on Supercomputing (CDROM)*, pages 2–2.
- [21] Rao, A. and Sarma, R. 2000. On local gouging in five-axis sculptured surface machining using flat-end tools. *Computer-Aided Design*, 32(7):409–420.
- [22] Roberts, F. S. 1984. Applied combinatorics. Prentice-Hall, Inc., Upper Saddle River, NJ, USA.
- [23] Sagan, H. 1994. Space-Filling Curves. Springer-Verlag, New York.
- [24] Schamberger, S. and Wierum, J.-M. 2005. Partitioning finite element meshes using space-filling curves. Future Generation Computer Systems, 21(5):759–766.
- [25] Song, Z. and Roussopoulos, N. 2000. Using Hilbert curve in image storing and retrieving. In MULTIMEDIA '00: Proceedings of the 2000 ACM workshops on Multimedia, pages 167–170.
- [26] Velho, L. and Gomes, J. 1991. Digital halftoning with space filling curves. In SIGGRAPH '91: Proceedings of the 18th annual conference on Computer graphics and interactive techniques, pages 81–90.
- [27] Yang, K.-M., Wu, L., and Mills, M. 1988. Fractal based image coding scheme using Peano scanning. In *Proceedings of 1988 IEEE International* Symposium on Circuits and Systems, pages 2301–2304.
- [28] Zhang, Y. and Webber, R. E. 1993. Space diffusion: an improved parallel halftoning technique using space-filling curves. In SIGGRAPH '93: Proceedings of the 20th annual conference on Computer graphics and interactive techniques, pages 305–312.

## Tool Paths in Adaptive Curvilinear Coordinates

## 5.1 Introduction

Space-filling curves tool path generation technique presented in Chap. 4 has been designed for surfaces represented in such a way that the parametric coordinates are changing within a rectangular region. Once a minimal machining strip is evaluated, constructing a basic grid for the SFC generation in the rectangular region is trivial (see Sect. 4.3.1). However, such a grid is often inefficient since a small step between the tracks could be required only in certain areas. The rectangular grid is also inefficient in the case of a complex boundary of the so-called trimmed surfaces. These surfaces are characterized by the boundaries created by intersections with other surfaces. The complex boundaries also occur in the case of pocket milling when the parametric region includes internal boundaries around one or several pockets. From the viewpoint of computational mathematics the above are classic situations when a numerically generated adaptive curvilinear grid should be introduced. The grid may be easily converted to the zigzag tool path or replace the basic grid required at the first step of the SFC tool path generation method.

In this chapter we introduce and analyze the both possibilities. The first approach is a modification of a classic grid generation based on the Euler-Lagrange equations for a functional which represents desired properties of the grid such as smoothness, adaptivity to the boundaries and to a certain weight (control) function [15, 81]. Therefore, Sect. 5.3 presents a concatenation of the grid generation approach and the tool path optimization. In this framework, proposed in [49, 51], the weight function is represented by the kinematics error. The minimization is subjected to constrains relevant to the heights of scallops between the successive tool tracks.

However, the above techniques have a number of drawbacks. In particular, they may converge slowly for complicated constraints. Besides, the approach requires equal number of the cutter contact points on each track of the tool. Therefore, if the kinematics error changes sharply from track to track, the method may require an excessive number of points.

Section 5.4 introduces another modification of the grid refinement which fits better to the framework of tool path optimization. The method does not require equal number of points on each track. It automatically evaluates the number of the required grid lines. As opposed to the first approach, where the weight function represents either the kinematics error or an estimate of the kinematics error (such as the surface curvature or the rotation angles), the proposed algorithm iteratively constructs an adaptive control function designed to represent the scallop height constraints. This important modification makes it possible to consider an arbitrary number of points along the tool tracks. Consequently, the kinematics error is reduced by means of inserting additional points along the resulting curvilinear coordinates<sup>1</sup>. In other words, this approach replaces the scallop constraints by a weight function and then treats the kinematics error independently. Additionally, instead of the Winslow functional the new optimization is based on the harmonic functional derived from the theory of harmonic maps [25, 36]. The functional not only provides the smoothness and the adaptivity but under certain conditions guarantees the numerical convergence as well. Finally, this approach merges with the SFC techniques. In this case, the grid is not converted to the tool path directly. Instead, it becomes the basic grid required for SFC generation which replaces the rectangular grid (see Chap. 4). With this modification, the SFC tool path can be constructed to machine surfaces with complex irregular boundaries, cuts off, pockets, islands, etc. Besides, the adaptive grid allows to efficiently treat complex spatial variability of the constraints in such a way that the SFC is being created on a grid having the small cells only where necessary.

## 5.2 A Historical Note on Grid Generation

Grid generation has been developed as a sub-discipline of computational fluid dynamics (CFD), heat and mass transfer and structural analysis. Nowadays, grid generation is employed in many other areas including CAD/CAM, mechanical engineering and manufacturing.

Structured grid generation has its roots in the US in the works of Winslow with Lawerence Livermore National Lab in the late 1960s [81]. About the

Curvilinear coordinates are a coordinate system based on some transformation of the standard coordinate system. For example, consider the 2D case, instead of Cartesian coordinates x and y one can use e.g. p and q where p=p(x,y) and q=q(x,y). The level curves of p and q in the (x,y) plane, as well as those of x and y in the (p,q) plane are in general curved. It is required that the transformation is locally invertible at each point. This means that a point can be converted in one coordinate system to its curvilinear coordinates and back. Depending on the application, a curvilinear coordinate system may be simpler than the Cartesian coordinate system. This also has consequences that the concepts in vector calculus can be expressed in Cartesian coordinates and also in curvilinear coordinates [1].

same time the structured grid generation was proposed in Russia by Godunov and Prokopov with Keldysh Institute of Applied Mathematics in Moscow and Computing Center of the Siberian Branch of the USSR Academy of Sciences [32]. Some ideas, foreshadowed the modern grid generation, were presented by Tikhonov and Gorbunov [75], Sidorov [67] and Bahvalov [6].

The unifying idea of grid generation is based on an estimate of a certain weight (cost) function combined with the equi-distribution principle which imposes such a distribution of the nodes that a product of the grid spacing and the weight function remains constant through the entire region. Some pioneering papers introducing this idea are [17, 22, 35, 58, 62, 72].

A variety of weight functions suitable for solutions of problems occurring in CFD has been proposed in [2, 3, 5, 13–15, 21, 23, 24, 27, 28, 52, 53, 55, 74, 79, 80].

A general viewpoint on the problem is represented by the concept of the so-called *informative-computational space* [2, 40, 54, 72]. The grid is characterized by the so-called *elliptic property* interpreted as *intercommunication* of observers. A motion of an observer to a suitable position implies that his neighbors follow him. The term *elliptic* originates from the fact that such intercommunication can be simulated by elliptic partial derivative equations such as the Laplace equation. A number of semi-heuristic methods employing various interpretations of the informative computational space have been proposed by Baker [7], Berger and Oliger [8], Blacker and R.J. [10], Blacker and Stephenson [11], Dannenhoffer [20], Frey and Field [30], Jiang and Carey [43], Kennon and Anderson [44], Kennon and Dulikravich [45], Pardhanani and Carey [56], Rank and Babushka [60], Samareh-Abolhassani and Stewart [65], Soni [68], Vabistchevitch [78].

Furthermore, the term *structured* means that the curvilinear grid is topologically equivalent to a rectangular grid. In other words, the curvilinear grid can be obtained by applying certain kind of deformations to the rectangular one. Eventually this idea evolved into the idea of constructing a grid which represents a discrete version of a one-to-one mapping of the so-called *physical region*, where the curvilinear grid is defined, onto a parametric square (or cube in 3D) defined in the so-called *computational region*, where the image of the grid becomes rectangular [32, 33, 73].

It turned out that construction of such grids can be performed by means of variational methods which employ Euler equations to optimize a weighted average of the grid quality measures. The grid quality measures include a number of criteria such as smoothness of the grid, orthogonality, adaptation to a certain weight function in accordance with the equi distribution principle, the total length of the grid lines, cell aspect ratio and many others [64].

Considerable effort has been spent on elimination of self-intersected and twisted cells and nodes located outside the prescribed region when the mapping becomes unacceptable [37]. Such grid is called the *degenerate* grid. An efficient approach to construct non-degenerate grids is based on the concept of *orthogonal grid* proposed and analyzed in [4, 14, 15, 59, 66, 70]. An orthogonal grid proposed are spent of the concept of the concept

onal grid generator involves a measure of orthogonality represented by a dot product between the vectors tangential to the grid lines [13, 15, 63].

Another approach to construct a grid without degenerate cells is based on *multi-block grid strategies* employing a decomposition of the complex-shaped regions into blocks [32, 73, 76]. However, the discontinuities at the boundary between blocks is the chief drawback of the method [18, 69].

The concept of convex grid has been proposed by Ivanenko [38]. The grid which consists of convex quadrilaterals ensures a non-degenerate grid at the continuous as well as at the discreet level [36, 61]. Furthermore, the concept of non-degenerate grids can be represented in the framework of the harmonic maps [26]. The use of the harmonic maps as a suitable grid generation strategy was proposed by Dvinsky [25] and Ivanenko [36]. The map constructed on the surface of the graph of the weight function provides the required adaptation of the grid in accordance with the equi distribution principle. The advantage that the theory features over other grid generation strategies is that in 2D it guarantees (under some conditions) the existence and the uniqueness of the map. Besides, harmonic grid generation has been shown to be parameterization-independent [46], namely, that the resulting grid in physical space is independent of the choice of parameterization for the physical domain.

As far as the tool path generation is concerned, construction of the tool paths of industrial milling machines in the framework of grid generation technologies was first introduced in [49] and developed in [50]. The grid generation techniques are surprisingly well-adapted to tool path optimizations. As a matter of fact, the concept of a grid refinement contains almost all the main ingredients for tool path planning, such as: grid adaptation to the regions of large milling errors, possibility to easily construct curvilinear versions of the conventional zigzag and spiral patterns and adaptation to constraints related to the tool diameter and the scallop height. Moreover, in contrast to the standard techniques characterized by a local error estimate, grid generation deals with a global spatial error and consequently adapts all the CL points simultaneously.

The ideas were further developed in [51], specifically for five-axis machining and in the framework of the harmonic maps. Bieterman and Sandstrom [9] suggested a similar approach based on the Laplacian grid generator independently.

It should be noted that application of grid generation for tool path optimization has not been fully exploited. For example, unstructured grids are generally far more flexible and robust when applied to complicated regions [12, 31, 34, 57]. However, application of such grids for tool path generation is an open problem.

Note that our references are related to selected pioneering papers introducing basic concepts of structured grid generation and harmonic maps. As far as the entire scope of modern grid generation methods is concerned, the interested reader should refer to excellent texts of Carey [16], Farrashkhalvat

and Miles [29], Liseikin [46, 47], Steinberg [71], Thompson et al. [73], Tucker [77].

Finally, in spite of success of grid generation in many areas, the process is still not made easy enough and automatic. The generation of grids could become the most time consuming part of calculations requiring hours and even days of calculations.

# 5.3 Variational Grid Generation for Tool Path Optimization

## 5.3.1 Preliminary Examples

A preliminary example is a surface having sharp variations along a sinus shaped curve Fig. 5.1. The corresponding curvilinear grid is depicted in Fig. 5.2. The tool will move along one family of the coordinate curves. It is plain that such curves are more appropriate for cutting and require the same data structures as those employed for rectangular grids.

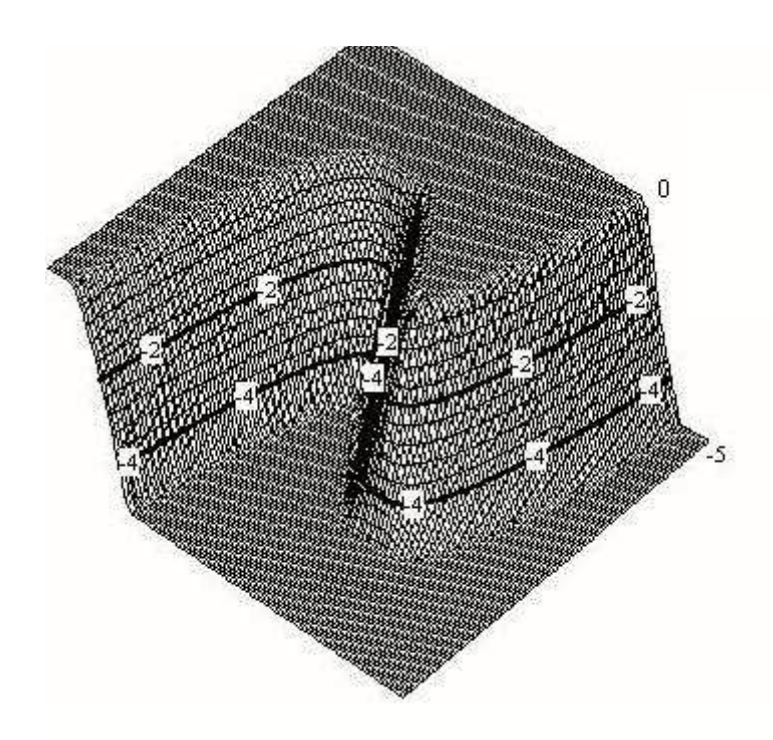
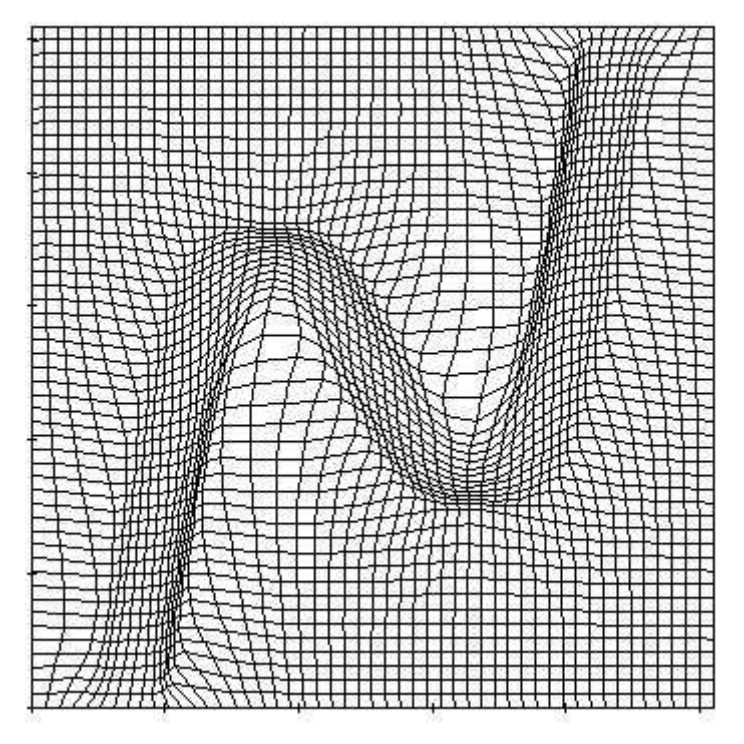


Fig. 5.1. Surface with a curvilinear zone of large gradients



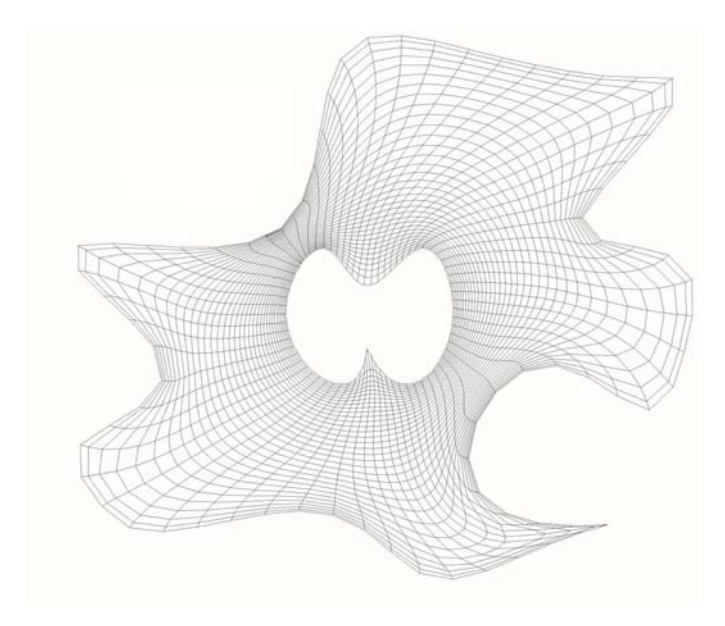
**Fig. 5.2.** Curvilinear grid which can be converted into a tool path to machine the surface in Fig. 5.1

Furthermore, the grid generation techniques are applicable to generate a tool path in the case of complex boundaries such as the case of a complex shaped domain in Fig. 5.3. Jeong and Kim [41] address this domain as an example of complex pocket milling which may not be solved by means of a regular zigzag pattern. However, the generated grid shows that the techniques enable us to simultaneously generate appropriate curvilinear zigzags and curvilinear spirals. The grid is well adapted to the internal and external boundaries. Besides, the flexibility of the grid generation approach allows for further adaptation to the regions requiring more accurate machining.

#### 5.3.2 Variational Method and Functionals

In this section we present basic principles of variational grid generation methods and show how these techniques can be applied to tool path optimization. As far as the grid generation techniques are concerned, we follow the classical variational approach of Winslow [81] and Brackbill and Saltzman [15]. The tool path optimization based of adaptive grids follows [49, 51].

Recall that  $S \equiv S(u,v) \equiv (x(u,v),y(u,v),z(u,v))$  denotes a surface to be machined. As usual u and v are the parametric variables. Consider a set



 ${f Fig.~5.3.}$  A grid which can be converted into a tool path for a complex shaped region

of cutter location points  $\{u_{ij}, v_{ij}\}, 0 \leq i \leq N_{\xi}, 0 \leq j \leq N_{\eta}$  arranged as a curvilinear grid. Mathematically, it means that  $\{u_{ij}, v_{ij}\}$  is a discrete analogy of a mapping from the computational region  $\Delta = \{0 \leq \xi \leq N_{\xi}, 0 \leq \eta \leq N_{\eta}\}$  onto a parametric region defined in the parametric coordinates u, v. In other words there exists a pair of functions  $u(\xi, \eta), v(\xi, \eta)$  such that a rectangular grid  $\{i, j\}$  being fed to  $u(\xi, \eta), v(\xi, \eta)$  becomes  $\{u_{ij}, v_{ij}\}$  (Fig. 5.4).

Recall that the general tool path optimization problem is given by

$$\min_{S,\Pi,\mathfrak{T},\mathfrak{M}} C,$$

where C denotes a criteria vector. The vector may include the kinematics error, the length of the path, the negative of the machining strip, the machining time, etc. Furthermore,  $\Pi$  is the tool path,  $\mathfrak M$  is a set of the parameters related to the setup and configuration of the machine, and  $\mathfrak T$  is the parameters of the tool. Usually, the optimization is subjected to constraints which may include the scallop height, gouging avoidance constrains, etc.

Note that optimization criteria and constraints may be interchangeable depending on the machining problem. For example, the minimization can be performed with regard to the kinematics error subject to the scallop height constraint. Alternatively, the scallops can be minimized subject to a prescribed maximum error. A weighted sum of the scallops and the tool tip errors can be also considered as a single criteria.

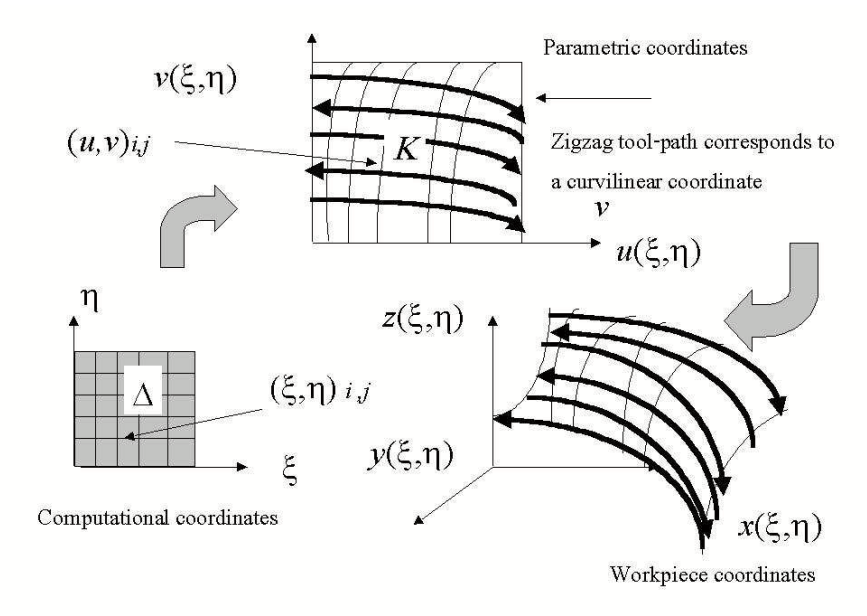


Fig. 5.4. Tool path as a mapping from the computational to the parametric (physical) domain

In this section we consider the criteria vector C, consisting of a single element given by  $C = ||\epsilon||$ , where  $\epsilon = |S(\xi, \eta) - T(\xi, \eta)|$  and  $T(\xi, \eta)$  is a machined surface. An approximation of T can be obtained using a variety of techniques including solid modeling, the sweep volume methods, etc (see Introduction).

As an example of a simple approximation consider  $T(\xi, \eta)$  composed from subsurfaces (patches)  $T_{i+1/2,j+1/2}(\xi,\eta)$  spanned onto a grid-cell  $\{(u,v)_{i,j}, (u,v)_{i+1,j}, (u,v)_{i,j+1}, (u,v)_{i+1,j+1}\}$ , where  $T_{i+1/2,j+1/2}(\xi,\eta)$  is obtained by linear interpolation between the tool trajectories (Fig. 5.5).

Since the tool path  $\Pi$  is now represented by the grid of points  $\{u_{ij}, v_{ij}\}$ , we arrive at the following optimization.

$$\min_{u_{ij}, v_{ij}} ||\epsilon||. \tag{5.1}$$

Furthermore, keeping (5.1) in mind, let us introduce grid generation techniques based on variational principles. Following [15, 81], the required grid is a discretized solution of a minimization problem given by

$$\min (F_s + \lambda_v F_v + \lambda_o F_o), \tag{5.2}$$

where

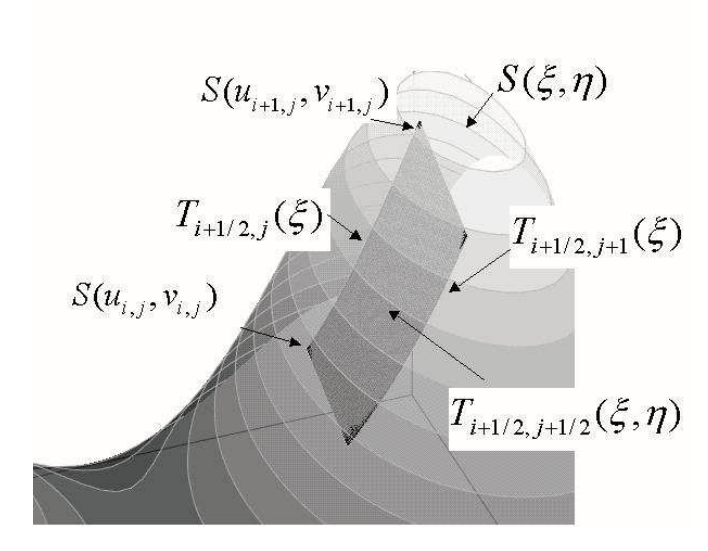


**Fig. 5.5.** Constructing surface  $T(\xi, \eta)$  from patches

$$F_s \equiv \iint_{\Delta} [(\Delta \xi)^2 + (\Delta \eta)^2] \ du dv, \tag{5.3}$$

$$F_v \equiv \iint_{\Lambda} J\epsilon \ dudv, \tag{5.4}$$

$$F_o \equiv \iint_{\Delta} \Delta \xi \cdot \Delta \eta \ du dv. \tag{5.5}$$

 $\Delta \equiv (\frac{\partial}{\partial u}, \frac{\partial}{\partial v}), \, J$  denotes the Jacobian of the mapping given by  $J = \frac{\partial u}{\partial \xi} \frac{\partial v}{\partial \eta} - \frac{\partial v}{\partial \xi} \frac{\partial v}{\partial \eta}, \, \lambda_v, \, \lambda_o$  are the calibration parameters. Furthermore,  $F_s$  is the Winslow functional which measures the smoothness of the mapping. A mapping that minimizes the functional produces a grid which does not have discontinuities or sharp corners and fits to the boundary of the physical region.

 $F_o$  is the so-called orthogonality functional. Its minimum  $F_o=0$  is reached when all the conjugate lines of the grid are orthogonal. The functional can be used as an additional measure which improves the quality of the grid i.e. eliminates twisted and degenerate cells. However, in the context of tool path generation  $F_o$  does not represent an important machining criteria.

Finally,  $F_v$  is the measure of the equi distribution with regard to weight function  $\epsilon$ . The product of the area of the grid cell (which is nothing else than the discretized Jacobian J) and the weight function  $\epsilon$  should be constant through the entire grid.

This is where the problem of the error minimization meets the grid generation. Since the error tends to zero as the area of the grid cell tends to zero, the grid generator adapts the cells in such a way that the error is reduced or even minimized while keeping the basic grid structure. However,  $F_v$  can not be minimized individually because the solution is not unique or may not exist. For example,  $J = \infty$  minimizes  $F_v$ , however, this mapping is singular and, therefore, does not produce a curvilinear grid. Let us omit the orthogonality functional and consider  $F = F_s + \lambda_v F_v$ . (Further analysis of the orthogonality functional can be found in [15, 42]).

Changing variables in  $F_s$  and  $F_v$  yields

$$F_s = \iint_{\Lambda} J^{-1} \left[ \left( \frac{\partial u}{\partial \xi} \right)^2 + \left( \frac{\partial u}{\partial \eta} \right)^2 + \left( \frac{\partial v}{\partial \xi} \right)^2 + \left( \frac{\partial v}{\partial \eta} \right)^2 \right] d\xi d\eta, \tag{5.6}$$

$$F_v = \iint_{\Lambda} J^2 \epsilon \, \mathrm{d}\xi \mathrm{d}\eta. \tag{5.7}$$

There is a variety of ways to proceed from that point. One of them is employing the Euler equations to minimize the weighted sum of the functionals  $F_s + \lambda F_v$ . The Euler equations are given by

$$\frac{\partial F}{\partial x} - \frac{\partial}{\partial \xi} \frac{\partial F}{\partial x_{\xi}} - \frac{\partial}{\partial \eta} \frac{\partial F}{\partial x_{\eta}} = 0,$$

$$\frac{\partial F}{\partial y} - \frac{\partial}{\partial \xi} \frac{\partial F}{\partial y_{\xi}} - \frac{\partial}{\partial \eta} \frac{\partial F}{\partial y_{\eta}} = 0.$$

Next, the partial derivatives should be replaced by the finite differences and the system of the finite difference equations should be solved numerically.

Alternatively, functionals  $F_s$  and  $F_v$  are approximated by quadratures  $I_s$  and  $I_v$ . The resulting discrete functional  $I=I_s+\lambda_vI_v$  should be minimized using the conditions

$$\frac{\partial I}{\partial u_{ij}} = 0, \frac{\partial I}{\partial v_{ij}} = 0.$$

The both methods produce the same system of finite difference equations when the standard second order approximations are being used for the first method ( $\frac{\partial^2 u}{\partial \xi^2} \approx u_{i+1,j} - 2u_{i,j} + u_{i-1,j}$ ,  $\frac{\partial u}{\partial \eta} \approx \frac{u_{i+1,j} - u_{i-1,j}}{2}$ , etc.) and when the standard trapezoidal rule with  $\Delta \xi = \Delta \eta = 1$  is applied to discretize  $F_s$  and  $F_v$  for the second method.

It is not hard to demonstrate that the system of finite difference equations is given by

$$\tilde{R}_{u} \equiv a_{1}u_{\xi\xi} + a_{2}u_{\xi\eta} + a_{3}u_{\eta\eta} + c_{1}v_{\xi\xi} + c_{2}v_{\xi\eta} + c_{3}v_{\eta\eta} + J^{2}\epsilon_{v}, 
\tilde{R}_{v} \equiv b_{1}u_{\xi\xi} + b_{2}u_{\xi\eta} + b_{3}u_{\eta\eta} + a_{1}v_{\xi\xi} + a_{2}v_{\xi\eta} + a_{3}v_{\eta\eta} + J^{2}\epsilon_{u},$$
(5.8)

where the subscripts  $\xi$ ,  $\eta$ , u and v correspond to the finite differences at  $(\xi_i, \eta_j)$  and  $(u_{ij}, v_{ij})$ , respectively.

The coefficients at the derivatives of the second order are given by

$$\begin{split} a_k &= a_{s,k} + \lambda_v a_{v,k}, \ b_k = b_{s,k} + \lambda_v b_{v,k}, \ c_k = c_{s,k} + \lambda_v c_{v,k}, \ k = 1,2,3, \\ a_{s,1} &= -A\alpha, \ b_{s,1} = B\alpha, \ c_{s,1} = C\alpha, \\ a_{s,2} &= 2A\beta, \ b_{s,2} = -2A\beta, \ c_{s,2} = -2C\beta, \\ a_{s,3} &= -A\gamma, \ b_{s,3} = B\gamma, \ c_{s,3} = C\gamma, \\ A &= u_\xi v_\xi + u_\eta v_\eta, \ B = v_\xi^2 + v_\eta^2, \ C = u_\xi^2 + u_\eta^2, \\ a_{v,1} &= -u_\eta v_\eta, \ b_{v,1} = v_\xi^2, \ c_{v,1} = u_\eta^2, \\ a_{v,2} &= u_\xi v_\eta + u_\eta v_\xi, \ b_{v,2} = -2v_\xi v_\eta, \ c_{v,2} = -2u_\xi u_\eta, \\ a_{v,3} &= -u_\xi v_\eta, \ b_{v,3} = v_\xi^2, \ c_{v,3} = u_\xi^2, \end{split}$$

Let us now evaluate the machining strip in the midpoint between two consecutive tracks of the tool  $\eta_j$  and  $\eta_{j+1}$ . Consider the flat-end cutter and for simplicity suppose that the tool is aligned with the normal to the surface. Consider a vertical plane through points  $S(\xi_i, \eta_j)$  and  $S(\xi_i, \eta_{j+1})$ . In this plane we approximate the corresponding section of the surface by a circle with the radius R, where R is the radius of the curvature in that direction. A simple geometric reasoning (Fig. 5.6) yields

$$w = 2|R|\sqrt{\frac{2|R|h + h^2}{|R| + h}}$$
 (5.9)

Additionally the tool radius r must satisfy  $r \geq 2\sqrt{2|R|h+h^2}$ . Note that, if the tool must be inclined, (5.9) must be replaced by a formula which includes the effective cutting radius of the tool  $r_e$  given by (3.36) (see Sect. 3.3). For instance, for  $h \ll r_e$ ,  $h \ll R$ , Lo [48] suggested a formula similar to (3.34) given by

$$w = \sqrt{\frac{8hr_eR}{R - r_e}}.$$

In order to construct a tool path simultaneously adapted to the milling errors  $\epsilon$  and to the constraints related to the prescribed scallop height, we introduce the following conditions:

$$D_{i,j+1/2} \ge 0, (5.10)$$

where  $D_{i,j+1/2} = w_{i,j+1/2}^2 - d_{i,j+1/2}^2$  and d denotes the distance between the points on the adjusted curves  $\eta_j$  and  $\eta_{j+1}$  on the surface S(u,v) given by

$$d_{i,j+1/2} = \sqrt{(x_{i,j+1} - x_{i,j})^2 + (y_{i,j+1} - y_{i,j})^2 + (z_{i,j+1} - z_{i,j})^2}$$
 (5.11)

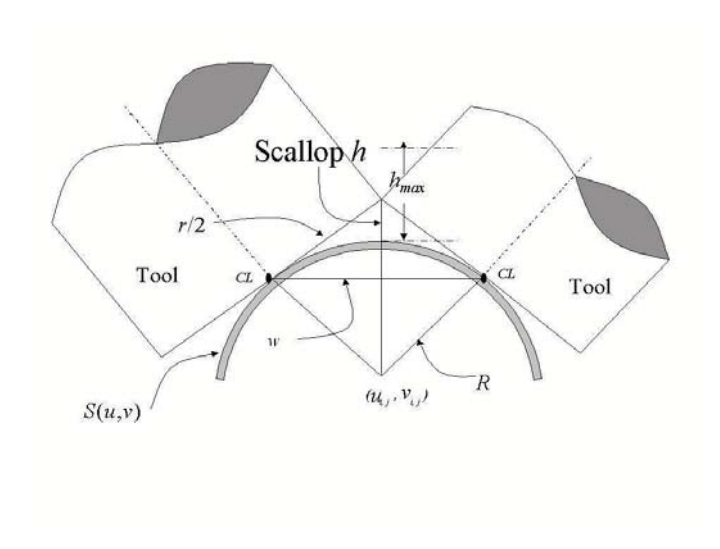


Fig. 5.6. The scallop height evaluation for convex surfaces

and w is evaluated by (5.9).

Thus, we arrived at the following problem: solve equations (5.8) subject to constrains (5.10) to find a minimizer of functional I. In order to solve the constraint minimization, we introduce a penalty function p(D). It is a convex decreasing function such that, p(D) = 0 if  $D \geq 0$  and  $p(D) \to \infty$  when  $D \to -\infty$ .

Next, we define a discrete penalty functional given by

$$I_p = \lambda_p \sum_{i,j} \lambda_{ij} p(D_{i,j+1/2}),$$

where  $\{\lambda_{ij}\}$  are the penalty coefficients and  $\lambda_p$  is the weight coefficient.  $p(D), D \in (-\infty, 0)$ , is a convex decreasing function,  $p(D) \to \infty$  if  $D \to -\infty$ .

Next, the derivatives of  $\lambda_p I_p$  with regard to  $u_{ij}, v_{ij}$  are added to the left hand side of the above finite difference equations, namely,

$$R_u = \tilde{R}_u + \lambda_p \frac{\partial I_p}{\partial u_{ij}} = 0, \ R_v = \tilde{R}_v + \lambda_p \frac{\partial I_p}{\partial v_{ij}} = 0.$$

Example 5.1. Suppose that  $S(u,v)\equiv(x,y,z)=(u,v,u^2+v^2)$ . Consider a penalty function given by  $p(D)=[\min(0,D)]^2$ . Then for D<0 we have

$$p(D_{i,j+1/2}) = D_{i,j+1/2}^2,$$

$$= [w^2 - ((u_{i,j+1} - u_{i,j})^2 + (v_{i,j+1} - v_{i,j})^2 + (u_{i,j+1}^2 + v_{i,j+1}^2 - u_{i,j}^2 - v_{i,j}^2)^2)]^2.$$

Differentiation with regard to  $u_{i,j}$  yields a penalty term given by

$$\begin{split} \frac{\partial I_p}{\partial u_{i,j}} = & 2D_{i,j+1/2} \big[ 2(u_{i,j+1} - u_{i,j}) \\ & + 4(u_{i,j+1}^2 + v_{i,j+1}^2 - u_{i,j}^2 - v_{i,j}^2) u_{i,j} \big] \lambda_{i,j+1/2} \\ & - 2D_{i,j-1/2} \big[ 2(u_{i,j} - u_{i,j-1}) \\ & + 4(u_{i,j}^2 + v_{i,j}^2 - u_{i,j-1}^2 - v_{i,j-1}^2) u_{i,j} \big] \lambda_{i,j-1/2}. \end{split}$$

Note that p(D) is not differentiable at D=0. Therefore, one has to perform an appropriate regularization near D=0. For instance,

$$p_{\text{reg}}(D) = \begin{cases} p(D), & \text{if } D \ge \epsilon, \\ H(D), & \text{if } 0 < D < \epsilon, \\ 0, & \text{otherwise,} \end{cases}$$

where H(D) is a Hermite polynomial satisfying  $H(\epsilon) = p(\epsilon)$ ,  $\frac{dH(\epsilon)}{dD} = \frac{dp(\epsilon)}{dD}$ , H(0) = 0.

The corresponding system can be solved by quasi Newtonian iterations given by

$$u_{i,j}^{n+1} = u_{i,j}^{n} - \left[ \tau \left( R_{u} \frac{\partial R_{v}}{\partial v} - R_{v} \frac{\partial R_{u}}{\partial v} \right) \left( \frac{\partial R_{u}}{\partial u} \frac{\partial R_{v}}{\partial v} - \frac{\partial R_{v}}{\partial u} \frac{\partial R_{u}}{\partial v} \right)^{-1} \right]_{i,j},$$

$$v_{i,j}^{n+1} = v_{i,j}^{n} - \left[ \tau \left( R_{v} \frac{\partial R_{u}}{\partial u} - R_{u} \frac{\partial R_{v}}{\partial u} \right) \left( \frac{\partial R_{u}}{\partial u} \frac{\partial R_{v}}{\partial v} - \frac{\partial R_{v}}{\partial u} \frac{\partial R_{u}}{\partial v} \right)^{-1} \right]_{i,j},$$

where n is the iteration index and  $\tau$  is the iteration parameter. The penalty coefficients are updated by the iterative procedure

$$\lambda_{i,j+1/2}^{l+1} = \left\{ \begin{array}{l} \lambda_{i,j}^l + \delta \lambda_{i,j}^l, \text{ if } D_{i,j+1/2} < 0, \\ \lambda_{i,j}^l, & \text{otherwise,} \end{array} \right.$$

where l is the index of the penalty iterations and  $\delta \lambda_{i,j}^l$  denotes the corresponding increment. In order to improve the stability of the algorithm, we use the following linear relaxation

$$(u_{i,j}^{n+1})_{\text{new}} = u_{i,j}^{n+1} (1 - \theta) + u_{i,j}^{n} \theta,$$
  
$$(v_{i,j}^{n+1})_{\text{new}} = u_{i,j}^{n+1} (1 - \theta) + u_{i,j}^{n} \theta,$$

where  $0 \le \theta \le 1$ .

## 5.3.3 The Harmonic Functional

The sum of two functionals  $F_s$  and  $F_v$  in (5.2) can be replaced by a single functional given by

$$I = \int \frac{(u_{\xi}^2 + u_{\eta}^2)(1 + f_u^2) + (v_{\xi}^2 + v_{\eta}^2)(1 + f_v^2) + 2f_u f_v (u_{\xi} v_{\xi} + u_{\eta} v_{\eta})}{(u_{\xi} v_{\eta} - u_{\eta} v_{\xi})\sqrt{1 + f_u^2 + f_v^2}} d\xi d\eta.$$
(5.12)

(5.12) is called the harmonic functional and is a generalization of Winslow functional to the case of *error surfaces* described explicitly by f(u, v). The subscripts  $u, v, \xi, \eta$  denote partial derivatives and f is the weight function.

The harmonic functional can be derived from the theory of harmonic maps [25, 36]. It has been proven that the functional minimizes an energy of mapping (see details [42]) and produces a grid adapted to the regions of large gradients of f. Note that if  $f_u \equiv f_v \equiv 0$ , then the harmonic functional (5.12) becomes the Winslow functional (5.3). It is important though to understand that I adapts the grid to the gradients of f rather than to f itself. Therefore, it works differently as compared with  $F_v$ . Besides, minimization of (5.12) could be 10 times more computationally expensive that minimization of (5.2) [19]. However, (5.12) has some points in its favor. In particular, it is possible to construct a computational procedure which (under certain conditions) always converges to a non degenerate grid [42]. The constraint minimization of (5.12) subject to the scallop height conditions can be performed by the penalty type techniques similar to those presented in the preceding section. The required modifications and the approximation of the harmonic functional are given in Sect. 5.4.

## 5.3.4 Examples of the Tool Path Optimization

This section illustrates the performance of the proposed procedures by educational examples.

## Example 5.2. Adaptation to a curvilinear zone

The example illustrates convergence of the tool path generation method for a workpiece having curvilinear boundaries and a sin-shaped zone of large milling errors depicted in Fig. 5.7.

For simplicity let us specify constraints (5.9)-(5.10) without defining the actual surface. Suppose we cut the surface by a flat-end cutter and suppose that the minimum radius of the curvature of the surface R=45. We will require that the maximum scallops do not exceed h=0.1 mm. Substituting R=45, h=0.1 into (5.9) yields d<1.25. We will impose this constraint for the entire region, although at many points the minimal distance will be underestimated. Furthermore, the error is *emulated* by (see Fig. 5.7)

$$\epsilon = \exp\left(-\left|y - 0.5\left(L_y - 6\right)\sin\left(\frac{\pi x}{L_x - 0.5}\right) + 0.5\right|\right).$$

Figure 5.7 displays generation of the curvilinear tool path satisfying the prescribed constraints generated by  $p(D) = [\min(D,0)]^2$ ,  $\delta\lambda = 1$ ,  $\lambda_v = 10$ ,  $\lambda_p = 0.9$ .